

NACA RM L55F14

7632

USAF TECHNICAL LIBRARY
HOLLOMAN AIR FORCE BASE
ALAMOGORDO, NEW MEXICO

NACA

SEP 1955

TECH LIBRARY KAFB, NM



0144167

RESEARCH MEMORANDUM

COLLECTION AND SUMMARY OF
 FLAP-TYPE-AILERON ROLLING-EFFECTIVENESS DATA AT ZERO
 LIFT AS DETERMINED BY ROCKET-POWERED MODEL TESTS AT MACH
 NUMBERS BETWEEN 0.6 AND 1.6

By H. Kurt Strass, Emily W. Stephens, E. M. Fields,
 and Eugene D. Schult

Langley Aeronautical Laboratory
 Langley Field, Va.

**NATIONAL ADVISORY COMMITTEE
 FOR AERONAUTICS**

WASHINGTON
 September 2, 1955



NATIONAL ADVISORY COMMITTEE FOR AERONAUTICS

RESEARCH MEMORANDUM

COLLECTION AND SUMMARY OF
FLAP-TYPE-AILERON ROLLING-EFFECTIVENESS DATA AT ZERO
LIFT AS DETERMINED BY ROCKET-POWERED MODEL TESTS AT MACH
NUMBERS BETWEEN 0.6 AND 1.6

By H. Kurt Strass, Emily W. Stephens, E. M. Fields,
and Eugene D. Schult

SUMMARY

A collection and summary have been made of the wing-aileron rolling-effectiveness data which have been obtained as a part of a general investigation of lateral control being conducted by the Langley Pilotless Aircraft Research Division utilizing rocket-powered test vehicles in free flight over a range of Mach number from 0.6 to 1.6. Some effects of trailing-edge angle, aileron-chord ratio, aileron span and location, aspect ratio, wing sweepback, and wing-tail interference are presented. Rough design charts have been prepared to show some effects of aileron trailing-edge angle at two sweepback angles, aileron-chord ratio, wing aspect ratio, and spanwise extent and location of aileron. These rough design charts have been prepared for use in the preliminary design stage, and estimates from these charts were in fair agreement with measured rocket-model data for several configurations simulating existing or proposed aircraft wing-aileron combinations.

INTRODUCTION

A general investigation of lateral control at transonic and supersonic speeds is being conducted by the Langley Pilotless Aircraft Research Division utilizing rocket-powered test vehicles in free flight. The first successful roll test was achieved in May 1946 and since that time a large number of successful test vehicles, comprising a variety of wing-control configurations, have been flown at the Langley Pilotless Aircraft Research Station at Wallops Island, Va. It is the purpose of this report to collect and summarize the rigid-wing flap-type aileron data obtained from these tests under one cover in order to aid in the design of aircraft intended

to be flown at transonic and supersonic speeds. A major portion of these data has been reported in references 1 to 33. The data for a few models (see refs. 1 to 4 and 6 to 10) were obtained during the earlier phases of the development of the testing technique, and although they were believed to be reliable as to trends and magnitude, they do not meet the standards of accuracy of the present report and are not included. Data for only the solid-steel-wing model (ref. 19) have been included since the other models had such large aeroelastic corrections as to make the calculated rigid-wing results questionable.

It should be noted that the data in the present paper represent a rigid-wing tailless (except where noted) configuration in essentially steady-state roll at zero lift and zero yaw, with each aileron differentially deflected 3° to 7° . No data concerning the variation of rolling effectiveness with aileron deflection or wing stiffness are shown.

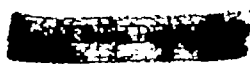
In the following sections an attempt has been made to separate the effects of the major geometric variables of the wing and aileron on rolling effectiveness. Except for the effects of trailing-edge angle, the data obtained by varying a major geometric parameter are first presented as rolling effectiveness plotted against Mach number and then cross-plotted against the major geometric variable for several Mach numbers. These cross plots may be considered rough design charts showing some effects on rolling effectiveness of aileron trailing-edge angle at two wing sweepback angles, aileron-chord ratio, wing aspect ratio, and aileron spanwise extent and location. All the aforementioned cross plots unavoidably contain some effects of trailing-edge angle.

The design charts have been used to estimate the rolling effectiveness of an assortment of wing-aileron combinations simulating the wing-aileron combinations (without fixed tails) of some existing or proposed aircraft. These estimates have been compared with measured data from rocket-model tests to indicate the applicability of the design charts for preliminary design purposes.

The geometry, pertinent wing-control parameters, and sources of published data for each of the test vehicles are listed in table I.

An index to the figures which shows the effects of the major geometric variables on the rolling effectiveness has been included as table II.

SYMBOLS

- A aspect ratio, b^2/s
b diameter of circle swept by wing tips, ft
- 
- 

- C_l rolling-moment coefficient
- c wing chord, parallel to model center line, ft
- \bar{c} mean exposed wing chord, $\frac{c_r + c_t}{2}$, ft
- h wing thickness at trailing edge, ft

$$K_A = \frac{\left(\frac{pb/2V}{\delta}\right)_A}{\left(\frac{pb/2V}{\delta}\right)_{A=3.7}}$$

$$K_c = \frac{\left(\frac{pb/2V}{\delta}\right)_{c_a/c}}{\left(\frac{pb/2V}{\delta}\right)_{c_a/c=1}}$$

$$K_\eta = \frac{\left(\frac{pb/2V}{\delta}\right)_{\text{part-span aileron}}}{\left(\frac{pb/2V}{\delta}\right)_{\text{full-span aileron}}} \quad \text{or} \quad \frac{\left(\frac{C_l/\delta}\right)_{\text{part-span control}}}{\left(\frac{C_l/\delta}\right)_{\text{full-span control}}}$$

- L length of model fuselage, 4.58 ft
- M Mach number
- p rolling velocity, positive when right wing is moving downward, radians/sec
- q dynamic pressure, lb/sq ft
- R Reynolds number

- S area of two wings to model center line, sq ft
- t wing local maximum thickness, ft
- V velocity, ft/sec
- X distance from model nose to quarter-chord point of \bar{c} , ft
- y distance from model center line, measured in a plane perpendicular to model center line, ft
- $pb/2V$ rolling-effectiveness parameter (wing-tip helix angle), radians
- $\frac{pb/2V}{\delta}$ rolling-effectiveness parameter $\left(\text{not } \frac{\partial(pb/2V)}{\partial\delta}\right)$, radians/deg
- δ average aileron deflection for one wing in a plane parallel to model center line, positive for trailing edge up on right wing, deg
- $\eta = \frac{y}{b/2}$
- Λ angle of sweepback of quarter-chord line, except where noted, deg
- λ ratio of tip chord to chord at model center line
- ϕ trailing-edge angle, defined as the angle measured in a plane parallel to model center line between straight lines drawn between 0.97 chord and 1.00 chord on upper and lower surfaces, deg

Subscripts:

- a aileron
- i inboard
- o outboard
- R rigid-wing rolling effectiveness
- r wing-fuselage intersection
- t wing tip

MODELS

A general arrangement of typical test vehicles is illustrated in figure 1. The geometry, pertinent wing-control parameters, and sources of the published data for each of the test vehicles are listed in table I. More detailed information regarding most of the models can be obtained from the appropriate references. The airfoil sections for all models, except where specifically noted in table I, were taken in a direction parallel to the model center line. All the models had constant percent-chord ailerons. It may be noted in table I that in some cases the trailing-edge angle varies between models having the same airfoil section. This variation generally arises from the hand-finishing operations near the extreme trailing edge during model construction.

A few of the models (2, 4, 6, 8, 83, 85, 89, and 93) having a simplified construction were used in order to provide additional data on the effects of wing aspect ratio and aileron-chord ratio. A typical model of this series (model 89) is shown in figure 2. The wings of this series were made of 1/2-inch-thick aluminum alloy and had wedge-shaped leading edges extending to 0.20 chord. The dark spanwise strip near the trailing edge is the filled-in slot along the aileron hinge line, the slot having been cut to allow bending the aileron to the desired deflection. Welded fittings were used to attach the wings to the rocket-motor case which also served as the fuselage. A tapered sleeve was used as a fairing behind the standard spinsonde head.

In the investigation of the effects of wing location and number of wings on rolling effectiveness, the wings were located at a more forward position on the body and some of these models had a free-to-roll tail for directional stability. Each free-to-roll tail consisted of four fins and two ball-bearing assemblies lubricated with a special wide-temperature-range silicone grease. The photographs presented in figure 3 are typical of the sweptback configurations.

TEST TECHNIQUE

The flight tests were made at the Langley Pilotless Aircraft Research Station at Wallops Island, Va. The test vehicles were propelled by a two-stage rocket-propulsion system to a maximum Mach number of approximately 1.6 to 1.8 in about 3 seconds. During the following 10 to 20 seconds of coasting flight, time histories of the rolling velocity measured in zero-lift flight were obtained with special radio equipment (designated spinsonde; see ref. 34), the flight-path velocity was obtained through the use of CW Doppler radar, and the model space coordinates were obtained

through the use of modified SCR 584 tracking radar. These data, in conjunction with atmospheric data obtained with radiosondes, permit the evaluation of the rolling effectiveness in terms of the parameter $pb/2V$ as a function of Mach number. The variation of Reynolds number and dynamic pressure with Mach number is presented in figure 4.

ACCURACY AND CORRECTIONS

General Discussion

During the course of a general investigation of rolling effectiveness which has been conducted by the Langley Pilotless Aircraft Research Division for the past 8 years, many changes have been made in the design and construction of the test vehicles and in the testing technique in order to improve the accuracy and reliability of the data. As a result, the data have been corrected to a standardized set of conditions to allow direct comparison of the data obtained at various stages in the evolution of the present technique.

The rolling-effectiveness data were obtained under essentially zero-lift conditions and have been corrected to rigid-wing values and are presented in terms of the parameter $\frac{pb/2V}{\delta}$, where $pb/2V$ results from the aileron deflection δ and should not be confused with $\frac{\partial(pb/2V)}{\partial\delta}$.

Accuracy

The following factors must be considered in the assessment of the overall probable accuracy of the data presented here.

(1) The accuracy of measurement of $pb/2V$ at a given Mach number for any given test model is dependent upon the following values:

M	±0.01
p, radians/sec	±1.5
V, ft/sec	±5.0
b/2	Negligible error

The maximum probable error in $pb/2V$ from these sources is estimated to be ±0.0020 at subsonic speeds and ±0.0010 at supersonic speeds.

(2) The systematic errors caused by deviations from the desired model geometry, a result of constructional tolerances which can alter

████████████████████

the roll effectiveness, normally are limited to variations in aileron deflection and wing alinement. The method of model measurement used is capable of measuring the angular deviation to within approximately $\pm \frac{0.0083}{\text{Chord}}$ degrees per foot of wing or aileron chord. The accuracy of measurement for a typical model (model 28) can be illustrated as follows:

$$\delta \text{ (average of models 28a, b, and c) } = 5.22^\circ \pm 0.071^\circ$$

$$i_\omega \text{ (not published, average of models 28a, b, and c) } = 0.02^\circ \pm 0.018^\circ$$

where i_ω is the average angle of wing misalignment (differential incidence), positive when tending to roll the model in a clockwise direction as seen from the rear, and is based upon distance from leading edge to aileron hinge line (0.472 foot).

Corrections

Incidence.- The data were corrected for deviations in wing incidence from the nominal value of $i_\omega = 0^\circ$ by use of the following equation which was derived by using very simple aerodynamic assumptions:

$$\frac{pb}{2V} = \frac{2i_\omega}{57.3} \frac{1 + 2\lambda}{1 + 3\lambda}$$

The validity of this correction was demonstrated in reference 21 wherein it is shown that this simple formula provides good estimates of $pb/2V$ resulting from differential incidence for a wide range of wing plan forms. It is estimated from the data published in reference 21 and additional unpublished data that the probable accuracy of prediction of this formula is within ± 15 percent for most configurations. (Relatively thick unswept wings, NACA 65A009, show an abrupt discontinuity in the variation of $pb/2V$ with M at $M \approx 0.92$ which is not predicted by the theory.)

Aileron deflection.- Corrections for deviations in δ were made simply by presenting the data as $\frac{pb/2V}{\delta}$.

As an example, the probable errors in $\frac{pb/2V}{\delta}$ for model 28 resulting from the previously mentioned limitations are tabulated as follows:

M	$\frac{pb/2V}{\delta}$ nominal	Sources of probable error in $\frac{pb/2V}{\delta}$				Total
		Random	δ_a , deg	i_w , deg		
				Measurement	Calculated correction (a)	
0.8	0.02040	± 0.00036	± 0.00028	± 0.00009	± 0.00001	± 0.00074
1.4	0.00510	± 0.00018	± 0.00007	± 0.00009	± 0.00001	± 0.00035

^aEstimated at ± 15 percent of theoretical correction.

Aeroelasticity corrections.- It was necessary to correct all the data for the effects of aeroelasticity, and the large number of models which were tested precluded the use of very refined methods of aeroelastic analysis. For this reason, a special engineering method was developed and is presented in reference 25. The probable errors in the values of $\frac{pb/2V}{\delta}$ resulting from the application of this method are very difficult to assess and are dependent upon a large number of variables. Unless otherwise specified, it is believed that errors from this source are negligible as the test wings in most instances were very stiff and needed a relatively small correction.

Effect of model roll inertia.- For one-degree-of-freedom configurations such as the rolling-effectiveness models of this report, the equation governing their behavior is

$$C_{L_p} \frac{pb}{2V} + C_{L_\delta} \delta = \frac{I_x}{qS'b} \frac{d\delta}{dt}$$

or

$$\left(\frac{pb}{2V}\right)_{\text{steady state}} = \left(\frac{pb}{2V}\right)_{\text{meas}} - \frac{I_x}{C_{L_p} qS'b} \frac{d\delta}{dt}$$

where

$$C_l = \frac{\text{Rolling moment}}{qS'b}$$

$$C_{l_p} = -\frac{dC_l}{d(pb/2V)}$$

$$C_{l_\delta} = \frac{dC_l}{d\delta}$$

I_x measured model moment of inertia about roll axis, slug-ft²

S' area of three wings to model center line, ft²

t time, sec

See the section on "SYMBOLS" for additional definitions.

The data for a model with large rolling accelerations (model 27a) have been corrected for roll inertia effects and the results are shown in figure 5. Physical constants for the model were $I_x = 0.0697$ slug-ft², $b = 2.18$ ft, and $S' = 1.93$ ft²; and C_{l_p} values for this configuration were obtained from reference 35. The maximum rolling acceleration for the model was 175 radians/sec².

Figure 5 shows that the differences between measured rolling effectiveness and steady-state rolling effectiveness are negligible for this model despite the very large values of rolling acceleration. Very few of the models in this report have rolling-acceleration values even approaching those for model 27a, and no inertia corrections have been made to any of the data presented in this report.

DISCUSSION OF RESULTS

Effect of Trailing-Edge Angle

General comments.- Aileron rolling effectiveness is affected by the contour of the entire wing, and particularly the contour over the aileron.

Thus, two ailerons differing widely in contour but having the same trailing-edge angles may have different values of rolling effectiveness.

It was shown in reference 20 that the rolling effectiveness of untapered wings with 0° and 45° sweepback and employing full-exposed-span ailerons could be correlated as a function of the trailing-edge angle for a wide range of airfoil profiles and thicknesses. In general, the correlation was good but the scatter of the data indicated that the trailing-edge angle was not the only variable; however, it was obvious that it was a very important factor. Since that initial effort, several attempts have been made to improve the correlation by making use of the transonic similarity laws. The $pb/2V$ values were plotted against parameters containing various combinations of airfoil thickness ratio and trailing-edge angle at constant Mach number and constant parameters containing Mach number, airfoil thickness ratio, and trailing-edge angle in combination. None of these attempts provided any marked improvement over the original correlation against trailing-edge angle in reference 20 and, in addition, they were much more complicated to use.

Figure 6 presents the rolling-effectiveness data correlated against trailing-edge angle and includes some additional data not available at the time of publication of reference 20. In addition, an improved method of correcting for the effects of aeroelasticity was used (ref. 25) which primarily affected the data for the sweptback wings.

Unswept wings.- For unswept wings it is apparent that trailing-edge angle has the greatest effect in the speed range between $M \approx 0.8$ to $M \approx 1.2$. At $M \approx 0.7$ and $M \approx 1.2$ the rolling effectiveness does not vary markedly with ϕ . In the transonic range there is considerable scatter and the only clear indication is that a small trailing-edge angle (approximately 7° or less) maintains rolling effectiveness throughout the speed range and that larger trailing-edge angles exhibit varying amounts of rolling-effectiveness loss or even reversal of control. There is an indication, although not shown as such in figure 6, that the 6-percent-thick wings appear to have generally higher rolling effectiveness than thicker wings of about the same trailing-edge angle. In view of the scatter of the data and the relatively small number of thickness ratios for comparison at a given trailing-edge angle, it is not clear whether a differentiation between various thickness ratios should be made, and so the trailing-edge angle has been the sole variable considered in fairing the data points.

Sweptback wings.- For wings swept back 45° , there was generally less scatter than for the unswept wings and the effects of trailing-edge angle were evident at a lower subsonic Mach number. No direct data are available for very low trailing-edge angles on a wing having the aspect ratio of the wings used in this correlation ($A = 3.71$), but flat-plate data ($\phi = 0^\circ$) for aspect ratios of 2.31 and 8.00 (models 6 and 89) have been interpolated

to provide an estimated end point to aid in fairing the measured data to $\phi = 0^\circ$. The faired curve in the region near $\phi = 0^\circ$ is presented as a dashed line to indicate that it is essentially an extrapolation of the data.

Effect of airfoil thickness ratio.- Although it is evident that trailing-edge angle is a major factor in determining the level of rolling effectiveness for an aileron, it is also of interest to note the effects of changing the thickness ratio for a given family of airfoils. Such a change necessarily involves a corresponding change in trailing-edge angle so that it is not possible to determine the effects of thickness ratio divorced from the effects of trailing-edge angle without altering the basic profile of the family. Figure 7 presents a comparison of the rolling-effectiveness data for wings having several thickness ratios, aspect ratios, and plan forms.

Concluding comment.- The preceding discussion indicates that the trailing-edge angle of an aileron is a parameter of prime importance and most of the undesirable characteristics of increased trailing-edge angle, such as abrupt changes in $pb/2V$ with M and unusually large losses in rolling effectiveness, can be avoided by employing ailerons with trailing-edge angles of $\phi \leq 7^\circ$ for $\Lambda = 0^\circ$ wings and $\phi \leq 12^\circ$ for $\Lambda = 45^\circ$ wings. In actuality, most of the high-speed aircraft which are designed to fly at the speeds where large trailing-edge angles are to be avoided should experience little or no trouble from this source because drag considerations preclude the use of thick wings (which would normally have large trailing-edge angles).

Effect of Wing Sweepback

Figure 8 presents some effects of wing sweepback on aileron rolling effectiveness for a variety of test configurations employing full-exposed-span ailerons.

At subsonic speeds, increased sweepback generally resulted in decreased rolling effectiveness.

At transonic speeds, the most significant effect of increased sweepback was the smoothing effect on the variation of $\frac{pb/2V}{\delta}$ with Mach number. The rolling-effectiveness "bucket," characteristic of unswept wings at transonic speeds with moderate trailing-edge angles, was virtually eliminated as the sweepback was increased to 45° and disappeared completely at 60° sweepback.

At supersonic speeds, increased sweepback did not cause a consistent variation of $\frac{pb/2V}{\delta}$ with change in sweepback angle; however, the general tendency was a decreased rolling effectiveness with increased sweepback angle.

Effect of Aileron Chord Ratio

Some effects of aileron chord upon rolling effectiveness are shown in figure 9 for a wide range of wing plan forms and airfoil sections. Unless otherwise specified, the following discussion pertains to full-exposed-span ailerons.

NACA 65A009 airfoil sections.- Figure 9(a) presents the effect of aileron chord as measured on unswept wings. The variation of $\frac{pb/2V}{\delta}$ with Mach number for all the aileron configurations is characterized by an abrupt dip near $M \approx 0.9$. This is a wing dropping phenomenon which on the basis of past experience is restricted primarily to unswept wings employing trailing-edge angles greater than $\phi \approx 7^\circ$ and thickness ratios greater than $t/c \approx 0.06$. (See refs. 20 and 36.) Aerodynamic control reversal was measured for the 0.1-chord ailerons in this region. It should be noted that a similar reversal of rolling effectiveness has been obtained for full-chord ailerons at a very small angle of deflection. (See ref. 21.) The values of $\frac{pb/2V}{\delta}$ presented in figure 9 were obtained from models on which the ailerons were deflected approximately 5° . Other tests have shown that aerodynamic reversal may be eliminated by increasing the aileron deflection. (See ref. 10, for example.)

Similar data for 45° sweptback wings are presented in figure 9(b). The variation of $\frac{pb/2V}{\delta}$ with c_a/c is similar to that experienced by the unswept wings.

NACA 65A006 airfoil sections.- The effect of aileron chord as measured on tapered, sweptback wings is presented in figures 9(c) to 9(f) for outboard ailerons of various spanwise extents. With the exception of the full-exposed-span ailerons, the data for the full-chord ailerons (figs. 9(d), 9(e), and 9(f)) were obtained for ailerons of different spanwise extents than the partial-chord ailerons.

The 0.15-chord ailerons were approximately 60 percent as effective as the 0.30-chord ailerons for the two aileron configurations of greater span (figs. 9(c) and 9(d)) but became relatively more effective for the smaller spans (figs. 9(e) and 9(f)).

It may be of interest to note that, with the exception of the abrupt dip in effectiveness at $M \approx 0.9$ for the unswept wings (fig. 9(a)), all the full-chord ailerons exhibited very little variation of effectiveness with Mach number.

Flat plate airfoil sections.- Figures 9(g) to 9(j) present some data which show the effects of aileron chord upon rolling effectiveness for several wings all of which employed flat-plate airfoil sections ($\phi = 0^\circ$). The effect of aileron chord was approximately the same for all the models in that the 0.2-chord ailerons were approximately 75 to 85 percent as effective as the 0.4-chord ailerons at subsonic speeds with the relative effectiveness decreasing with increasing Mach number until at $M = 1.6$, the 0.2-chord ailerons were approximately 50 percent as effective as the 0.4-chord ailerons.

Correlation of data.- Where data are available for both part-chord and full-chord controls of the same span (figs. 9(a) to 9(f)), the part-chord $\frac{pb/2V}{\delta}$ have been divided by the full-chord $\frac{pb/2V}{\delta}$ and plotted as K_c at the appropriate c_a/c value in figure 10 to illustrate non-dimensionally the effects of aileron-chord ratio on rolling effectiveness. Because of the scatter and the relatively small number of tests available, only the theoretical two-dimensional curves for thin plates are shown for comparison with the test points.

The 0.1-chord ailerons on the unswept wings exhibited control reversal at $M = 0.9$ and zero effectiveness at $M = 0.93$. At $M = 0.96$, no control reversal was observed but all of the unswept wing-aileron configurations were appreciably less effective than the comparable swept-wing models. Figure 6 shows that the effectiveness of 0.2-chord ailerons can be greatly increased in this speed range by recourse to smaller trailing-edge angles. Although no direct evidence is available for 0.1-chord controls, there is no reason to suspect that a similar improvement could not be achieved on these controls by the use of small trailing-edge angles. It should be pointed out that swept wings with part-chord ailerons exhibit low $\frac{pb/2V}{\delta}$ values for large trailing-edge angles in this same speed range. (See ref. 20.)

Effect of Aspect Ratio

The effect of wing aspect ratio upon the rolling effectiveness of full-span ailerons is illustrated in figure 11 for untapered wings having sweepback angles of 0° , 45° , and 60° and several airfoil sections. Only two configurations (fig. 11(a)) have been tested which show the effect of aspect ratio upon 60° sweptback wings; these data do not conform with

the trend shown by the wings of lower sweep but show that increased aspect ratio caused an increase in $\frac{pb/2V}{\delta}$ at subsonic speeds and a very slight decrease at supersonic speeds.

Correlation of data.- In order to illustrate better the effects of aspect ratio, the data of figure 11 have been normalized as a fraction of the $A = 3.7$ values, and the resulting values of K_A , the normalized aspect-ratio factor, are cross-plotted against aspect ratio in figure 12. It is obvious that, although the general trend of the data is for the rolling effectiveness to decrease with increasing aspect ratio, considerable variation exists in the rate of change of the variation as is evidenced by comparison of the faired curves of the various test configurations.

At Mach numbers of 0.9 and greater, the effect of aspect ratio depends upon the configuration. For example, at $M = 0.9$, the rolling effectiveness of the unswept wings decreased rapidly with increasing aspect ratio, whereas the 45° sweptback wings showed little effect of aspect ratio. The aileron trailing-edge angle had considerable effect in that for a given sweepback angle there was greater sensitivity to changes in aspect ratio for the larger trailing-edge angles.

No plots are shown for the region between $M \approx 0.92$ and $M \approx 0.98$ because of the rapid variation of $\frac{pb/2V}{\delta}$ with Mach number in this region. Any plots of K_A against aspect ratio at these speeds would at best have doubtful value.

General discussion.- It is evident from the foregoing discussion that the variation of rolling effectiveness with aspect ratio is very complex and is dependent upon a number of variables of which Mach number and trailing-edge angle are of great importance. However, it is possible to generalize to some extent. With certain exceptions, increased aspect ratio apparently causes a decrease in rolling effectiveness. At transonic speeds the effect is very variable and is influenced to a large extent by the trailing-edge angle. Increased aspect ratio tends to decrease rolling effectiveness more at supersonic than at subsonic speeds.

Effect of Aileron Location

Some effects of aileron location and spanwise extent upon aileron rolling effectiveness are presented in figure 13 for a variety of wing-aileron configurations.

NACA 65A006 airfoil sections.- Figures 13(b), 13(c), and 13(d) show the rolling effectiveness of various ailerons (including full-chord ailerons) on sweptback wings having NACA 65A006 airfoil sections. Generally, the outboard half-exposed-span ailerons were from one-half to two-thirds as effective as the full-exposed-span ailerons. An inboard aileron was generally more effective than an outboard aileron of the same span at subsonic and transonic speeds, but the results were mixed at supersonic speeds. Although all the part-chord ailerons showed decreased effectiveness as the speed increased, the full-chord ailerons had essentially constant effectiveness throughout the speed range tested.

NACA 65A009 airfoil sections.- Figure 13(a) shows that on the unswept wing the outboard half-exposed-span control was more effective than the inboard half-exposed-span control, whereas on the sweptback wing the reverse is true. The outboard control was generally more than one-half as effective as the full-exposed-span control for the unswept wing, but about one-half as effective for the sweptback wing.

NACA 65A012 airfoil sections.- Figure 13(e) shows that the outboard half-exposed-span ailerons were more effective than the inboard half-exposed-span ailerons at subsonic speeds for both taper ratios. At speeds greater than $M = 1.0$, all the configurations had poor control characteristics, particularly near $M = 1.2$ where the controls were either completely ineffective or control reversal was observed.

Miscellaneous airfoil sections.- Several miscellaneous wing-aileron configurations having full-chord ailerons are presented in figure 13(f). These data, except for model 36, show a relatively constant rolling effectiveness throughout the speed range tested.

Comparison between experimental and estimated values.- Reference 37 presents a method for estimating the effect of aileron spanwise location on rolling effectiveness for unswept wings having various aspect ratios and taper ratios at low subsonic speeds, and reference 38 compares the results shown in reference 37 with experimental data for swept wings and presents a design chart based on the comparison. It is shown that aspect ratio has little effect on the spanwise variation of rolling-moment coefficient and that the effect of taper ratio is not of major importance. Figure 14 shows the design chart of reference 38 in nondimensional form which was obtained by dividing the value of $C_l/\Delta\alpha$ (equivalent to C_l/δ in the notation of the present report) at any span station by the full-span value.

The quantity of rocket-model data in figures 13(a), 13(b), 13(c), 13(d), and 13(f) is not considered to be sufficient to establish a general plot of the variation of rolling effectiveness with control spanwise location, so the data from figure 13 are compared in figure 14 with the

normalized design chart taken from reference 38. The comparisons in figure 14 have been made at two representative Mach numbers and are in reasonably good agreement; the data of figure 13(e) ($A = 8.0$) have not been included at $M = 1.4$ because of the poor control characteristics at this speed.

The data of figure 13 were normalized according to the procedure

$$K_{\eta} \left[\begin{array}{c} 1.0 \\ \eta_i \end{array} \right] = K_{\eta} \left[\begin{array}{c} 1.0 \\ \eta_r \end{array} \right] \frac{\left[\begin{array}{c} pb/2V \\ \delta \end{array} \right]^{1.0} \eta_i}{\left[\begin{array}{c} pb/2V \\ \delta \end{array} \right]^{1.0} \eta_r}$$

where K_{η} appearing on the right-hand side of the equation is the value for a full-exposed-span control from figure 14. The values of K_{η} thus obtained for outboard ailerons ($\eta_o = 1.0$) are plotted as data points on figure 14 at the appropriate value of η_i . The experimental K_{η} values for inboard ailerons are not shown in figure 14, but they agree fairly well with estimated values from figure 14.

Effects of Wing-Tail Interference, Wing

Location, and Number of Wings

General discussion.- All the data thus far discussed were obtained by the use of three-winged test vehicles which do not resemble typical airplane configurations. Some uncertainties exist regarding the application of these data to conventional aircraft. In order to partially clarify this situation, a limited investigation has been conducted to determine some effects upon aileron rolling effectiveness of wing-tail interference, wing location on the fuselage, and the number of wings.

Wing-tail interference.- In order to determine some effects of wing-tail interference upon the aileron rolling effectiveness at zero lift, an investigation employing five test models was conducted. The test models were constructed with two wings, instead of the usual three, in order to approximate an airplane-type configuration. (See fig. 3(b).) Two of

these models employed free-to-roll tail assemblies (models 54 and 58) which provided directional stability without introducing rolling moments. Bench tests of these free-to-roll tails, under simulated drag loads several magnitudes greater than those estimated for flight conditions, showed friction forces corresponding to a rolling moment of 0.17 ft-lb which is negligible when compared with the 40 to 50 ft-lb damping moment of the test wings. A more complete description of the test models with free-to-roll tails is given in reference 33. Figure 15 shows the results obtained with these models.

Inboard ailerons: Figure 15(a) shows that fixing the tail for inboard ailerons resulted in a considerable decrease in rolling effectiveness. The change in rolling effectiveness due to the fixed tail was approximately constant throughout the speed range tested and was enough to cause a slight roll reversal at speeds greater than $M \approx 1.3$. Whether this condition exists for other aileron deflections and tail fore-and-aft locations is not known at this time. Changing the location of the fixed tail from the plane of the wings to 0.18c above the plane of the wings had little effect on the fixed-tail rolling effectiveness.

Outboard ailerons: Figure 15(b) shows that fixing the tail did not cause any appreciable change in the rolling effectiveness of the outboard aileron at all speeds for which data are available.

General discussion: It is apparent from the limited data presented here that the rolling effectiveness of inboard ailerons is markedly affected by the fixed-tail assembly. Reference 33 shows that the additional damping in roll due to the addition of the fixed-tail assembly caused a decrease of about 15 percent in the rolling effectiveness at all speeds, a value which is outweighed by the large losses resulting when the aileron-generated downwash strikes the fixed tail. Reference 33 shows that the effects of the downwash could be estimated with fairly good accuracy by simple theoretical means.

Effect of wing location and number of wings.- Figure 16 shows the effects on rolling effectiveness of locating the wings at a more forward position on the fuselage and reducing the number of wings from three to two. All the wings were untapered, had NACA 65A009 airfoil sections, and 0.20-chord ailerons. The effects of wing forward location and number of wings were not appreciable except for the unswept wings at subsonic and transonic speeds (see fig. 16(a)) where any physical modification to the standard model (three wings aft) generally caused a decrease in rolling effectiveness.



ADDITIONAL TESTS

References 1 to 33 contain additional aileron rolling-effectiveness data not considered appropriate for inclusion in the present report. The type of investigation and corresponding references are listed as follows:

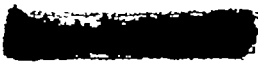
Type of investigation	Reference
Aeroelastic effects	16, 18, 19, 22, 23, 24, 25, 26, 28, 32
Delta wings	5, 12, 24
Leading-edge and trailing-edge ailerons in combination	6
Effects of aileron chord extension	10
Effects of airfoil nose shape	13
Horn-balanced ailerons	14
Wing-tip ailerons	17, 30
Effects of wing leading-edge roughness	27
Interference between ailerons and tip stores	30
Bellows-actuated ailerons	31
Effects of built-in wing twist	32

SPECIFIC WING-AILERON CONFIGURATIONS

Comparison Between Measured and Estimated Values

A number of models simulating existing or proposed airplane wing-aileron configurations without fixed tails did not fit handily into the basic data plots showing the effects of aspect ratio, trailing-edge angle, and so forth, and these special models have been included in figure 17. It was felt that these special models would provide some indication of the applicability of the preliminary design charts (figs. 6, 10, 12, and 14).

In estimating the rolling effectiveness of a given configuration, it was assumed that the rolling effectiveness could be approximated by considering only six major variables: (1) aileron trailing-edge angle, and (2) sweepback at the hinge line, figure 6; (3) ratio of aileron chord to wing chord, figure 10; (4) wing aspect ratio, figure 12; and (5) spanwise extent, and (6) location of aileron, figure 14. No consideration was given to the effects of wing location on the body, number of wings, and



so forth. No consideration was given to the effects of wing taper ratio, other than the use of the hinge line for the reference sweepback angle when using figure 6.

As shown in figure 17, the agreement between the measured rolling effectiveness and the estimated rolling effectiveness (from figs. 6, 10, 12, and 14) is fair on the whole.

Method Used in Estimation

For the purpose of estimating the rolling effectiveness, it is assumed that the rolling effectiveness for any configuration may be expressed as the rolling effectiveness for some arbitrary reference configuration with the proper corrections applied to account for deviations from the geometry of the reference configuration. In the present case, the reference configuration geometry is given in the legend of figure 6.

In order to indicate the procedure used in estimating the rolling effectiveness from figures 6, 10, 12, and 14 for a given configuration, a sample calculation is shown as follows for model 99 at $M = 1.00$:

$$A = 2.8$$

$$\Lambda = 38.5^\circ \quad (\text{hinge line, calculated})$$

$$\varphi = 11.6^\circ$$

$$\eta_1 = 0.41$$

$$\eta_0 = 0.75$$

$$\frac{c_a}{c} = 0.23$$

$$\frac{\overline{pb/2V}}{\delta} = \left(\frac{\overline{pb/2V}}{\delta} \right)_{\text{ref}} K_A K_\eta \frac{K_c}{K_{c\text{ref}}}$$

where $\left(\frac{\overline{pb/2V}}{\delta} \right)_{\text{ref}}$ is the rolling effectiveness for reference configuration having 38.5° sweepback at the hinge line and 11.6° trailing-edge angle, using straight-line interpolation for effect of hinge-line sweepback

$$\left(\frac{pb/2V}{\delta}\right)_{\text{ref}} = 0.0116 \quad (\text{interpolated from fig. 6(f)})$$

$$\frac{K_c}{K_{c_{\text{ref}}}} = \frac{(K_c)_{c_a/c=0.23}}{(K_c)_{c_a/c=0.20}}$$

$$= 1.15 \quad (\text{from } M > 1.0 \text{ theory curve, fig. 10(f)})$$

$$K_A = 1.12 \quad (\text{from } \Lambda = 45^\circ \text{ curve, fig. 12})$$

$$K_\eta = 0.76 - 0.24$$

$$= 0.52 \quad (\text{from } \Lambda_{LE} = 51.3^\circ \text{ curve, fig. 14})$$

therefore,

$$\frac{pb/2V}{\delta} = (0.0116)(1.12)(0.52)(1.15)$$

$$= 0.0078$$

CONCLUDING REMARKS

A collection and summary is presented of the wing-aileron rolling-effectiveness data which have been obtained with each aileron differentially deflected 3° to 7° during a general investigation of lateral control being conducted by the Langley Pilotless Aircraft Research Division. Some effects of trailing-edge angle, aileron chord ratio, spanwise extent and location of aileron, aspect ratio, wing sweepback, and wing-tail interference are presented. The quantity of data which has been obtained in each of these categories varies considerably.

It is felt that the effects of some parameters, such as aileron trailing-edge angle, are fairly well defined, whereas others, such as wing-tail interference, are not satisfactorily defined.

Rough design charts have been prepared to show some effects of aileron trailing-edge angle at two sweepback angles, aileron chord ratio, aileron span and spanwise location, and wing aspect ratio. These rough design charts have been prepared for use in the preliminary design stage, and estimates have been made from these charts for thirteen wing-aileron configurations (without fixed tails) simulating existing or proposed aircraft wing-aileron combinations. The estimated values were in fair agreement with measured rocket-model data.

These design charts should be used with caution when the configuration has a fixed tail assembly, since the limited data available indicate that in some cases the wing-tail interference appreciably affects the aileron rolling power.

Langley Aeronautical Laboratory,
National Advisory Committee for Aeronautics,
Langley Field, Va., June 8, 1955.

REFERENCES

1. Sandahl, Carl A., and Marino, Alfred A.: Free-Flight Investigation of Control Effectiveness of Full-Span 0.2-Chord Plain Ailerons at High Subsonic, Transonic, and Supersonic Speeds to Determine Some Effects of Section Thickness and Wing Sweepback. NACA RM L7D02, 1947.
2. Sandahl, Carl A.: Free-Flight Investigation of Control Effectiveness of Full-Span, 0.2-Chord Plain Ailerons at High Subsonic, Transonic, and Supersonic Speeds To Determine Some Effects of Wing Sweepback, Taper, Aspect Ratio, and Section Thickness Ratio. NACA RM L7F30, 1947.
3. Sandahl, Carl A., and Strass, H. Kurt: Additional Results in Free-Flight Investigation of Control Effectiveness of Full-Span, 0.2-Chord Plain Ailerons at High Subsonic, Transonic, and Supersonic Speeds To Determine Some Effects of Wing Sweepback, Aspect Ratio, Taper, and Section Thickness Ratio. NACA RM L7L01, 1948.
4. Sandahl, Carl A.: Preliminary Free-Flight Investigation of the Effect of Airfoil Section on Aileron Rolling Effectiveness at Transonic and Supersonic Speeds. NACA RM L8B26, 1948.
5. Sandahl, Carl A.: Free-Flight Investigation of the Rolling Effectiveness of Several Delta Wing-Aileron Configurations at Transonic and Supersonic Speeds. NACA RM L8D16, 1948.
6. Strass, H. Kurt: Free-Flight Investigation of the Rolling Effectiveness at High Subsonic, Transonic, and Supersonic Speeds of Leading-Edge and Trailing-Edge Ailerons in Conjunction With Tapered and Untapered Plan Forms. NACA RM L8E10, 1948.
7. Sandahl, Carl A.: Free-Flight Investigation at Transonic and Supersonic Speeds of the Rolling Effectiveness of a 42.7° Sweptback Wing Having Partial-Span Ailerons. NACA RM L8E25, 1948.
8. Sandahl, Carl A.: Free-Flight Investigation at Transonic and Supersonic Speeds of a Wing-Aileron Configuration Simulating the D-558-2 Airplane. NACA RM L8E28, 1948.
9. Sandahl, Carl A.: Free-Flight Investigation at Transonic and Supersonic Speeds of the Rolling Effectiveness of a Thin, Unswept Wing Having Partial-Span Ailerons. NACA RM L8G20a, 1948.
10. Sandahl, Carl A.: Free-Flight Investigation at Transonic and Supersonic Speeds of the Rolling Effectiveness of Several Aileron Configurations on a Tapered Wing Having 42.7° Sweepback. NACA RM L8K23, 1949.

11. Sandahl, Carl A., Bland, William M., Jr., and Strass, H. Kurt: Effects of Some Airfoil-Section Variations on Wing-Aileron Rolling Effectiveness and Drag as Determined in Free Flight at Transonic and Supersonic Speeds. NACA RM L9D12, 1949.
12. Sandahl, Carl A., and Strass, H. Kurt: Comparative Tests of the Rolling Effectiveness of Constant-Chord, Full-Delta, and Half-Delta Ailerons on Delta Wings at Transonic and Supersonic Speeds. NACA RM L9J26, 1949.
13. Strass, H. Kurt, and Fields, Edison M.: Flight Investigation of the Effect of Thickening the Aileron Trailing Edge on Control Effectiveness for Sweptback Tapered Wings Having Sharp- and Round-Nose Sections. NACA RM L9L19, 1950.
14. Strass, H. Kurt: The Effect of Spanwise Aileron Location on the Rolling Effectiveness of Wings With 0° and 45° Sweep at Subsonic, Transonic, and Supersonic Speeds. NACA RM L50A27, 1950.
15. Strass, H. Kurt, Fields, E. M., and Schult, E. D.: Free-Flight Investigation at Transonic and Supersonic Speeds of the Rolling Effectiveness of a Partial-Span Aileron on an Inversely Tapered Sweptback Wing. NACA RM L50B08, 1950.
16. Sandahl, Carl A., and Strass, H. Kurt: Rolling Effectiveness of a Thin Tapered Wing Having Partial-Span Ailerons As Determined by Rocket-Powered Test Vehicles. NACA RM L50D17, 1950.
17. Sandahl, Carl A., Strass, H. Kurt, and Piland, Robert O.: The Rolling Effectiveness of Wing-Tip Ailerons As Determined by Rocket-Powered Test Vehicles and Linear Supersonic Theory. NACA RM L50F21, 1950.
18. Strass, H. Kurt, Fields, E. M., and Purser, Paul E.: Experimental Determination of Effect of Structural Rigidity on Rolling Effectiveness of Some Straight and Swept Wings at Mach Numbers From 0.7 to 1.7. NACA RM L50G14b, 1950.
19. Strass, H. Kurt, Fields, E. M., and Schult, Eugene D.: Some Effects of Spanwise Aileron Location and Wing Structural Rigidity on the Rolling Effectiveness of 0.3-Chord Flap-Type Ailerons on a Tapered Wing Having 63° Sweepback at the Leading Edge and NACA 64A005 Airfoil Sections. NACA RM L51D18a, 1951.
20. Fields, E. M., and Strass, H. Kurt: Free-Flight Measurements at Mach Numbers From 0.7 to 1.6 of Some Effects of Airfoil-Thickness Distribution and Trailing-Edge Angle on Aileron Rolling Effectiveness and Drag for Wings With 0° and 45° Sweepback. NACA RM L51G27, 1951.

21. Strass, H. Kurt, and Marley, Edward T.: Rolling Effectiveness of All-Movable Wings at Small Angles of Incidence at Mach Numbers From 0.6 to 1.6. NACA RM L51H03, 1951.
22. Schult, Eugene D., Strass, H. Kurt, and Fields, E. M.: Free-Flight Measurements of Some Effects of Aileron Span, Chord, and Deflection and of Wing Flexibility on the Rolling Effectiveness of Ailerons on Sweptback Wings at Mach Numbers Between 0.8 to 1.6. NACA RM L51K16, 1952.
23. Strass, H. Kurt: Summary of Some Effective Aerodynamic Twisting-Moment Coefficients of Various Wing-Control Configurations at Mach Numbers From 0.6 to 1.7 As Determined From Rocket-Powered Models. NACA RM L51K20, 1952.
24. Marley, Edward T., and English, Roland D.: Some Effects of Aeroelasticity at Mach Numbers From 0.7 to 1.6 on the Rolling Effectiveness of Thin Flat-Plate Delta Wings Having 45° Swept Leading Edges and Full-Span Constant-Chord Ailerons. NACA RM L51L05, 1952.
25. Strass, H. Kurt, and Stephens, Emily W.: An Engineering Method for the Determination of Aeroelastic Effects Upon the Rolling Effectiveness of Ailerons on Swept Wings. NACA RM L53H14, 1953.
26. English, Roland D.: Some Effects of Aeroelasticity and Sweepback on the Rolling Effectiveness and Drag of a 1/11-Scale Model of the Bell X-5 Airplane Wing at Mach Numbers From 0.6 to 1.5. NACA RM L53I18b, 1953.
27. English, Roland D.: Some Effects of Leading-Edge Roughness on the Aileron Effectiveness and Drag of a Thin Rectangular Wing Employing a Full-Span Plain Aileron at Mach Numbers From 0.6 to 1.5. NACA RM L53I25, 1953.
28. Strass, H. Kurt: Summary of Some Rocket-Model Investigations of Effects of Wing Aspect Ratio and Thickness on Aileron Rolling Effectiveness Including Some Effects of Spanwise Aileron Location for Sweptback Wings With Aspect Ratio of 8.0. NACA RM L53L11, 1953.
29. English, Roland D.: Flight Investigation of an Aileron and a Spoiler on a Wing of the X-3 Airplane Plan Form at Mach Numbers From 0.5 to 1.6. NACA RM L54D26a, 1954.
30. English, Roland D.: Some Effects of External Wing Tip Stores on the Rolling Effectiveness and Drag of Plain and Half-Delta Tip Ailerons on a 4-Percent-Thick, Tapered, Unswept Wing. NACA RM L54F29a, 1954.

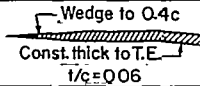
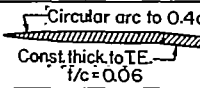
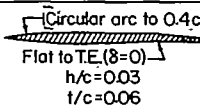
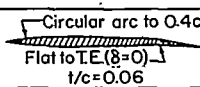
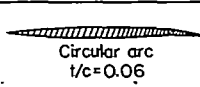
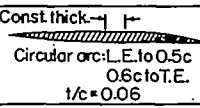
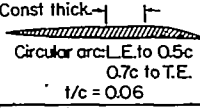
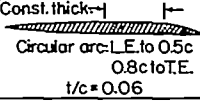
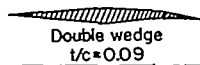
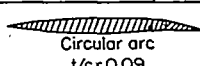
31. Schult, Eugene D.: Free-Flight Measurements of the Rolling Effectiveness and Operating Characteristics of a Bellows-Actuated Split-Flap Aileron Control on a 60° Delta Wing at Mach Numbers Between 0.8 and 1.8. NACA RM L54H17, 1954.
32. Strass, H. Kurt, and Tucker, Warren A.: Some Effects of Aileron Span, Aileron Chord, and Wing Twist on Rolling Effectiveness As Determined by Rocket-Powered Model Tests and Theoretical Estimates. NACA RM L54G13, 1954.
33. English, Roland D.: Free-Flight Investigation To Determine Some Effects of Tail Damping and Wing-Tail Interference on the Rolling Effectiveness of Inboard and Outboard Ailerons on an Untapered Sweptback Wing. NACA RM L54L17a, 1955.
34. Harris, Orville R.: Determination of the Rate of Roll of Pilotless Aircraft Research Models by Means of Polarized Radio Waves. NACA TN 2023, 1950.
35. Bland, William M., Jr., and Dietz, Albert E.: Some Effects of Fuselage Interference, Wing Interference, and Sweepback on the Damping in Roll of Untapered Wings As Determined by Techniques Employing Rocket-Propelled Vehicles. NACA RM L51D25, 1951.
36. Stone, David G.: Wing-Dropping Characteristics of Some Straight and Swept Wings at Transonic Speeds As Determined With Rocket-Powered Models. NACA RM L50C01, 1950.
37. Weick, Fred E., and Jones, Robert T.: Résumé and Analysis of N.A.C.A. Lateral Control Research. NACA Rep. 605, 1937.
38. Lowry, John G., and Schneiter, Leslie E.: Estimation of Effectiveness of Flap-Type Controls on Sweptback Wings. NACA TN 1674, 1948.

TABLE I
WING CONTROL CONFIGURATIONS

Configuration	Model	Wing Parameters							Control Parameters					X/L	Refs.		
		A	Λ (deg)	λ	Airfoil section (a)	b/2 (ft)	c_t (ft)	c_r (ft)	S_c (ft ²)	c_g c	η_i	η_o	ϕ (deg)			δ (deg)	
	1	0.7	80	0	Mod. Hexagonal L.E. radius = 0.001c h/c = 0.01 t/c = 0.02	0.80	0	3.37	3.65	1.00	0.26	1.0	2.0	0.67	0.73	—	
	2	2.3	0	1.0	Wedge to 0.2c Const. thick to T.E. t/c = 0.054	.88	.77	.77	1.36	.20	.15	1.0	0	4.59	.84	—	
	3	a			NACA 65A009						.24	1.0	11.5	5.00	.85	2,28	
	4				Wedge to 0.2c Const. thick to T.E. t/c = 0.054					.40	.15	1.0	0	4.90	.84	—	
	5	a	2.3	30	1.0	NACA 65A009	.88	.77	.77	1.36	.20	.24	1.0	10.5	4.84	.82	—
	b													10.7	4.69		
	6		2.3	45	1.0	Wedge to 0.2c Const. thick to T.E. t/c = 0.054	.88	.77	.77	1.36	.20	.15	1.0	0	5.00	.91	—
	7	a				NACA 65A009						.24	1.0	11.7	5.27	.81	28
	b													12.3	5.05		
	8					Wedge to 0.2c Const. thick to T.E. t/c = 0.054					.40	.15	1.0	0	4.95	.91	—
	9	a	2.3	60	1.0	NACA 65A009	.88	.77	.77	1.36	.20	.24	1.0	10.9	5.09	.84	—
	b													11.2	2.38		
	c													11.4	2.38		
	10	a	2.3	60	0	NACA 65A006	.98	0	1.34	1.68	1.00	.65	1.0	7.6	4.82	.86	12
	b													8.0	4.92		
	11	a				7.6° 15.2° Hexagonal L.E. radius: Wing 0.01c Aileron 0.05c t/c = 0.06								7.4	1.0		12
	b													4.9	7.65		
	12		2.9	0	1.0	NACA 65A009	.98	.68	.68	1.32	.20	.21	1.0	9.5	4.77	.85	28
	13		2.9	45	1.0	NACA 65A009	.98	.68	.68	1.32	.20	.21	1.0	10.4	4.88	.80	28
	14		3.7	0	1.0	NACA 65A009	1.09	.59	.59	1.29	.10	.19	1.0	10.9	4.00	.89	—

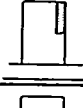
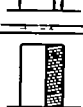
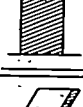
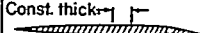
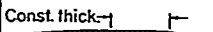
(a) Section is taken freestream unless noted otherwise.

TABLE I.- CONTINUED
WING CONTROL CONFIGURATIONS

Configuration	Model	Wing Parameters										Control Parameters				X L	Refs.
		A	Λ (deg)	λ	Airfoil section (a)	b/2 (ft)	c_t (ft)	c_r (ft)	S (ft ²)	c_d c	η_i	η_o	ϕ (deg)	δ (deg)			
	15	3.7	0	10	NACA 65A003	1.09	.59	.59	129	20	.19	1.0	3.5	4.91	.89	18,20 25,28	
	16				NACA 65A006								7.2	4.85		20,28	
	17												0	4.66		20	
	18												0	5.11		20	
	19												3.2	4.77		20	
	20												6.2	4.89		20	
	a	21												12.9	5.18		20
	b													13.2	5.07		
	c													13.6	4.68		
	d													13.6	4.78		
	a	22												13.5	4.43		20
	b													16.6	4.46		
	a	23												21.2	4.60		20
	b													21.2	4.68		
a	24												30.2	4.61		20	
b													31.2	4.88			
a	25												9.6	4.70		20	
b													9.8	4.81			
	26												20.4	5.09		20	
a	27				NACA 16-009								17.4	4.00		11,20	
b						19.8	3.58										
c						24.3	5.00										
d						24.8	4.98										
a	28				NACA 65A009								11.7	5.05		11,14 18,20 25	
b						11.7	5.15										
c						11.7	5.45										

(a) Section is taken freestream unless noted otherwise.

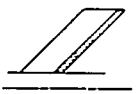
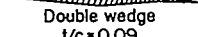
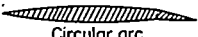
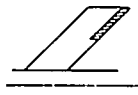
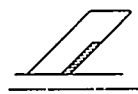
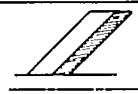
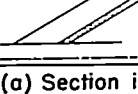
**TABLE I.- CONTINUED
WING CONTROL CONFIGURATIONS**

Configuration	Model	Wing Parameters										Control Parameters				X L	Refs.
		A	Δ (deg)	λ	Airfoil section (a)	b/2 (ft)	c_t (ft)	c_r (ft)	S_w (ft ²)	$\frac{c_a}{c}$	η_i	η_o	ϕ (deg)	δ (deg)			
	29	3.7	0	1.0	NACA 65A009	1.09	.59	.59	1.29	2.0	.19	1.0	11.2	5.28	.63	—	
	30 ^a												10.6	4.89		33	
	30 ^b												11.8	5.12		33	
	31												10.8	5.04		33	
	32				NACA 65A012								16.3	5.09	.89	28	
	33 ^a				NACA 65A009								9.8	4.35		—	
	33 ^b				NACA 65A009						.60	1.0	10.8	5.0		14	
	34 ^a												10.8	5.0		14	
	34 ^b									.19	.60		11.4	4.85		14	
	35 ^a									.40	.19	1.0	11.3	4.79		—	
	35 ^b												11.5	5.05		—	
	36 ^a									1.00	.19	1.0	12.3	0.97		3,18,21	
	37 ^a	3.7	30	1.0	NACA 65A009	1.09	.59	.59	1.29	2.0	.19	1.0	11.1	4.82		.83	—
	37 ^b												11.4	4.84		—	
	38	3.7	45	1.0	NACA 65A009	1.09	.59	.59	1.29	1.0	.19	1.0	9.9	4.82	.80	—	
	39				NACA 65A006						2.0	.19	1.0	7.1	5.14		20,28
	40 ^a												12.3	5.05		20,28	
	40 ^b				Circular arc								12.9	5.08		20	
	40 ^c				t/c=0.06								13.5	5.17		20	
	41 ^a				Const. thick- 								17.2	4.70		20	
	41 ^b				Circular arc: L.E. to 0.5c 0.6c to T.E. t/c=0.06 ^a								17.5	4.92		20	
	42 ^a				Const. thick- 								20.2	5.23		20	
42 ^b				Circular arc: L.E. to 0.5c 0.7c to T.E. t/c=0.06								20.6	4.95		20		
42 ^c												21.9	4.93		20		
42 ^d												22.0	4.91		20		
43 ^a				Const. thick- 								30.1	4.79		20		
43 ^b				Circular arc: L.E. to 0.5c 0.8c to T.E. t/c=0.06								30.2	4.86		20		
43 ^c												33.3	5.31		20		

(a) Section is taken freestream unless noted otherwise.

(b) 3 wings, free-to-roll tail.

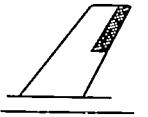
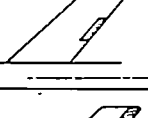
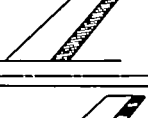
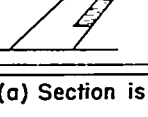
TABLE I.- CONTINUED
WING CONTROL CONFIGURATIONS

Configuration	Model	Wing Parameters										Control Parameters		X/L	Refs.				
		A	Δ (deg)	λ	Airfoil section (a)	b/2 (ft)	c_t (ft)	c_r (ft)	S (ft ²)	$\frac{c_g}{c}$	η_i	η_o	ϕ (deg)			δ (deg)			
	a	3.7	45	1.0	 Double wedge t/c=0.09	1.09	.59	.59	1.29	.20	.19	1.0	10.2	4.72	.80	11,20			
	b												10.4	4.74					
	a				 Circular arc t/c=0.09								16.4	5.47		11,20			
	b												17.3	5.51					
	c												17.4	5.14					
	a				NACA 16-009								19.7	5.05		11,20			
	b												20.3	4.84					
	a				NACA 65A009									11.3	3.44		20,28		
	b													11.7	3.70				
	c													11.9	5.25		11,14,18		
d													11.9	5.29		20,25			
e													11.9	4.77		8,20,28			
	48												13.6	4.67	.63	—			
(b)	49												10.9	4.82		—			
(c)	50												10.7	4.67		—			
	51				NACA 65 ₁ A012								16.4	5.12	.80	28			
	a				NACA 65A009									11.1	5.52		14		
	b											.60	1.0	11.8	5.31				
	c													12.0	5.55				
		53													13.4	4.71		.63	33
	(c)	54													13.5	4.69			33
(d)	55												11.7	4.70		33			
	a												19	.60	11.3	4.72	.80	14	
	b														11.3	4.84			
		57												12.8	4.61	.63	33		
	(c)	58												12.0	3.26		33		
	(d)	59												12.0	3.17		33		
(e)	60												11.8	5.26		33			
	61												40	.19	1.0	11.4	4.93	.80	—
	62												1.00	.19	1.0	11.3	0.97		21
	a	3.7	60	1.0	NACA 65A009	1.09	.59	.59	1.29	.20	.19	1.0	11.4	4.84		.92	—		
	b												11.5	4.93					

- (a) Section is taken freestream unless noted otherwise.
- (b) 3 wings, free-to-roll tail.
- (c) 2 wings, free-to-roll tail.
- (d) 2 wings, fixed-tail, horizontal tail in wing chord plane.
- (e) 2 wings, fixed-tail, horizontal tail $0.1 \frac{b}{2}$ above wing chord plane.



TABLE I.- CONTINUED
WING CONTROL CONFIGURATIONS

Configuration	Model	Wing Parameters										Control Parameters				X/L	Refs.
		A	Δ (deg)	λ	Airfoil section (a)	b/2 (ft)	c_t (ft)	c_r (ft)	S_w (ft ²)	c_g c	η_i	η_o	ϕ (deg)	δ (deg)			
	64	4.0	35	.60	NACA 65A006	1.50	.56	.88	225	.30	.14	1.0	7.8	4.35	.73	22	
	65	↓	↓	↓	↓	↓	↓	↓	↓	↓	↓	.57	1.0	7.8	4.05	22,25	
	66	4.0	45	.60	NACA 65A006	1.50	.56	.88	225	.15	.14	1.0	6.6	4.22	.74	22	
	67	↓	↓	↓	↓	↓	↓	↓	↓	↓	↓	.35	1.0	7.1	4.01	22	
	68	↓	↓	↓	↓	↓	↓	↓	↓	↓	↓	.57	1.0	6.8	4.02	22	
	69	↓	↓	↓	↓	↓	↓	↓	↓	↓	↓	.78	1.0	6.8	3.88	22	
	70	↓	↓	↓	↓	↓	↓	↓	↓	↓	↓	.35	.57	7.9	3.56	22	
	71	↓	↓	↓	↓	↓	↓	↓	↓	↓	↓	.30	.14	1.0	7.8	3.70	22,25
	72	↓	↓	↓	↓	↓	↓	↓	↓	↓	↓	.35	1.0	7.6	3.58	22	

(a) Section is taken freestream unless noted otherwise.

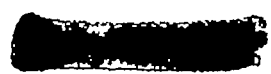
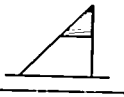
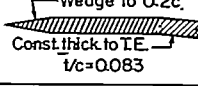
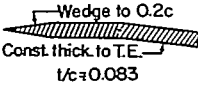
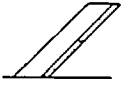
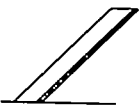
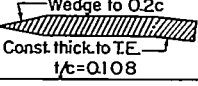
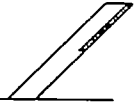
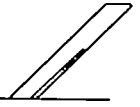
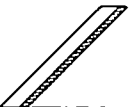
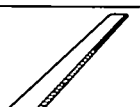
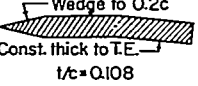
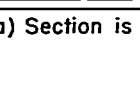


TABLE I.- CONTINUED
WING CONTROL CONFIGURATIONS

Configuration	Model	Wing Parameters										Control Parameters		X L	Refs.			
		A	Δ (deg)	λ	Airfoil section (a)	b/2 (ft)	c _t (ft)	c _r (ft)	S _w (ft ²)	c _d c	η_i	η_o	ϕ (deg)			δ (deg)		
	a													7.2	3.83			
	73	4.0	45	.60	NACA 65A006	1.50	.56	.88	225.30	.57	1.0					.74	22,25	
	b													7.7	3.78			
	74											.78	1.0	7.0	3.63		22	
	75											.14	.57	7.4	3.71		22,25	
	76											↑	.35	.57	7.3	3.74	22	
	77											1.0	.14	1.0	7.2	1.41	32	
	78												.49	1.0	8.6	1.63	32	
	79												.70	1.0	8.5	2.77	32	
	80												92	1.0	8.3	4.75	↑	32
	81	4.0	45 LE	0	NACA 65A006	1.23	0	1.02	1.51	1.0	.17	1.0	9.0	0.74	.89		21	

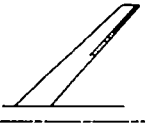
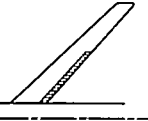
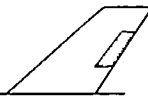
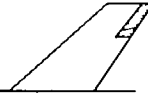
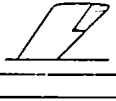
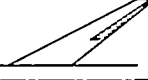
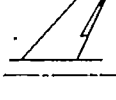
(a) Section is taken freestream unless noted otherwise.

TABLE I.- CONTINUED
WING CONTROL CONFIGURATIONS

Configuration	Model	Wing Parameters							Control Parameters					X/L	Refs.		
		A	Δ (deg)	λ	Airfoil section (a)	b/2 (ft)	c_t (ft)	c_r (ft)	S_D (ft ²)	$\frac{c_a}{c}$	η_i	η_o	ϕ (deg)			δ (deg)	
	a	82	4.0	45	0	NACA 65A006	1.23	0	1.02	1.51	1.0	.63	1.0	8.6	4.88	.89	12
	b													8.7	4.98		
	83	5.0	0	1.0		1.25	0.50	0.50	1.25	2.0	.11	1.0	0	4.89	.88		—
	84					NACA 65A009						.17	1.0	11.8	4.88		28
	85										.40	.11	1.0	0	5.07		
	a	86	5.0	45	1.0	NACA 65A009	1.25	0.50	0.50	1.25	2.0	.17	1.0	11.8	4.96	.82	—
	b					NACA 65A012								11.9	4.93		
	88	8.0	45	1.0	NACA 65A009	1.55	.39	.39	1.20	2.0	.13	1.0	10.0	4.67	.76	28	
	89											.09	1.0	0	4.11		—
	a	90				NACA 65A012						.13	1.0	15.7	5.24		28
	b													16.2	4.99		
	91											.57	1.0	15.6	5.08		28
	92											.13	.57	15.6	4.80		28
	93										.40	.09	1.0	0	4.57		—
	94	8.0	45	.50	NACA 65A012	1.59	.27	.50	1.26	2.0	.13	1.0	15.7	4.90	.76	28	

(a) Section is taken freestream unless noted otherwise.

TABLE I.- CONTINUED
WING CONTROL CONFIGURATIONS

Configuration	Model	Wing Parameters										Control Parameters				X L	Refs.
		A	A (deg)	λ	Airfoil section (a)	b/2 (ft)	c_t (ft)	c_r (ft)	S (ft ²)	c_g c	η_i	η_o	ϕ (deg)	δ (deg)			
	95	8.0	45	.50	NACA 65 ₁ A012	1.59	.27	.50	126	.20	.56	1.0	15.7	5.0	.76	28	
	96	↓	↓	↓	↓	↓	↓	↓	↓	↓	↓	1.3	15.6	15.9	4.39	↓	28
	97	2.8	16	.39	Hexagonal Wedges: L.E. to 0.3c 0.7c to T.E. t/c=0.045	1.02	.41	.87	148	.25	.68	1.0	8.9	4.60	.86	16	
	98	3.0	16	.40	↓	1.04	.39	.86	142	.25	.70	1.0	8.9	6.06	.60	29	
	99	2.8	45	.52	NACA 0008.6-116 38/1.14(modified)at root. NACA 0006.4-116 38/1.14(modified)at tip.	1.42	.69	1.23	2.87	.23	.41	7.5	11.6	8.34	.64	—	
	100	3.0	45	.50	NACA 0009-1.16 38/1.14(modified)at root. NACA 0007-1.16 38/1.14(modified)at tip.	1.42	.64	1.17	2.70	.25	.68	1.0	7.8	4.06	.80	—	
	101	3.1	35	1.63	Republic R-4, 40-1710x (modified) normal to 50- percent chord line.	.99	.80	.56	1.28	.27	.55	.94	9.2 9.4 9.6 9.9	4.74 5.04 4.74 5.08	.84	15	
	102	3.5	61	.25	NACA 65A005	1.12	.26	.88	1.44	.30	.50	1.0	6.4	4.80	.83	19	
	103	a 3.6	38	.45	NACA 0010-64 normal to 44.8 percent chord line	1.11	.39	0.76	1.38	.17	.50	1.0	16.4 17.5	4.73 5.01	.82	13	
	104	↓	↓	↓	Same as 103 except aileron is modified: $h = \frac{1}{2} (t)_{HL}$	↓	↓	↓	↓	↓	↓	↓	8.1	4.83	↓	13	
	105	4.0	0	.60	NACA 65A004	1.15	.43	.67	1.33	.15	.59	1.0	5.1	5.25	.60	30	

(a) Section is taken freestream unless noted otherwise.

TABLE I.- CONCLUDED
WING CONTROL CONFIGURATIONS

Configuration	Model	Wing Parameters							Control Parameters					X L	Refs.	
		A	Δ (deg)	λ	Airfoil section (a)	b/2 (ft)	c_f (ft)	c_r (ft)	S_w (ft ²)	$\frac{c_a}{c}$	η_i	η_o	ϕ (deg)			δ (deg)
	106	4.0	40	.50	10 percent circular arc normal to c/4 line	1.17	.39	.71	1.36	.20	.50	1.0	8.1	4.11	.80	10
	(c) 107	5.7	20	.45	NACA 64 ₍₁₀₎ A011 normal to 38-percent-chord line at root. NACA 64 ₍₀₈₎ A00828 normal to 38-percent-chord line at tip (f).	1.39 (g)	.30	.62	1.36	.18	.70	1.04	10.7	9.78	.60	25,26
	(c) 108	3.4	47	.44		1.096 (g)	.40	.80	1.42	.16	.62	1.00	10.7	8.13		25,26
	(c) 109	2.1	59	.43		.88 (g)	.51	1.04	1.52	.15	.60	.95	6.8	6.10		25,26

(a) Section is taken freestream unless noted otherwise.

(c) 2 wings, free-to-roll tail.

(f) Variable wing sweepback configuration. Wing pivots about axis normal to wing chord plane at intersection of fuselage and 38-percent-chord line.

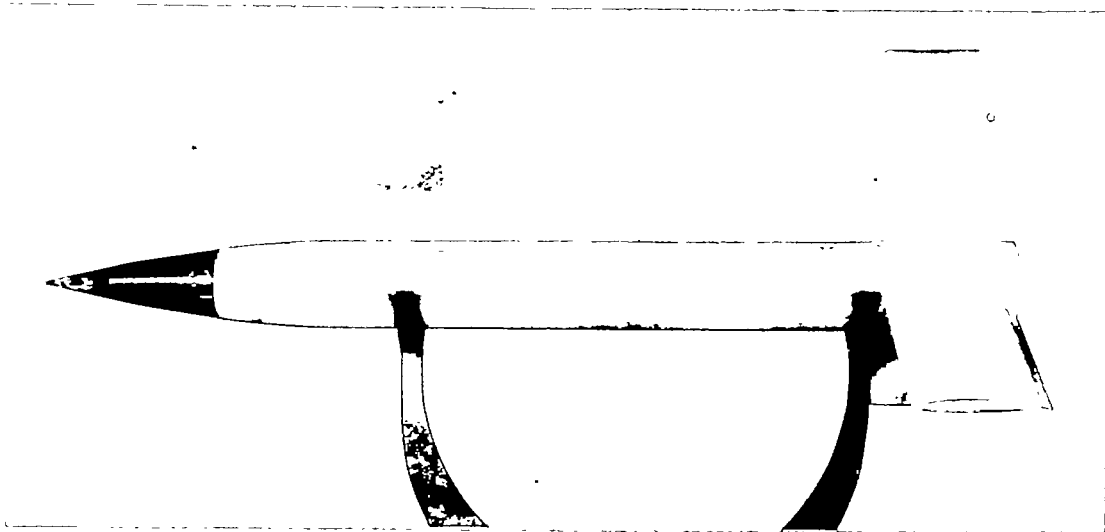
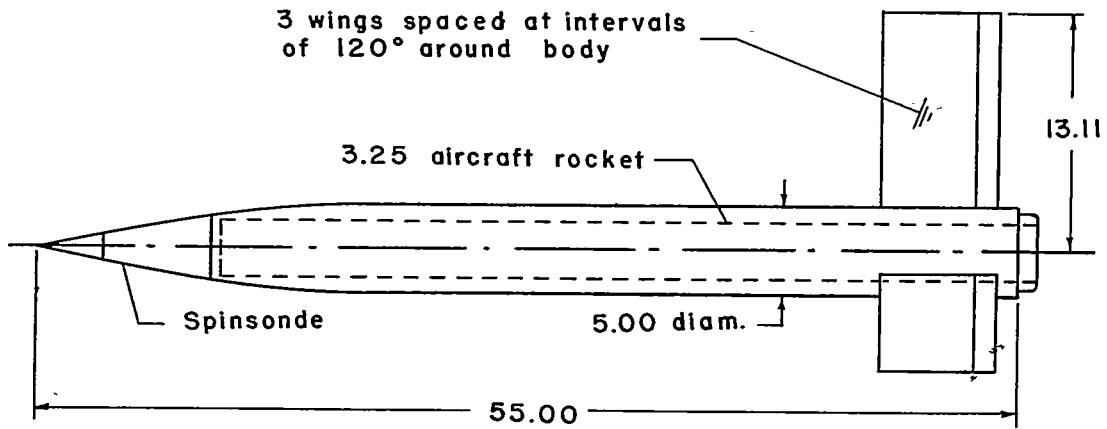
(g) To tip at 38-percent-chord line.

TABLE II

INDEX TO FIGURES

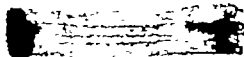
Variable	Basic data	Cross plots
	Figure	Figure
Trailing-edge angle	--	6
Airfoil thickness ratio	7	---
Sweepback	8	(a)
Aileron chord ratio	9	10
Aspect ratio	11	12
Aileron span and spanwise location . . .	13	14
Wing-tail interference	15	---
Wing location and number of wings	16	---
Comparison between measured and estimated values	17	---

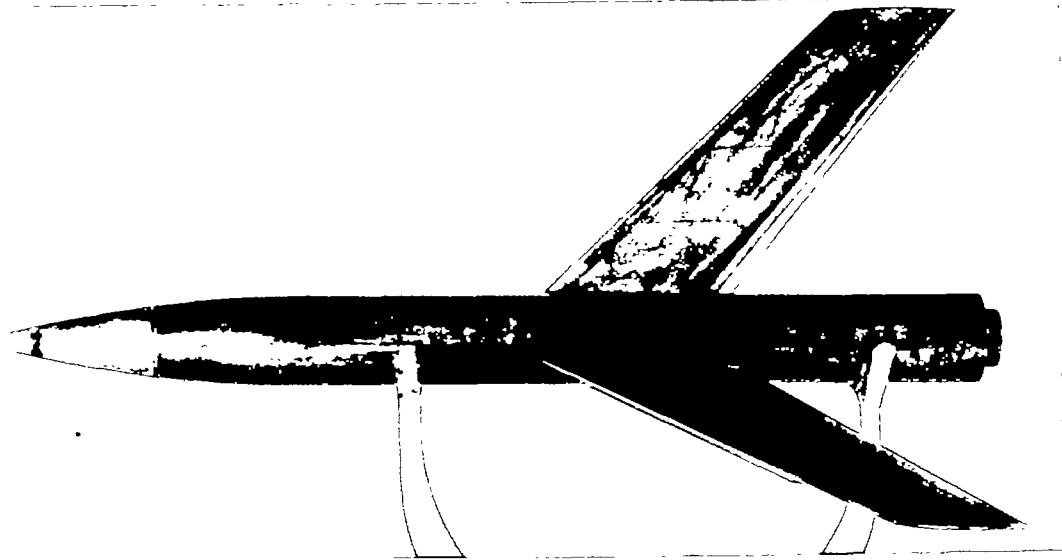
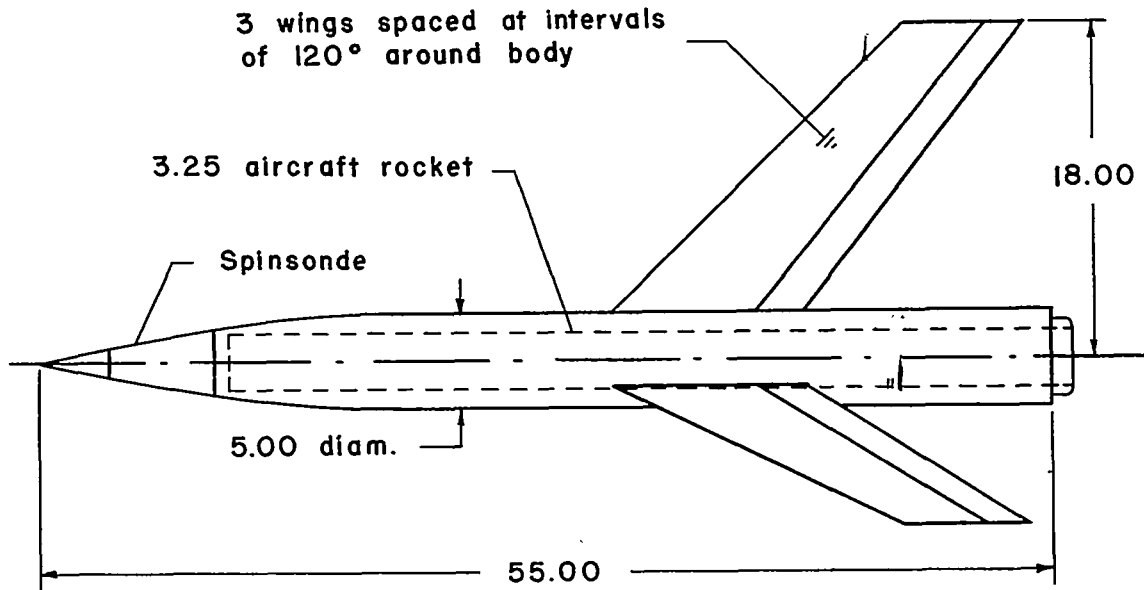
^aTrailing-edge angle plots show data at two wing sweepback angles.

(a) Model 28. $A = 3.7$; $\Lambda = 0^\circ$; $\lambda = 1.0$.

L-67857.1

Figure 1.- General arrangement of typical test vehicles. All dimensions are in inches.



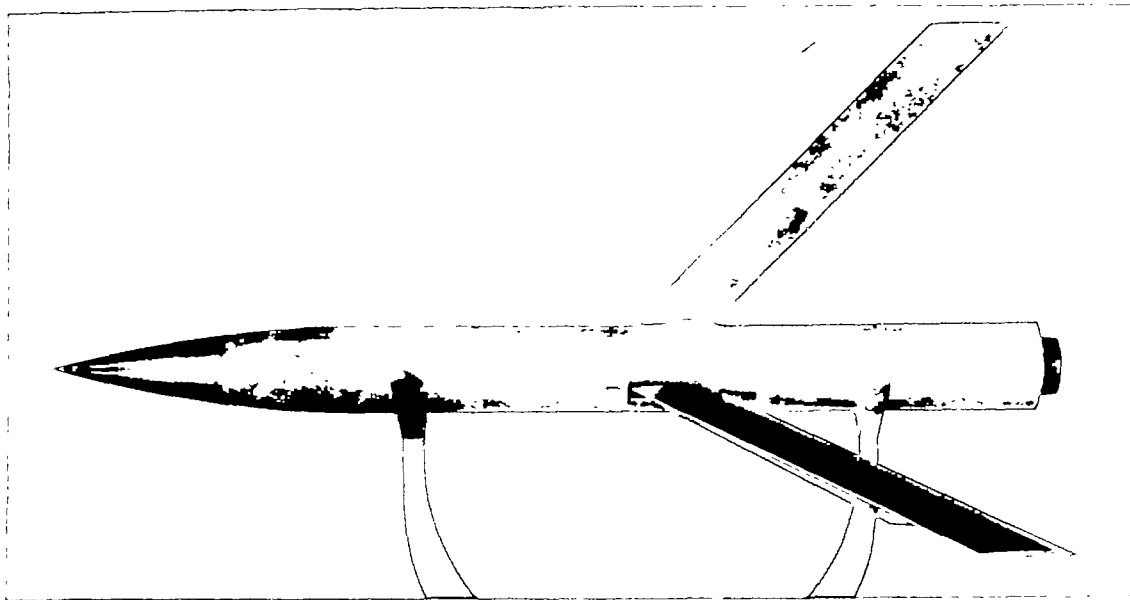
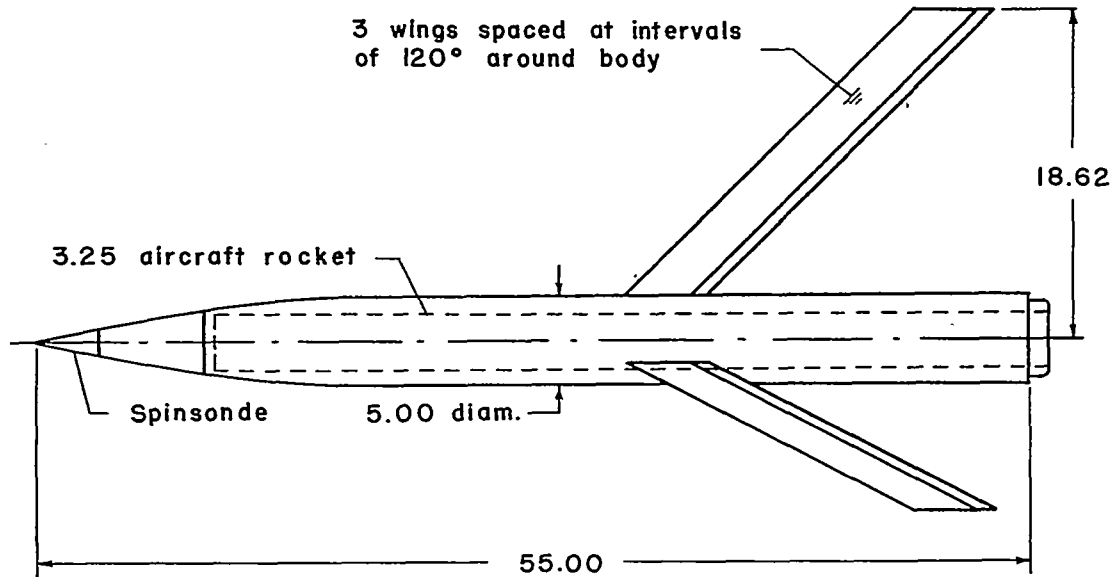


(b) Model 71. $A = 4.0$; $\Lambda = 45^\circ$; $\lambda = 0.60$.

L-73023.1

Figure 1.- Continued.

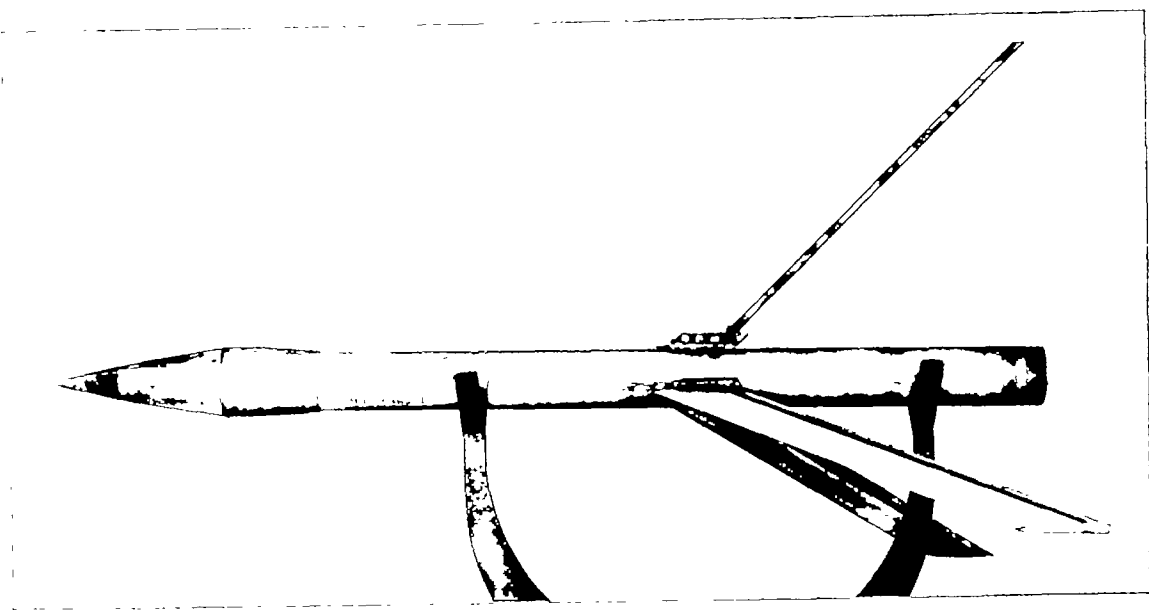
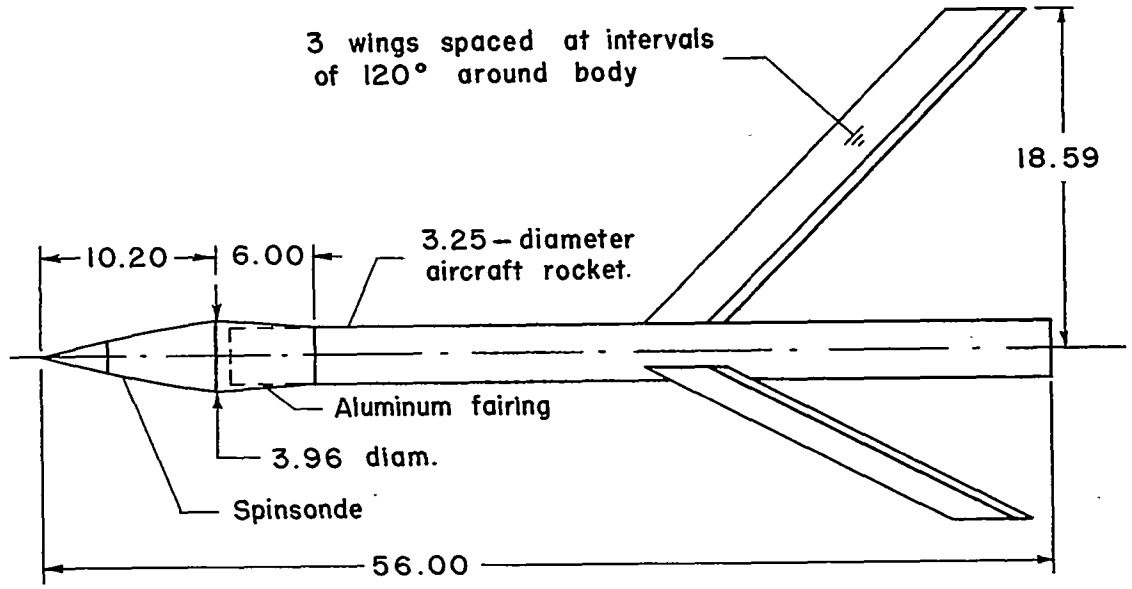
CONFIDENTIAL

(c) Model 88. $A = 8.0$; $\Lambda = 45^\circ$; $\lambda = 1.0$.

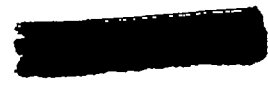
L-69353.1

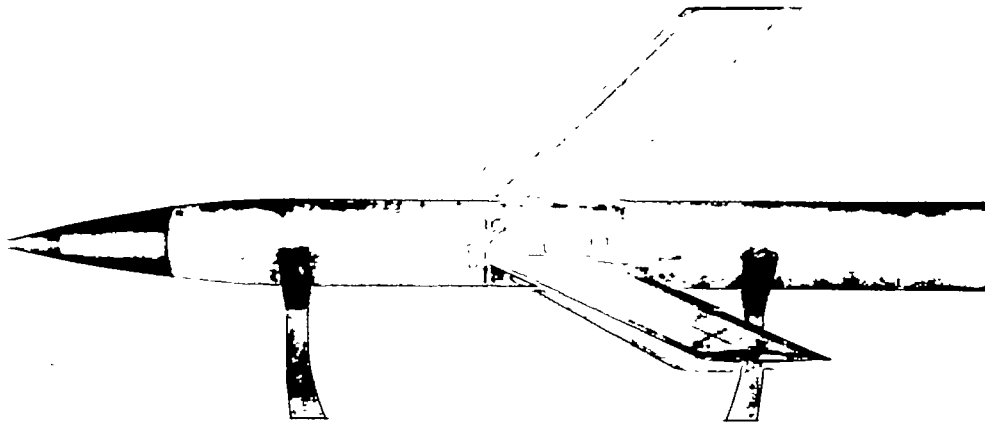
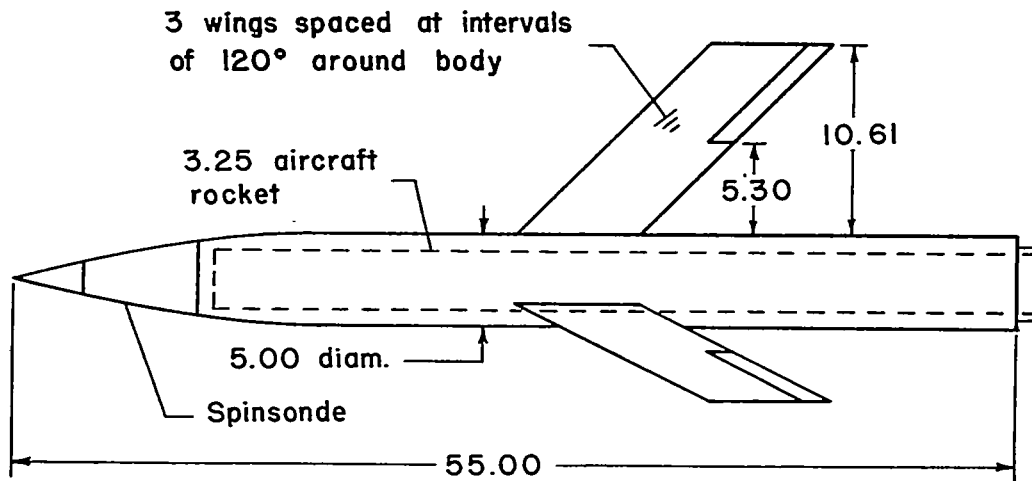
Figure 1.- Concluded.

CONFIDENTIAL



L-82789.1
Figure 2.- Photographs showing typical construction for models 2, 4, 6, 8, 83, 85, 89, and 93. All dimensions are in inches.



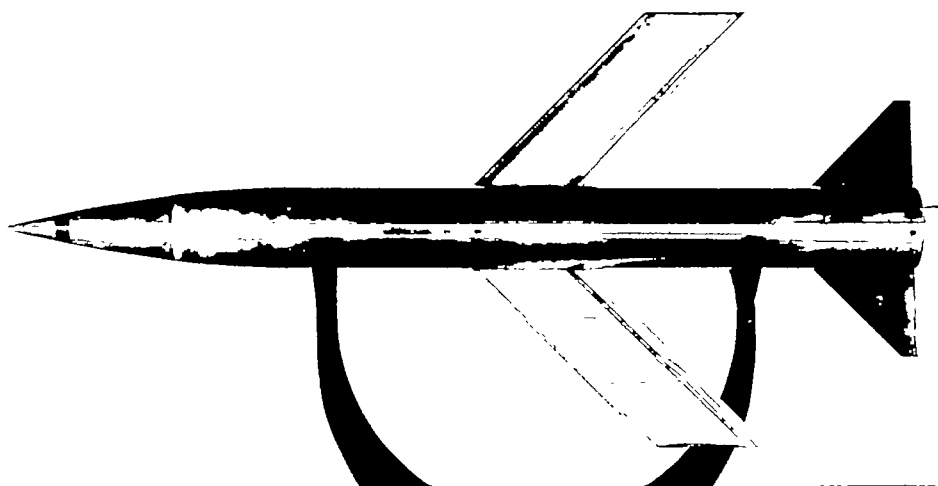
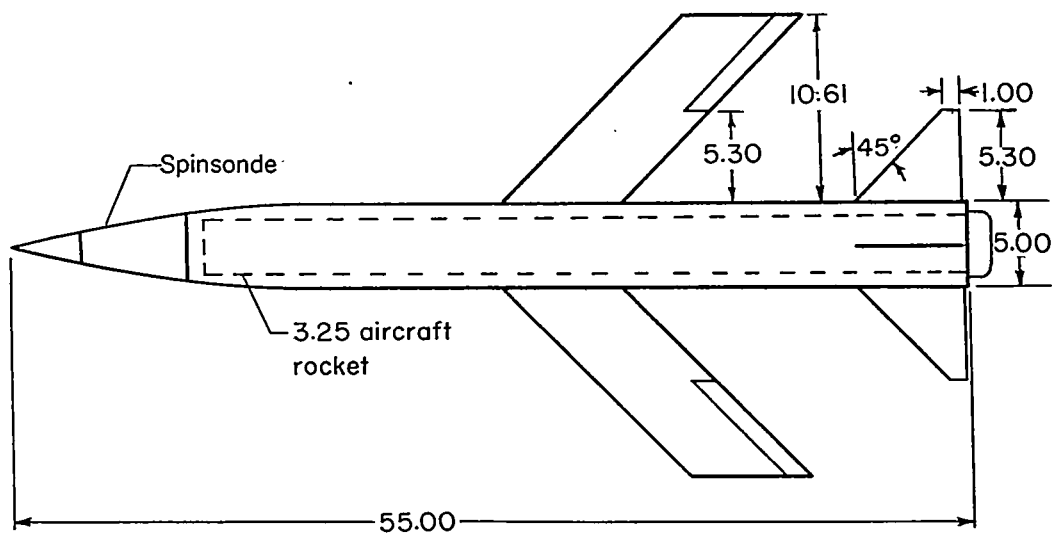


L-71131.1

(a) Three wings with outboard half-span aileron for investigation of effects of wing location. Model 53.

Figure 3.- Typical test vehicles for investigating the effects of wing location and wing-tail interference. All dimensions are in inches.

CONFIDENTIAL

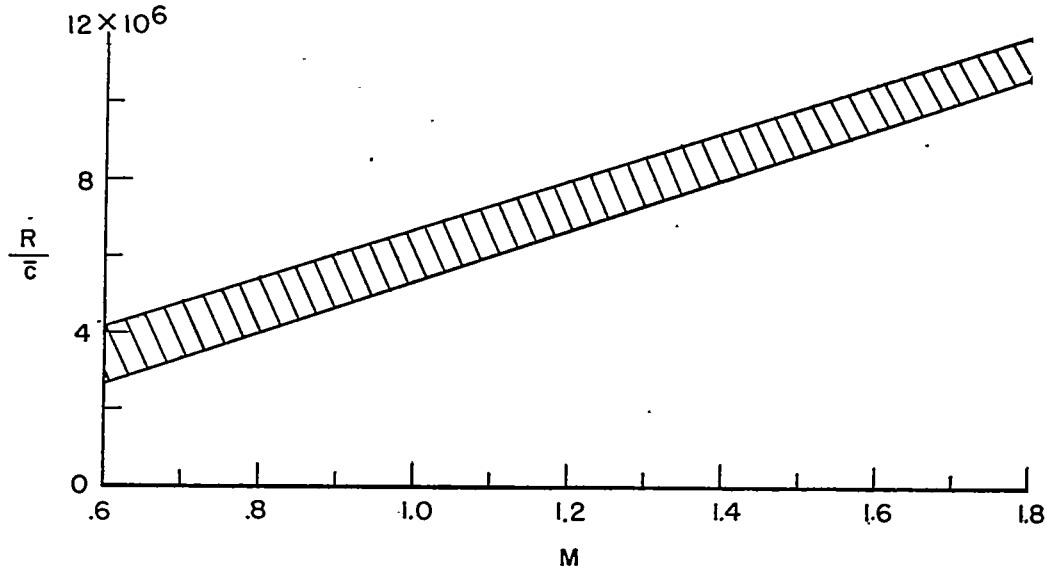


L-75895.1

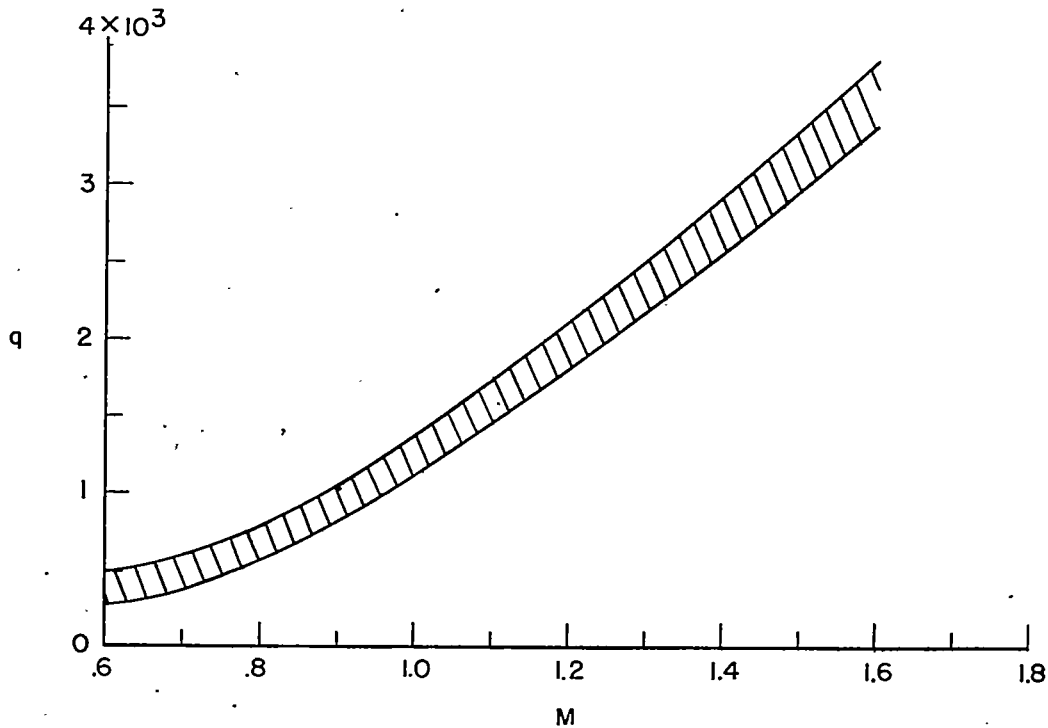
(b) Two wings with outboard half-span aileron with fixed tail for investigation of effects of wing-tail interference. Model 55.

Figure 3.- Concluded.

CONFIDENTIAL



(a) For all tests, the Reynolds number per foot R/\bar{c} fell within the shaded band. The minimum \bar{c} tested was approximately 0.4 foot.



(b) For all tests, the dynamic pressure q fell within the shaded band.

Figure 4.- Variation of Reynolds number and dynamic pressure with Mach number for all test vehicles.

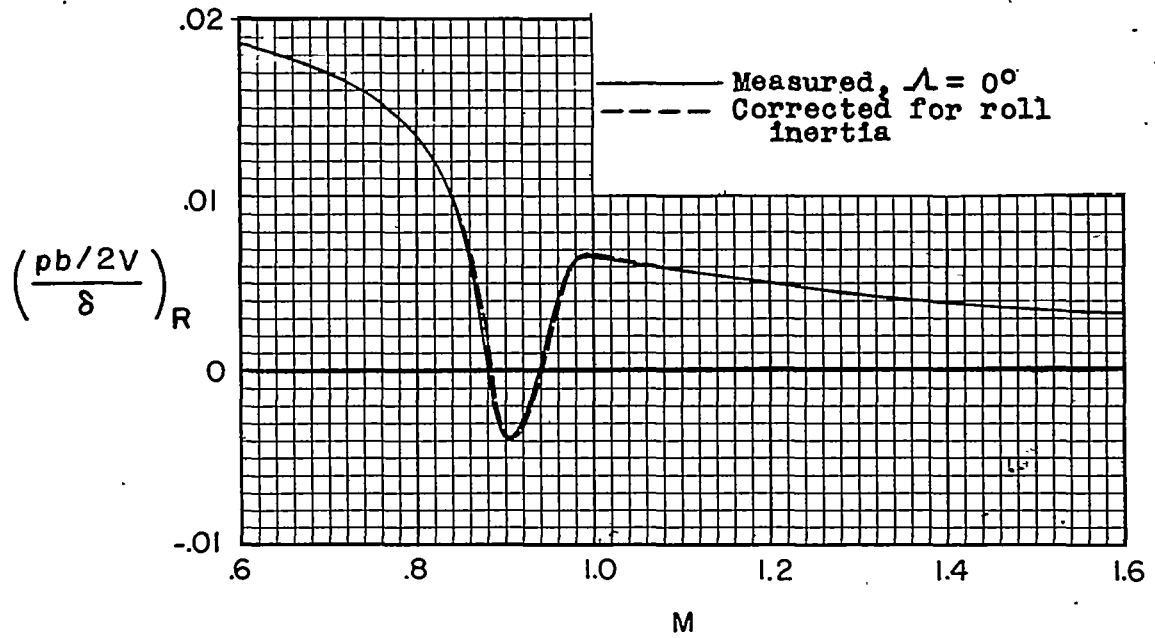


Figure 5.- Effect of model roll inertia on rolling effectiveness.
 Model 27a.

CONFIDENTIAL

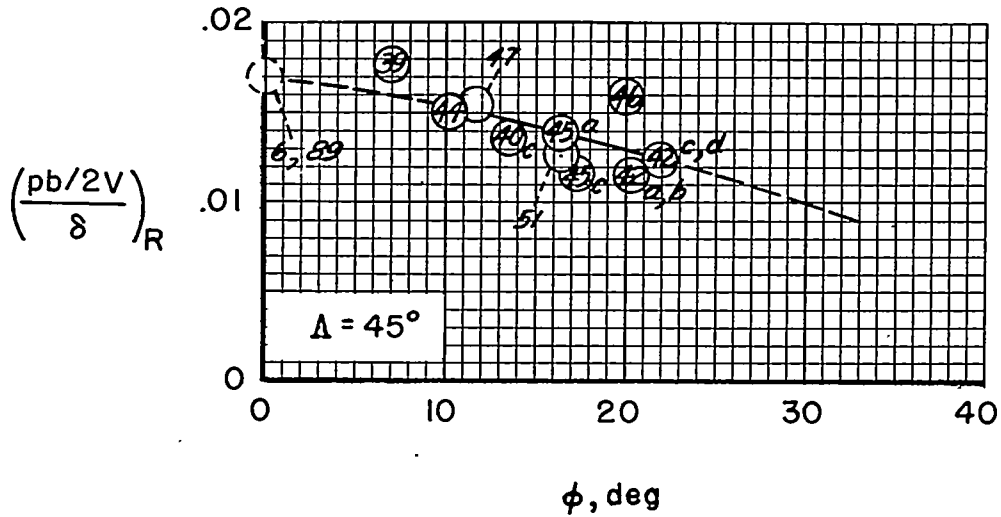
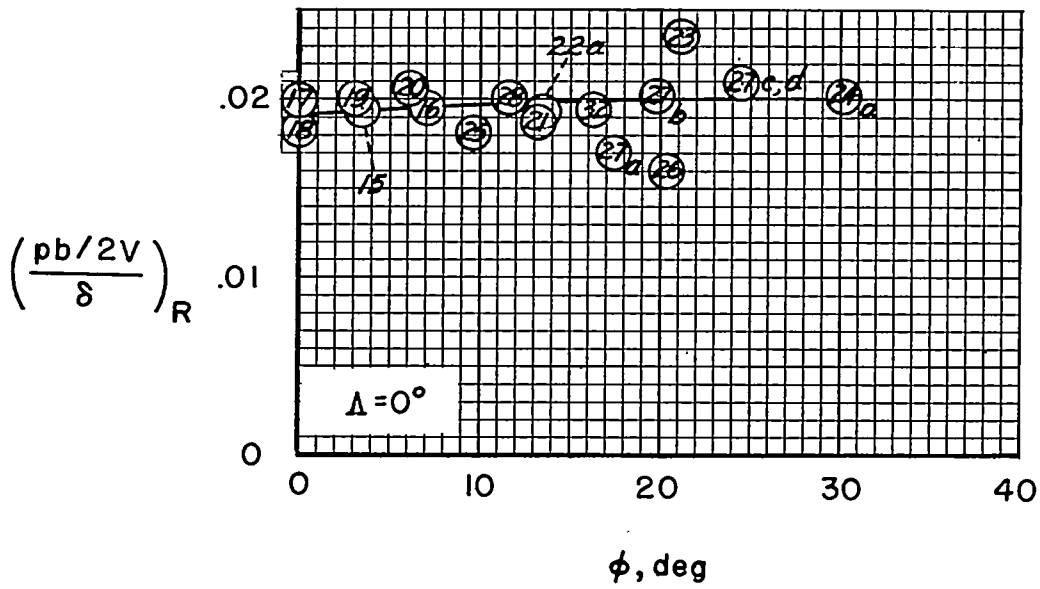
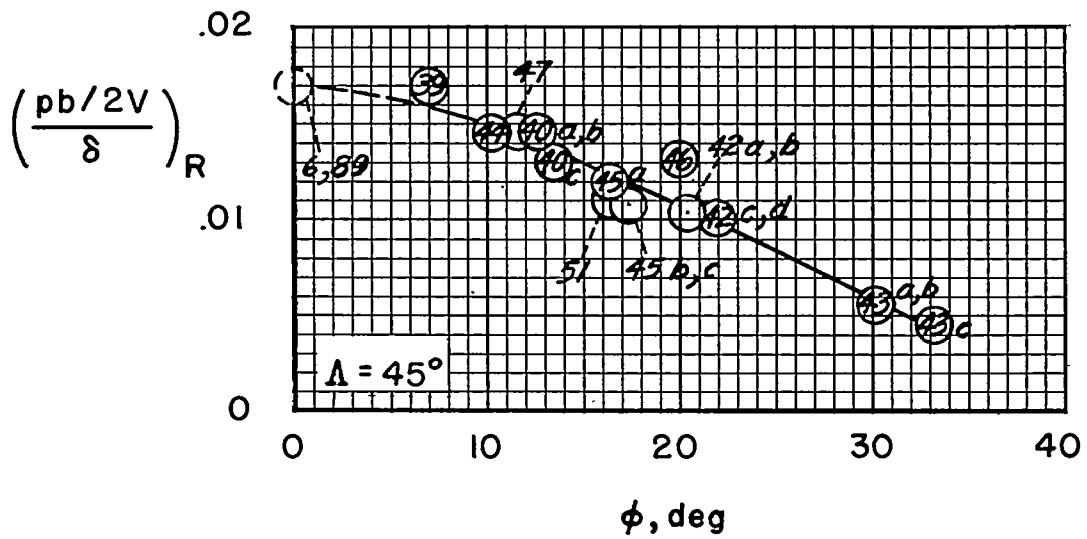
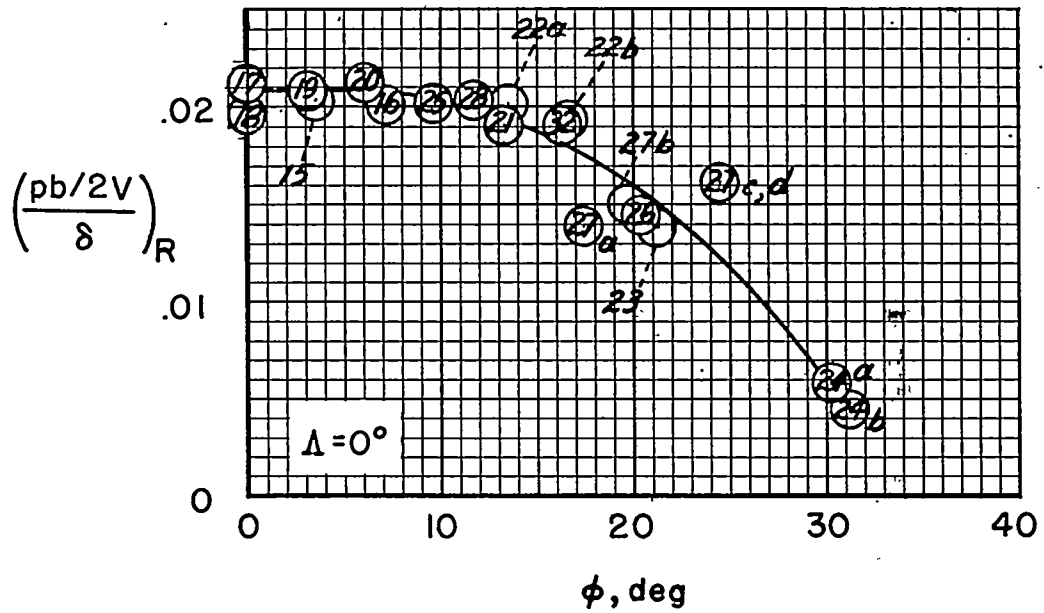
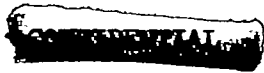
(a) $M = 0.70$.

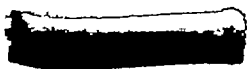
Figure 6.- Variation of rolling-effectiveness parameter $\frac{(pb/2V)}{\delta}$ with trailing-edge angle ϕ . Unless otherwise indicated, average values are plotted where two or more nominally identical models were tested. $A = 3.7$; $\lambda = 1.0$; $c_a/c = 0.20$; full-exposed-span ailerons ($\eta_r = 0.19$); $\delta \approx 3^\circ$ to 7° . Numbers in symbols denote model numbers.

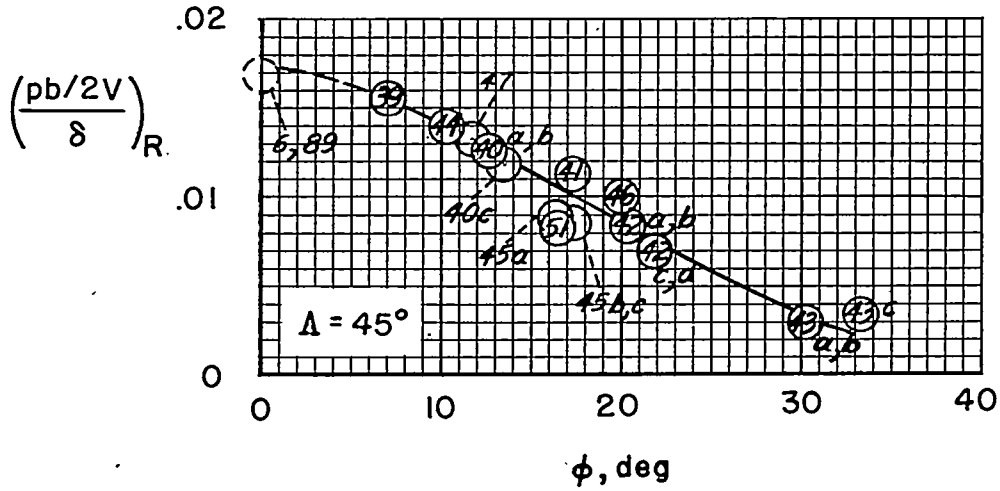
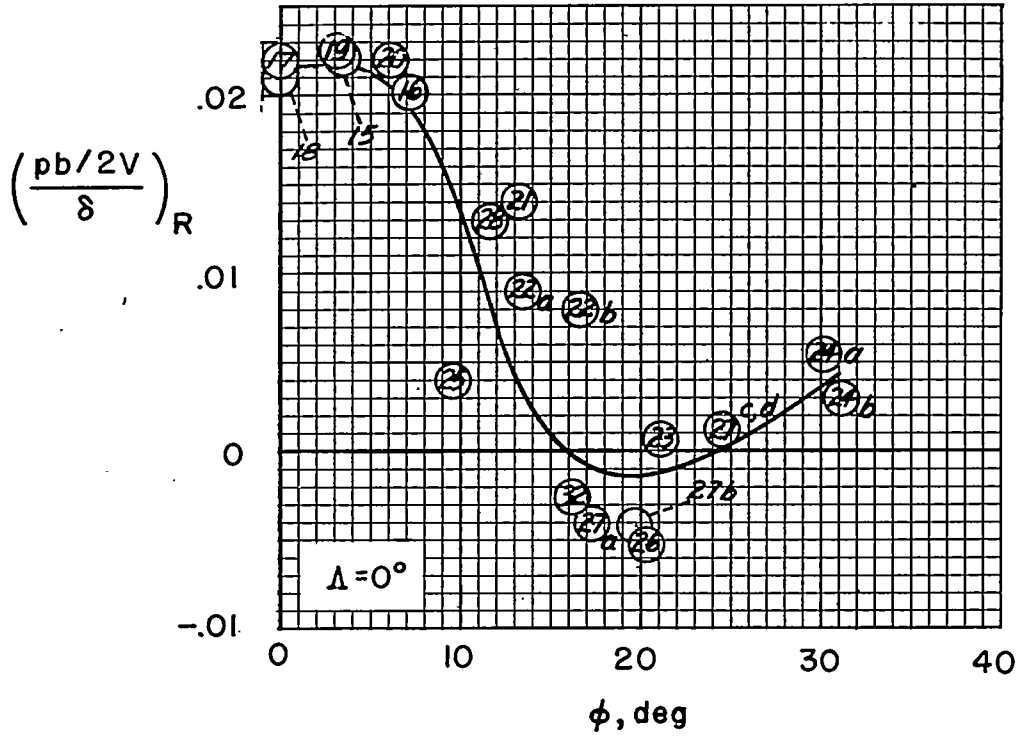
CONFIDENTIAL



(b) $M = 0.80$.

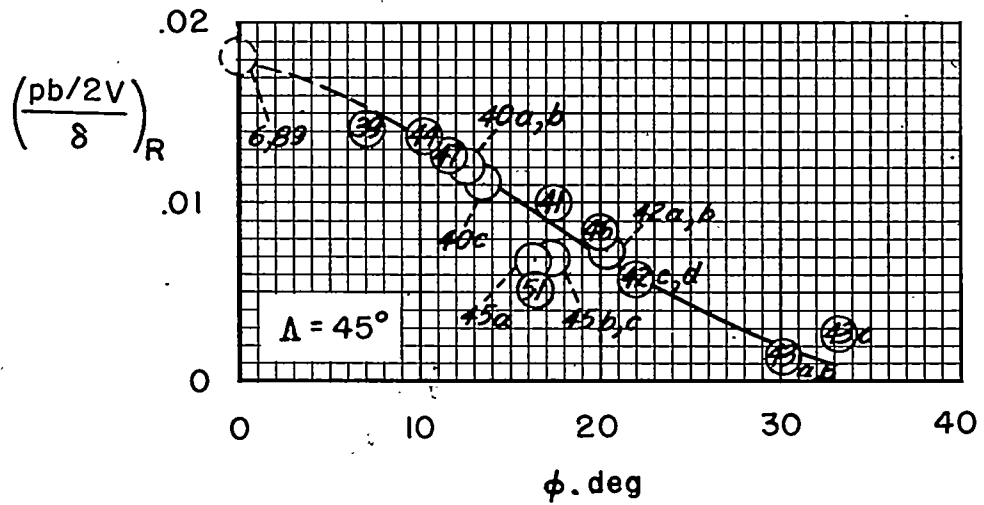
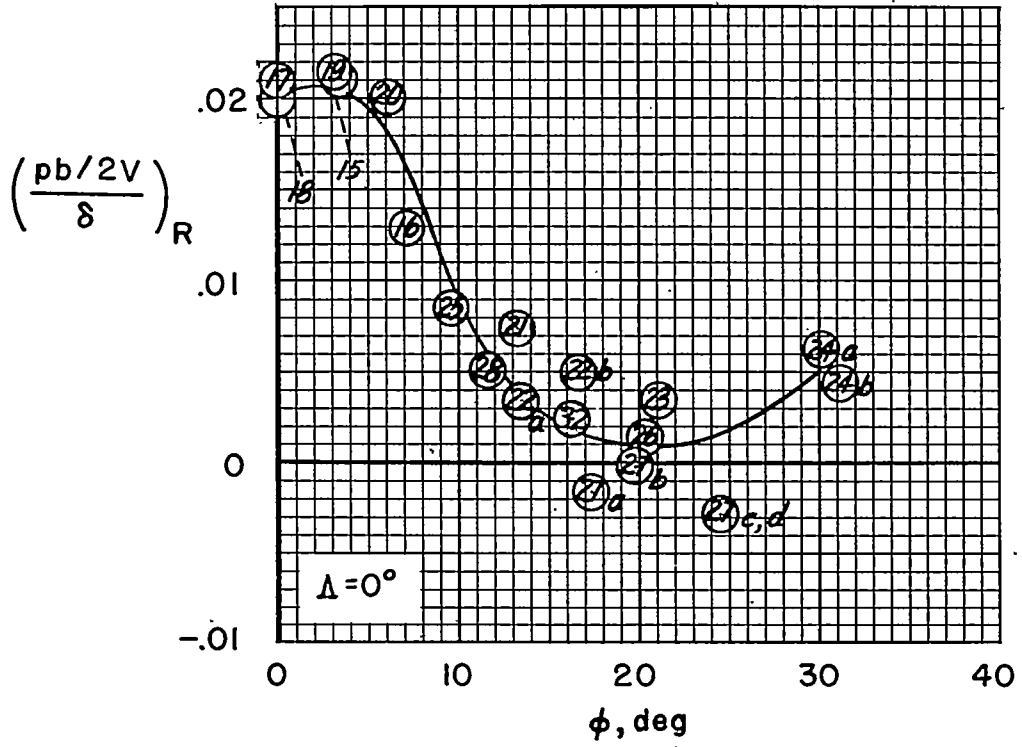
Figure 6.- Continued.





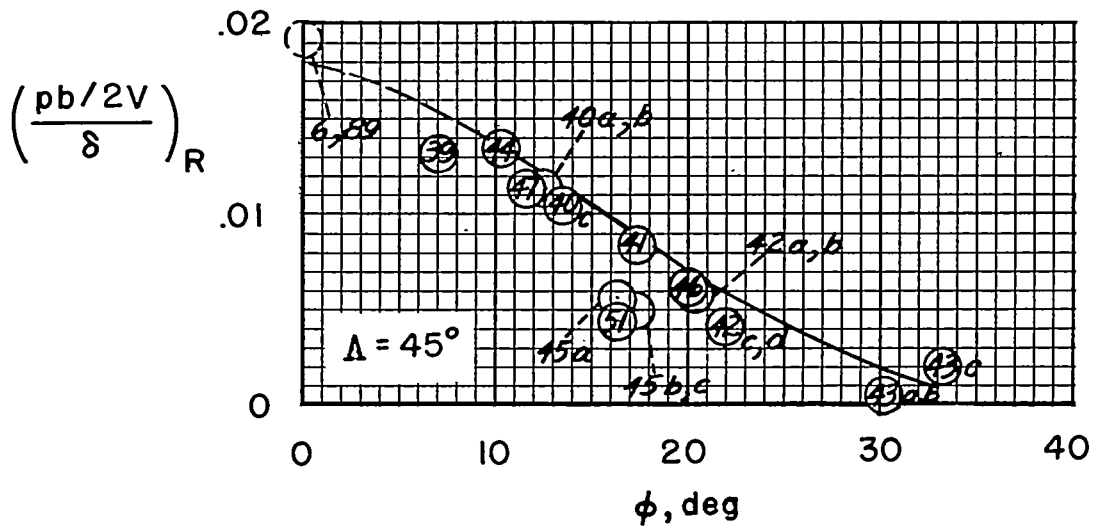
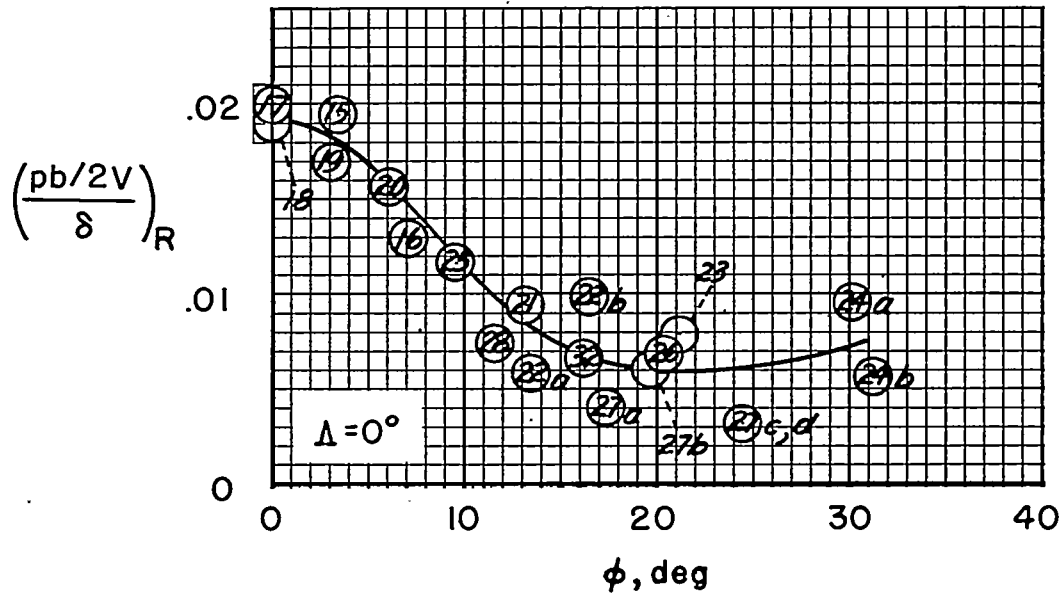
(c) $M = 0.90$.

Figure 6.- Continued.



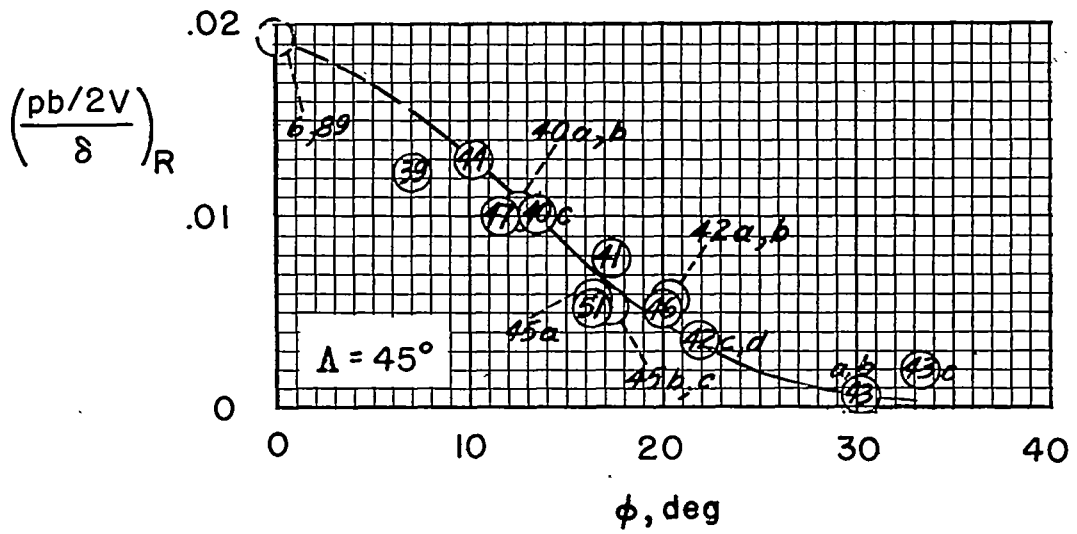
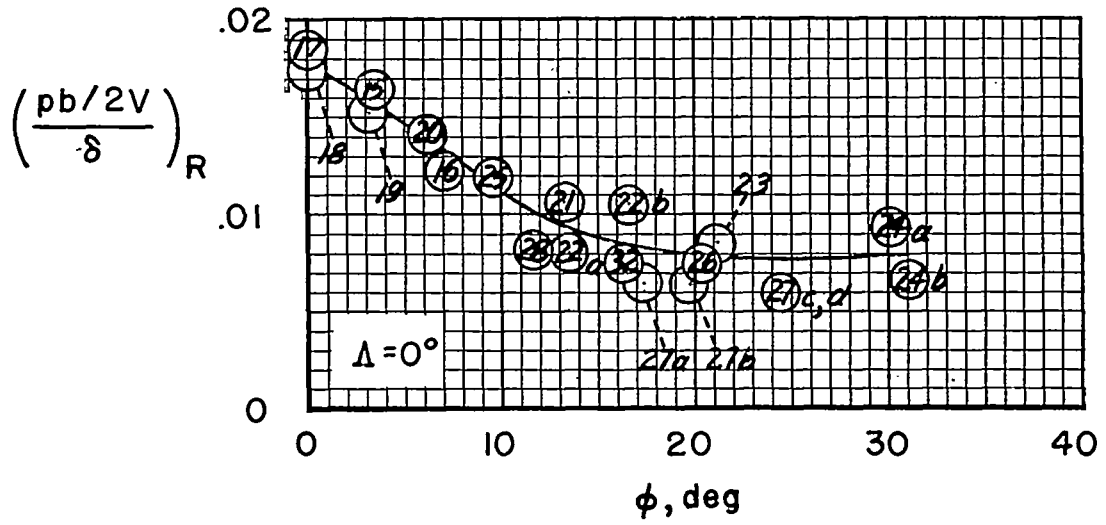
(d) $M = 0.93$.

Figure 6.- Continued.



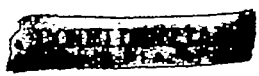
(e) $M = 0.96$.

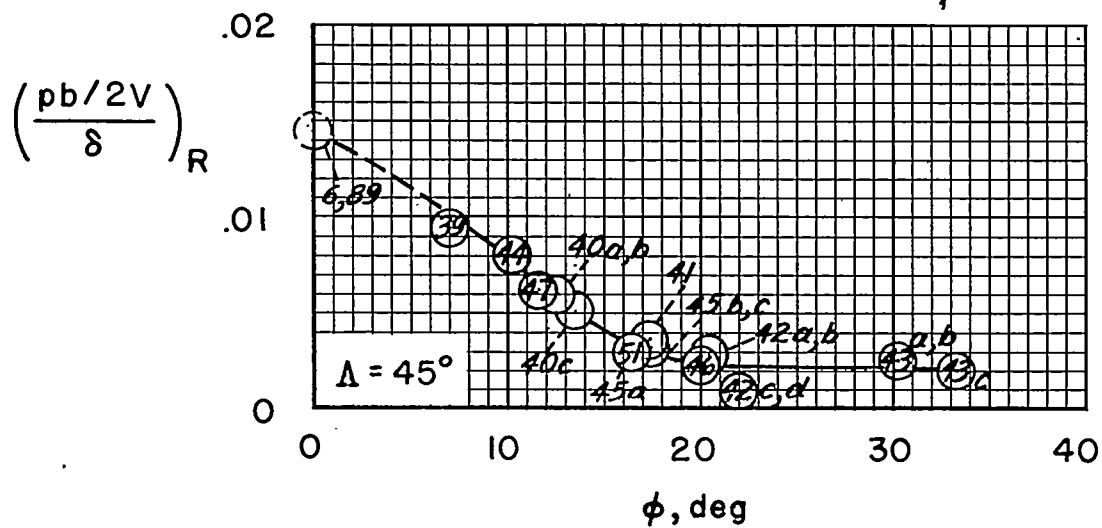
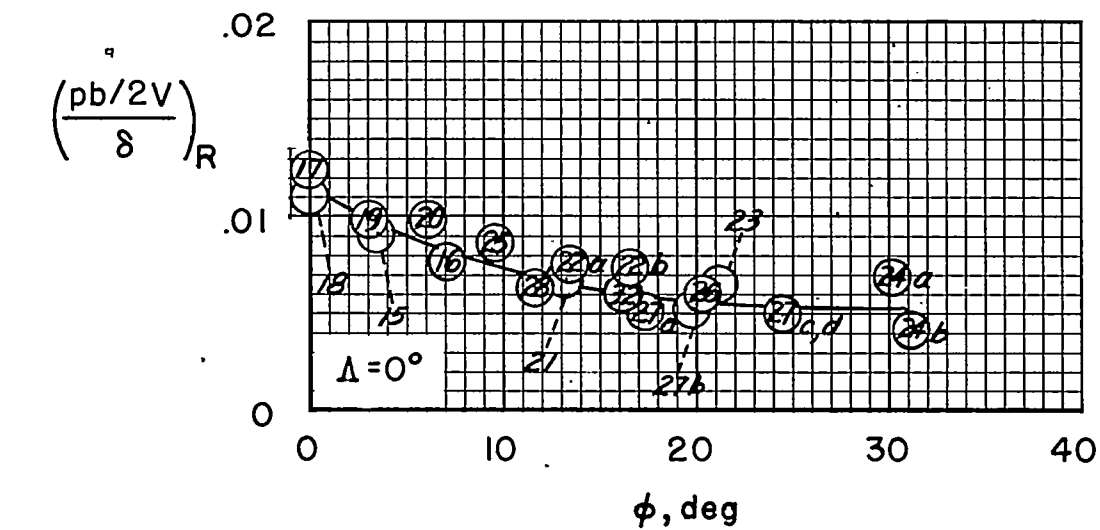
Figure 6.- Continued.



(f) $M = 1.00.$

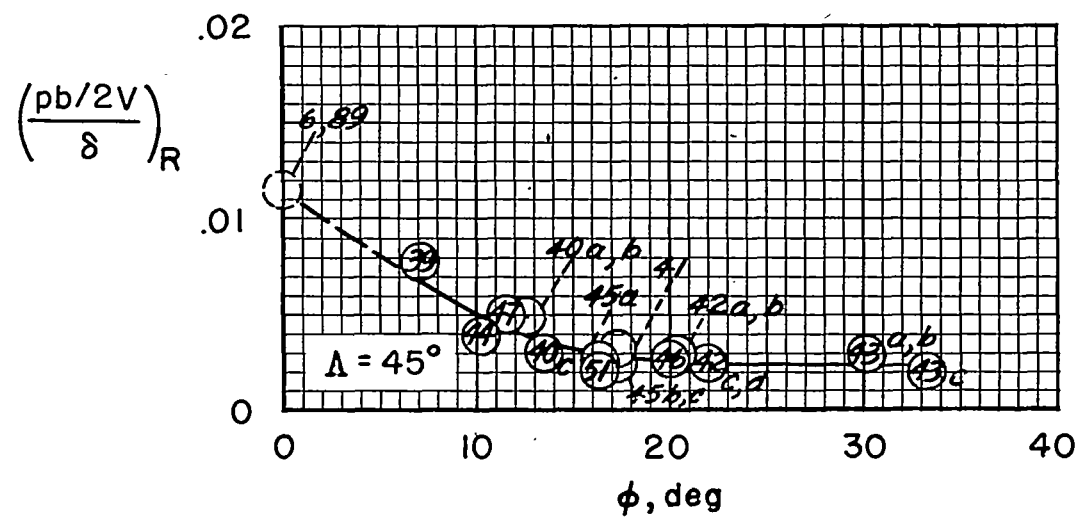
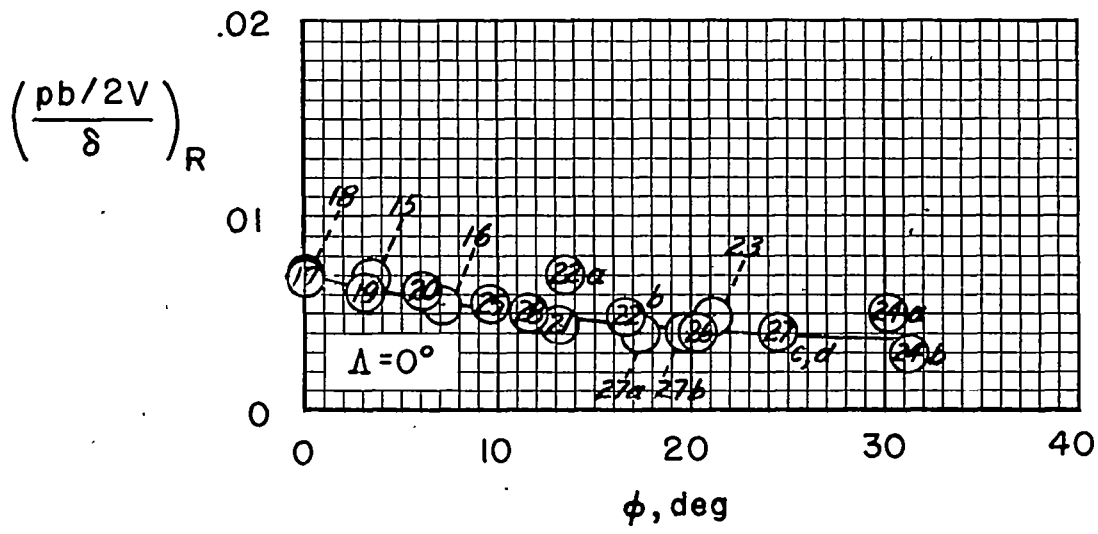
Figure 6.- Continued.





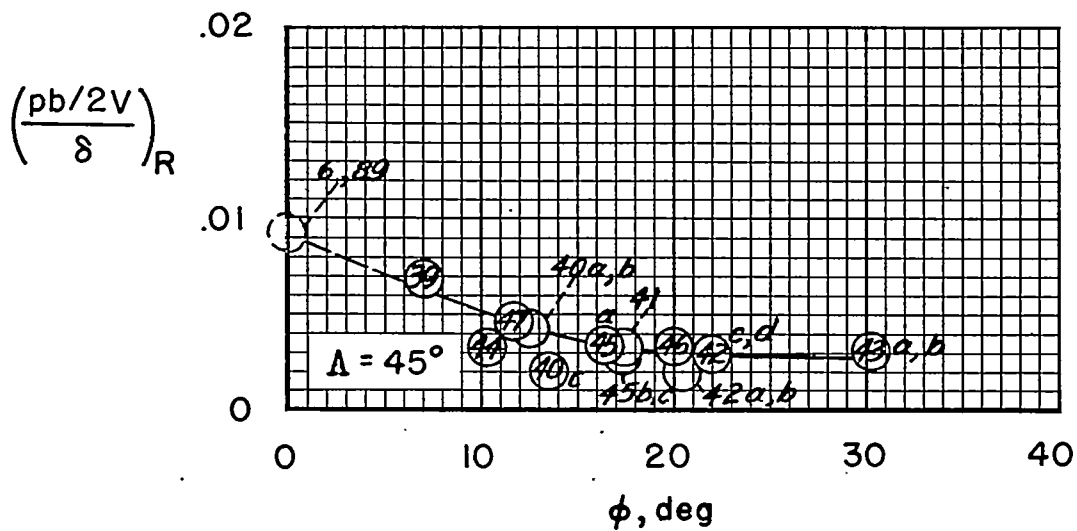
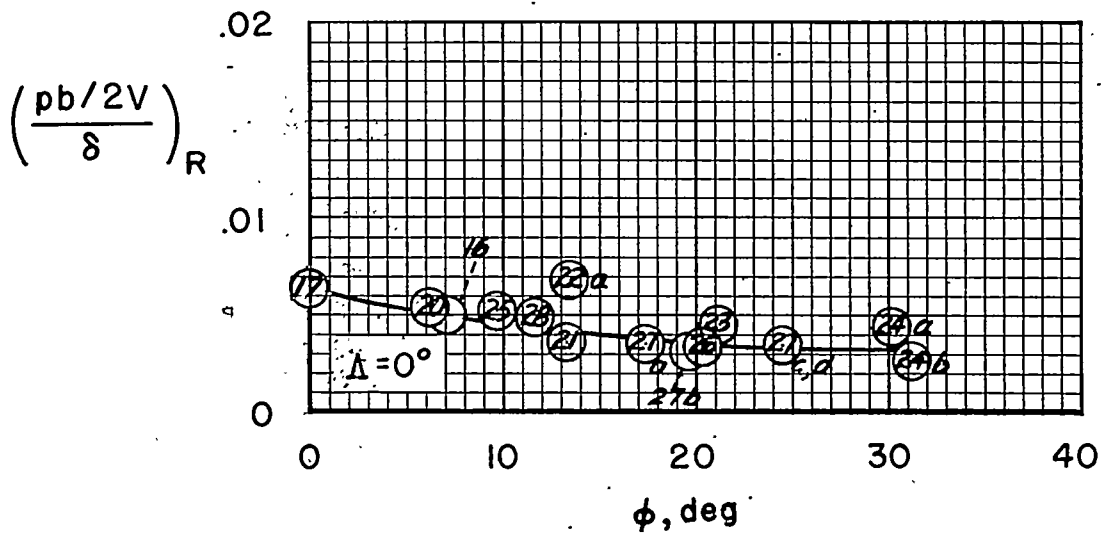
(g) $M = 1.20$.

Figure 6.- Continued.



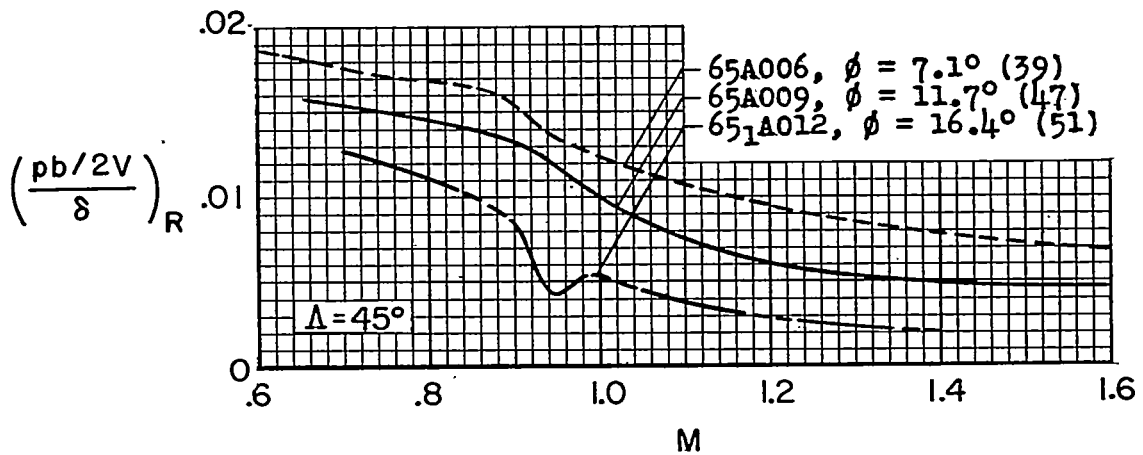
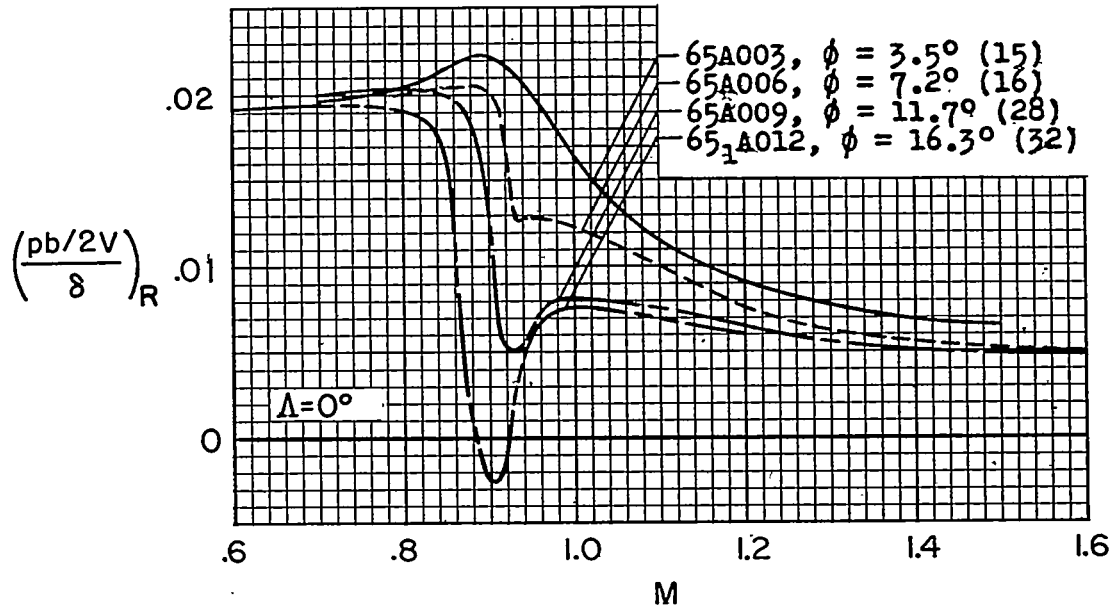
(h) $M = 1.40.$

Figure 6.- Continued.



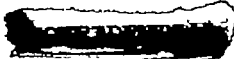
(1) $M = 1.60$.

Figure 6.- Concluded.



(a) $A = 3.71$.

Figure 7.- Effect of airfoil thickness ratio on aileron rolling effectiveness. Numbers in parentheses denote model numbers. NACA 65A0XX airfoil sections. $c_a/c = 0.20$; $\lambda = 1.0$; $\delta \approx 3^\circ$ to 7° .



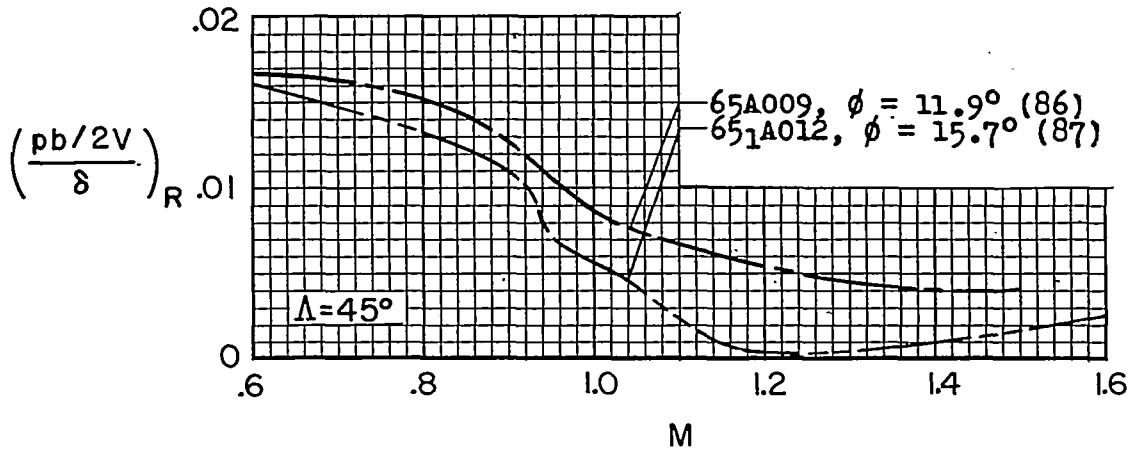
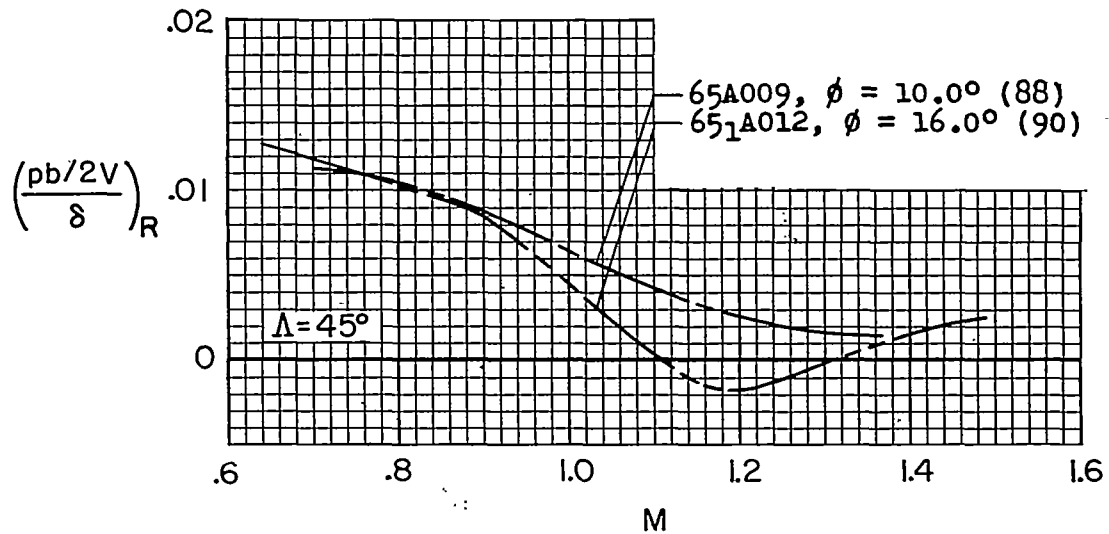
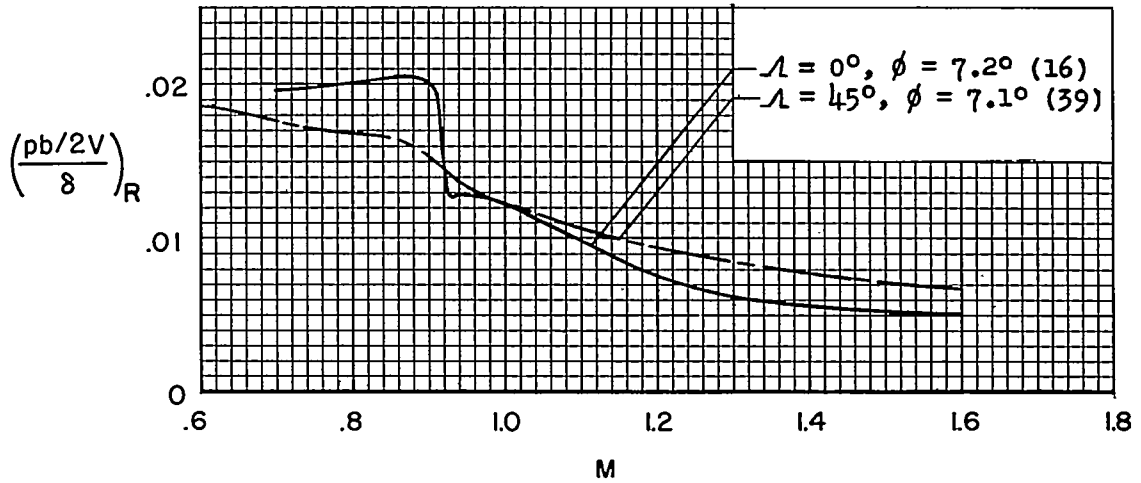
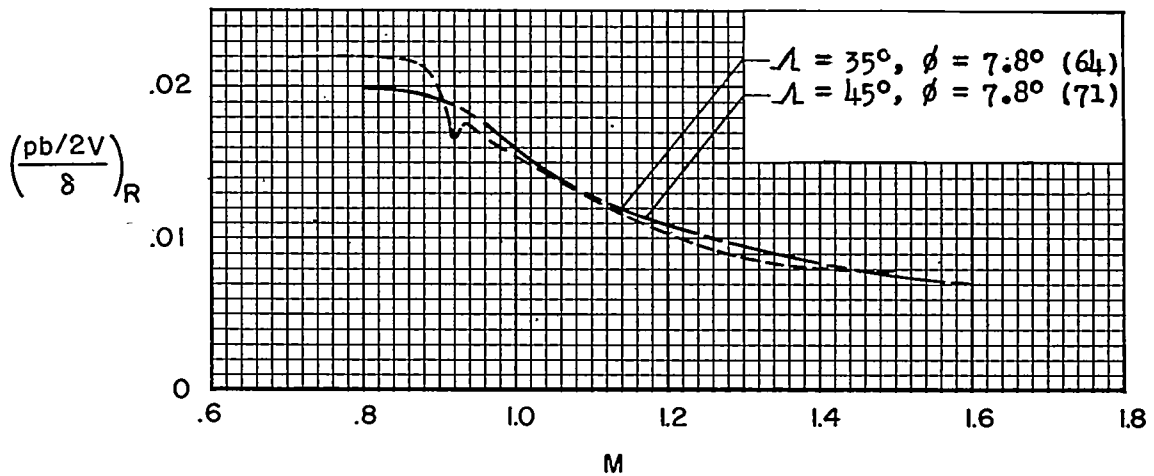
(b) $A = 5.0$.(c) $A = 8.0$.

Figure 7.- Concluded.

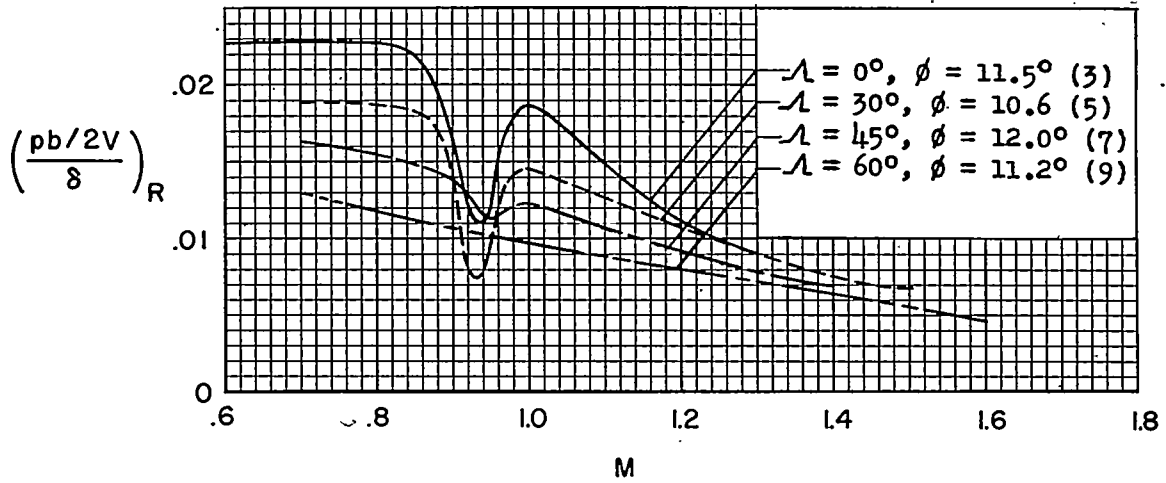


(a) $A = 3.7; \lambda = 1.0$; NACA 65A006 airfoil sections; $c_a/c = 0.20$.

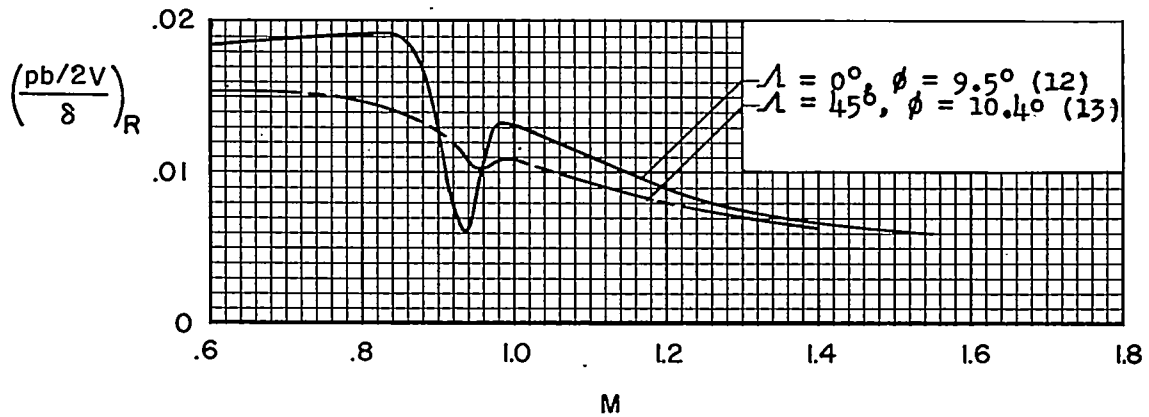


(b) $A = 4.0; \lambda = 0.6$; NACA 65A006 airfoil sections; $c_a/c = 0.30$.

Figure 8.- Some effects of wing sweepback on rolling effectiveness for full-exposed-span ailerons. Numbers in parentheses denote model numbers. $\delta \approx 3^\circ$ to 7° .

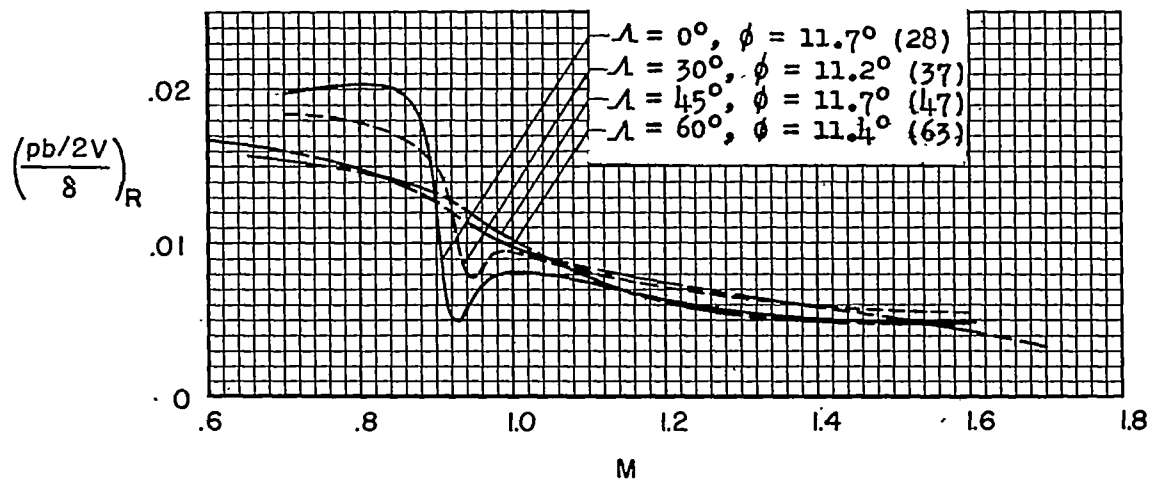


(c) $A = 2.3; \lambda = 1.0$; NACA 65A009 airfoil sections; $c_a/c = 0.20$.

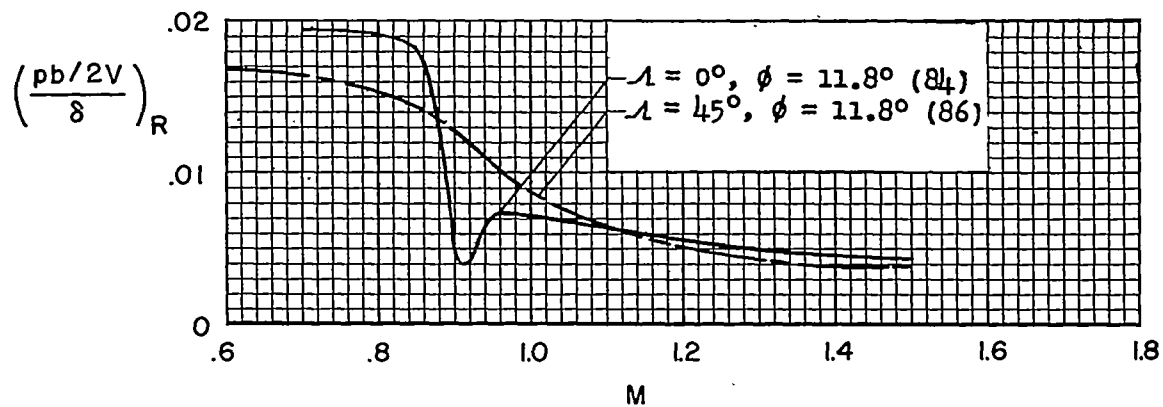


(d) $A = 2.9; \lambda = 1.0$; NACA 65A009 airfoil sections; $c_a/c = 0.20$.

Figure 8.- Continued.

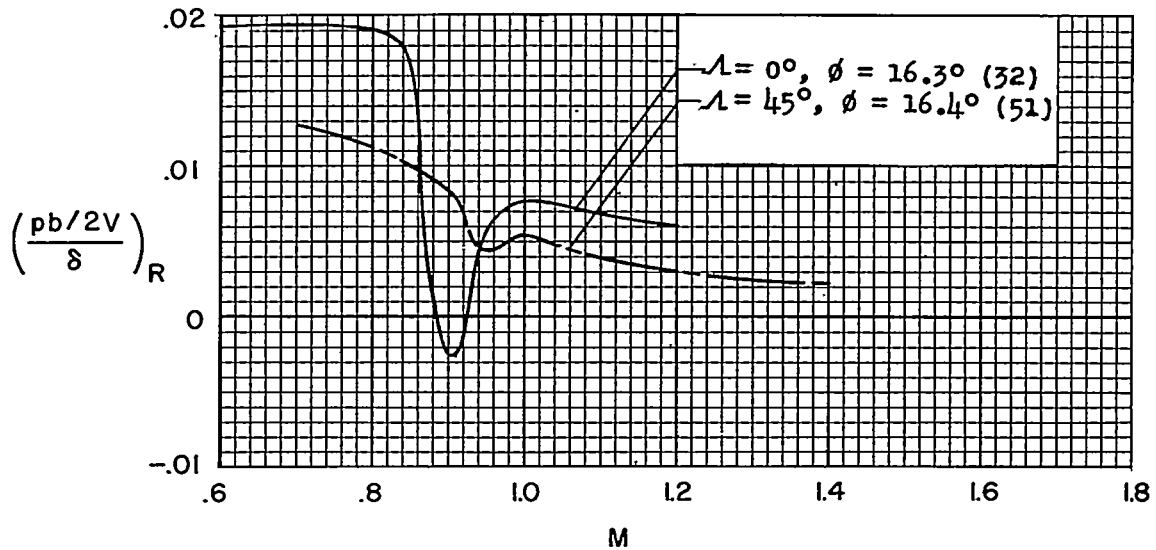


(e) $A = 3.7; \lambda = 1.0$; NACA 65A009 airfoil sections; $c_a/c = 0.20$.

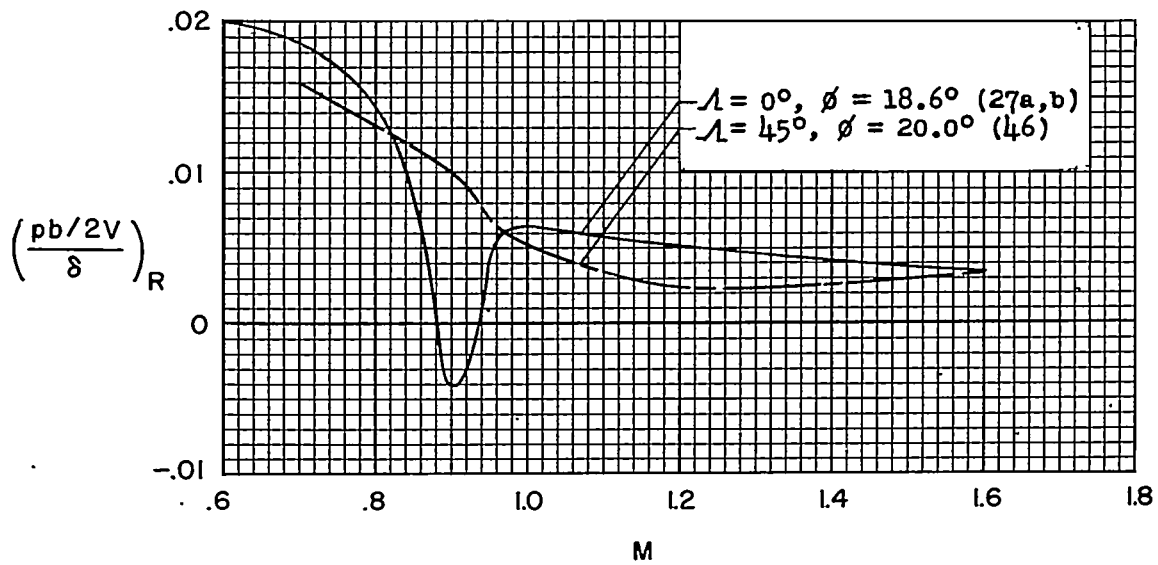


(f) $A = 5.0; \lambda = 1.0$; NACA 65A009 airfoil sections; $c_a/c = 0.20$.

Figure 8.- Continued.

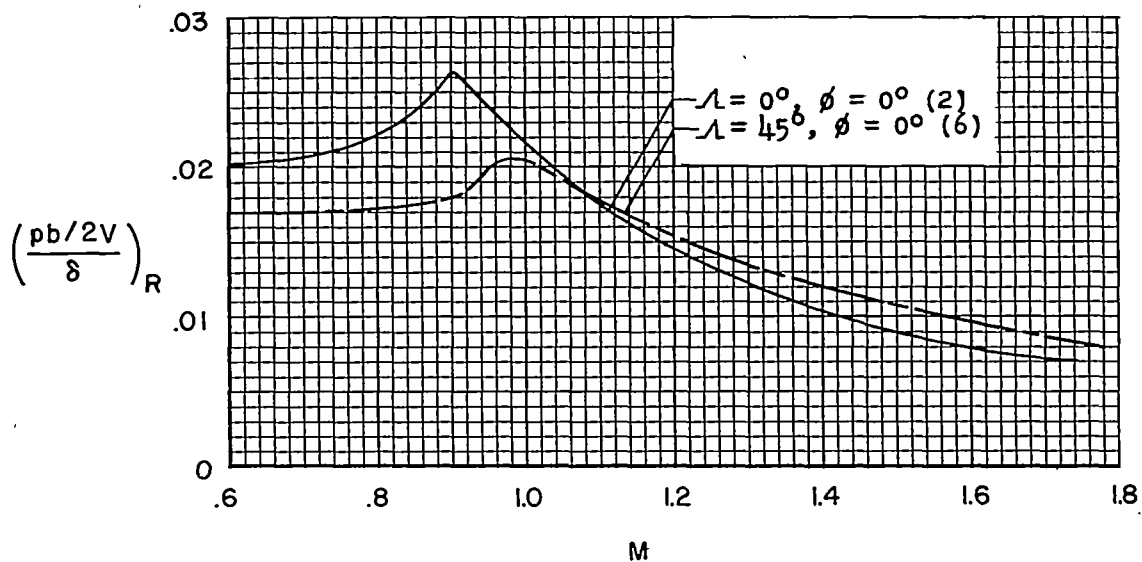


(g) $A = 3.7; \lambda = 1.0$; NACA 651A012 airfoil sections; $c_a/c = 0.20$.

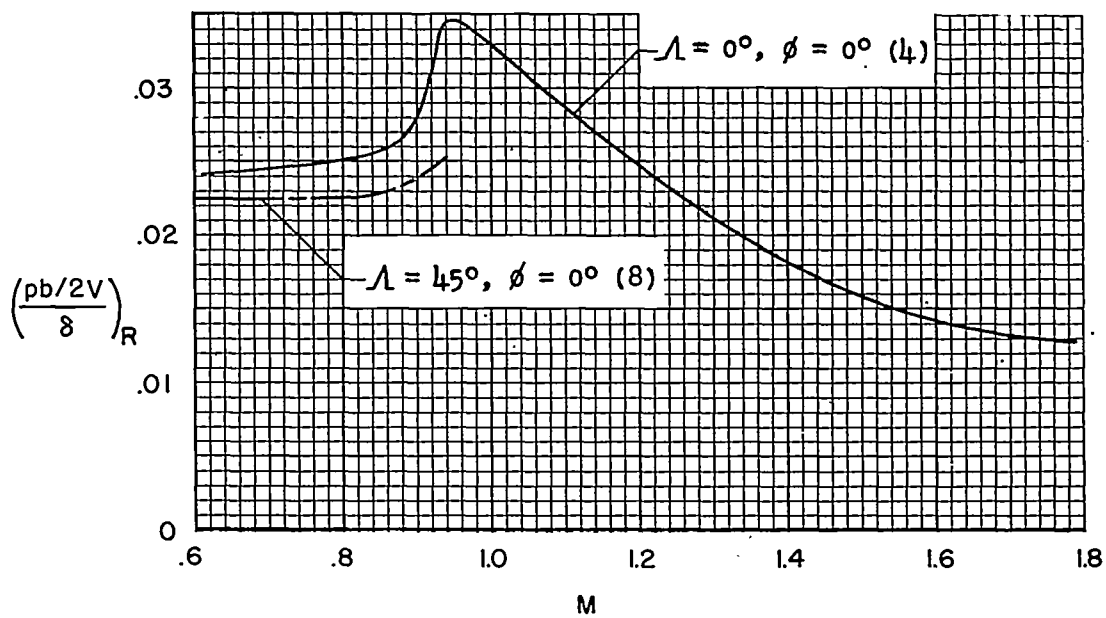


(h) $A = 3.7; \lambda = 1.0$; NACA 16-009 airfoil sections; $c_a/c = 0.20$.

Figure 8.- Continued.

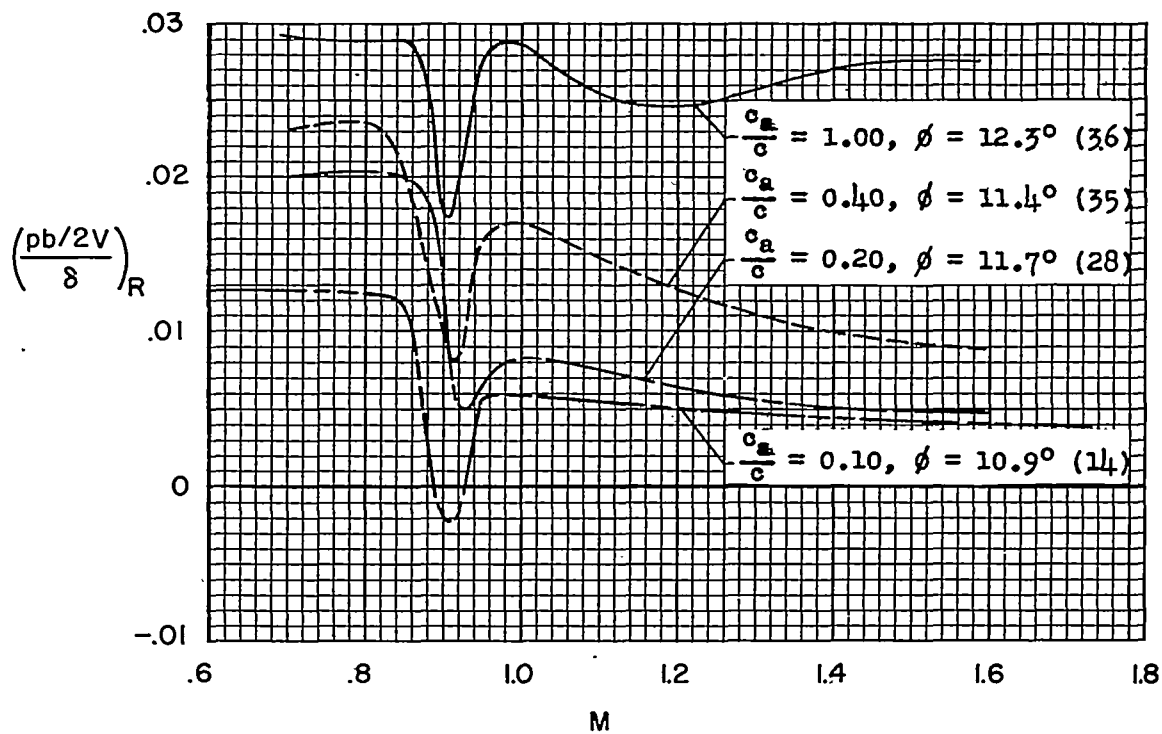
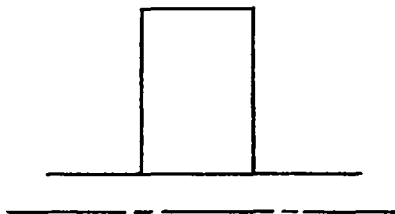


(i) $A = 2.3$; $\lambda = 1.0$; flat-plate airfoil sections; $c_a/c = 0.20$.



(j) $A = 2.3$; $\lambda = 1.0$; flat-plate airfoil sections; $c_a/c = 0.40$.

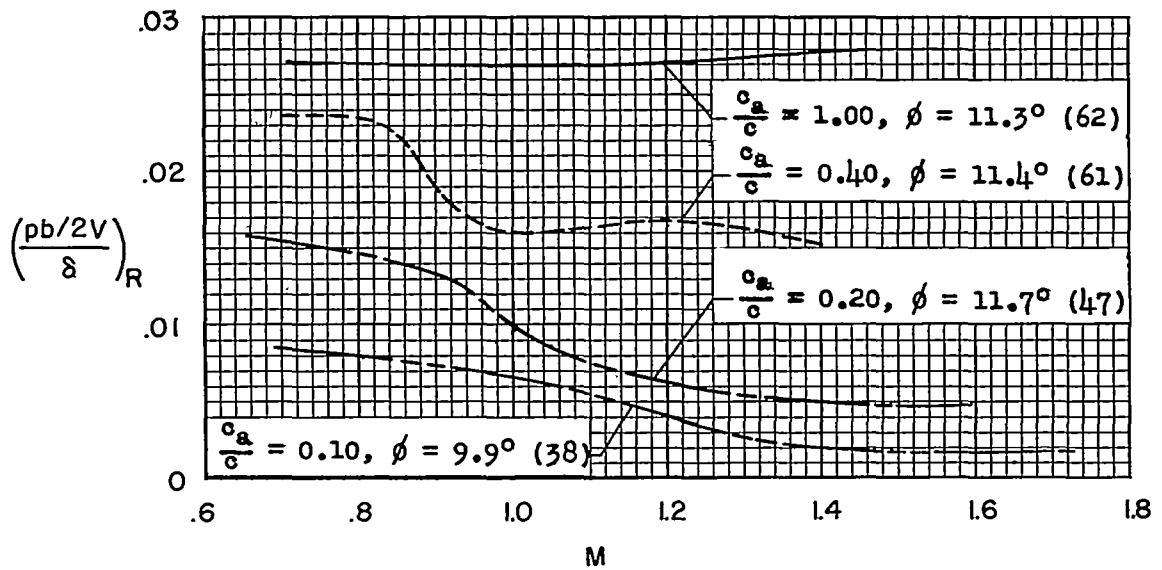
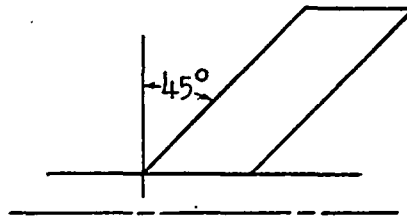
Figure 8.- Concluded.



(a) $\Lambda = 0^\circ$; $A = 3.7$; $\lambda = 1.0$; NACA 65A009 airfoil sections; full-exposed-span aileron.

Figure 9.- Effect of aileron chord ratio c_a/c on rolling effectiveness. $\delta \approx 3^\circ$ to 7° , except for $c_a/c = 1.0$. Numbers in parentheses denote model numbers.

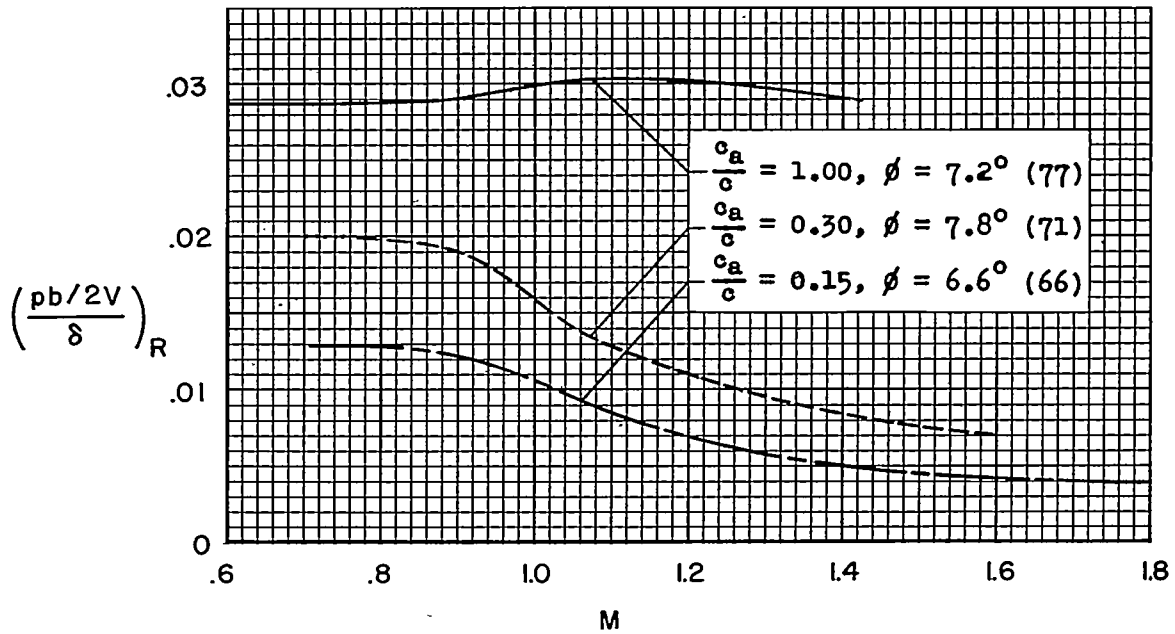
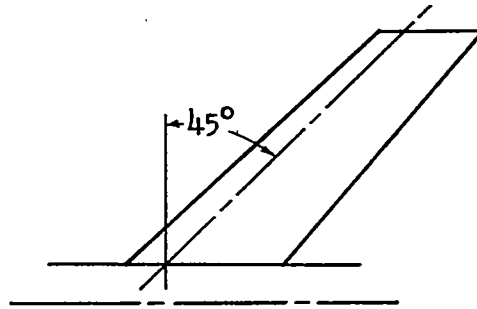
~~CONFIDENTIAL~~



(b) $\Lambda = 45^\circ$; $A = 3.7$; $\lambda = 1.0$; NACA 65A009 airfoil sections; full-exposed-span aileron.

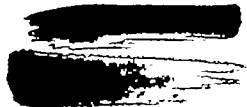
Figure 9.- Continued.

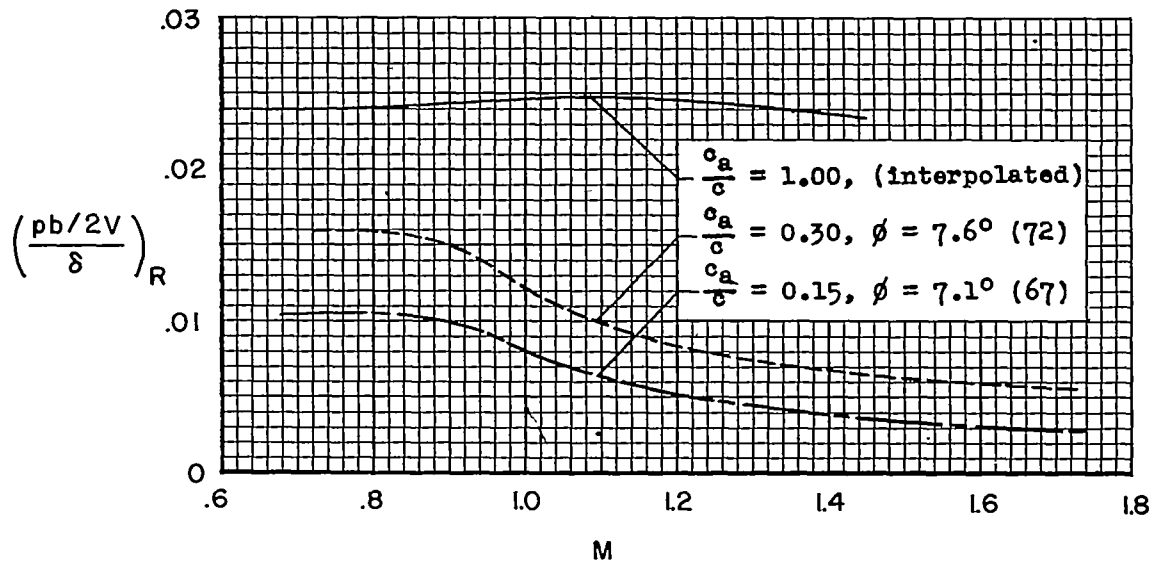
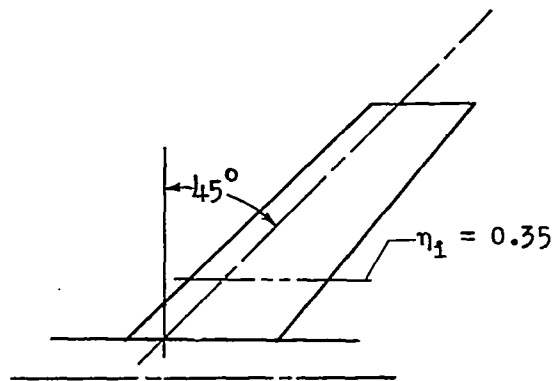
~~CONFIDENTIAL~~



(c) $\Lambda = 45^\circ$; $A = 4.0$; $\lambda = 0.60$; NACA 65A006 airfoil sections; full-exposed-span aileron.

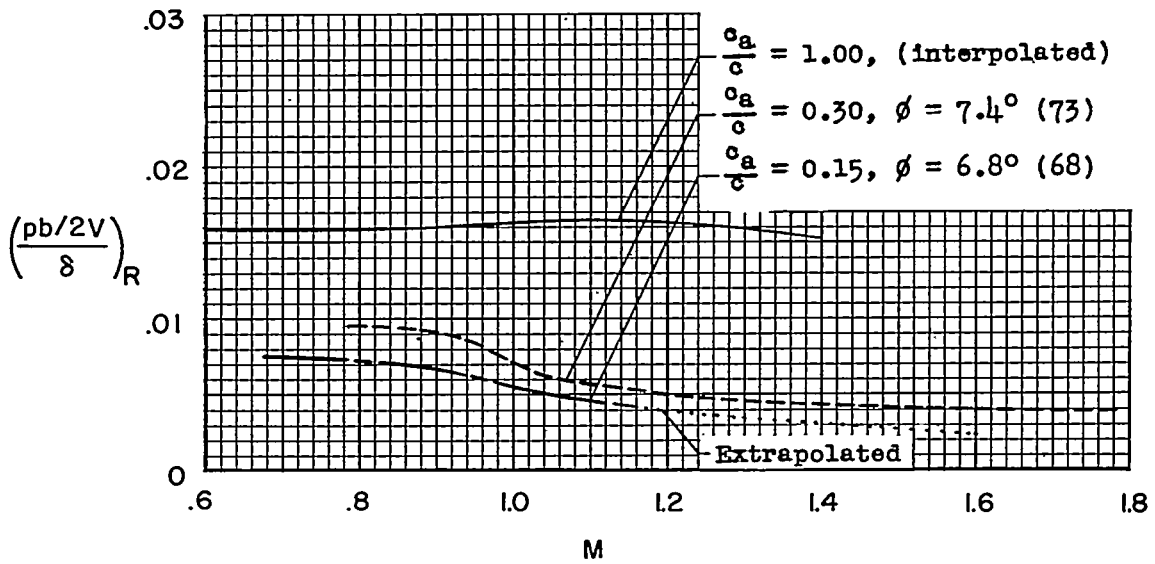
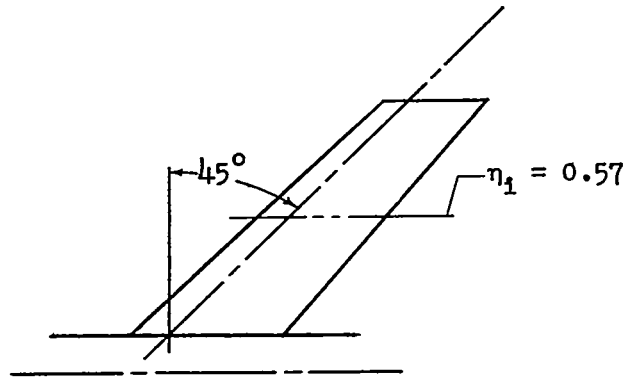
Figure 9.- Continued.





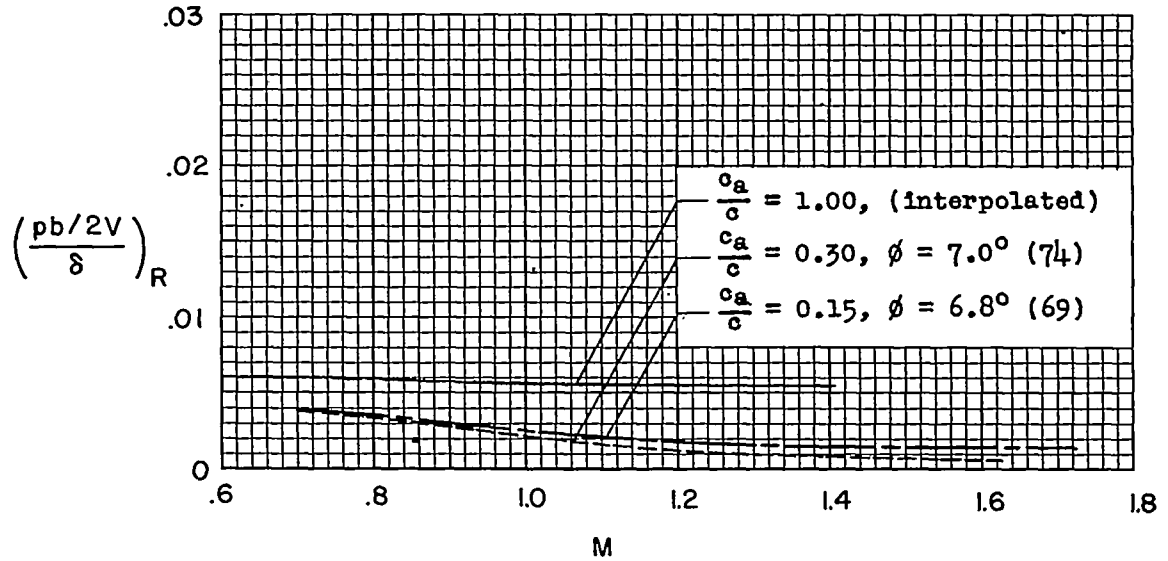
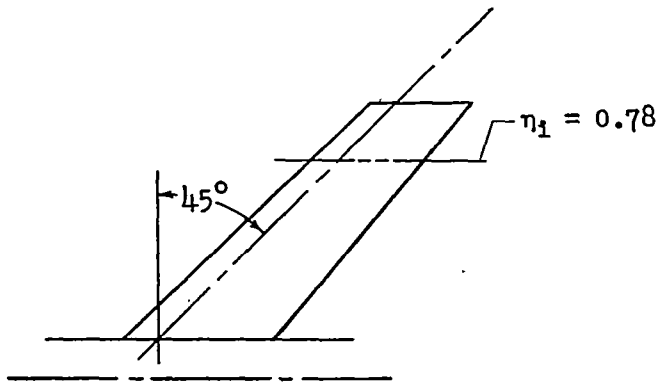
(d) $\Lambda = 45^\circ$; $A = 4.0$; $\lambda = 0.60$; NACA 65A006 airfoil sections; outboard three-quarter-span aileron.

Figure 9.- Continued.



(e) $\Lambda = 45^\circ$; $A = 4.0$; $\lambda = 0.60$; NACA 65A006 airfoil sections; outboard half-span aileron.

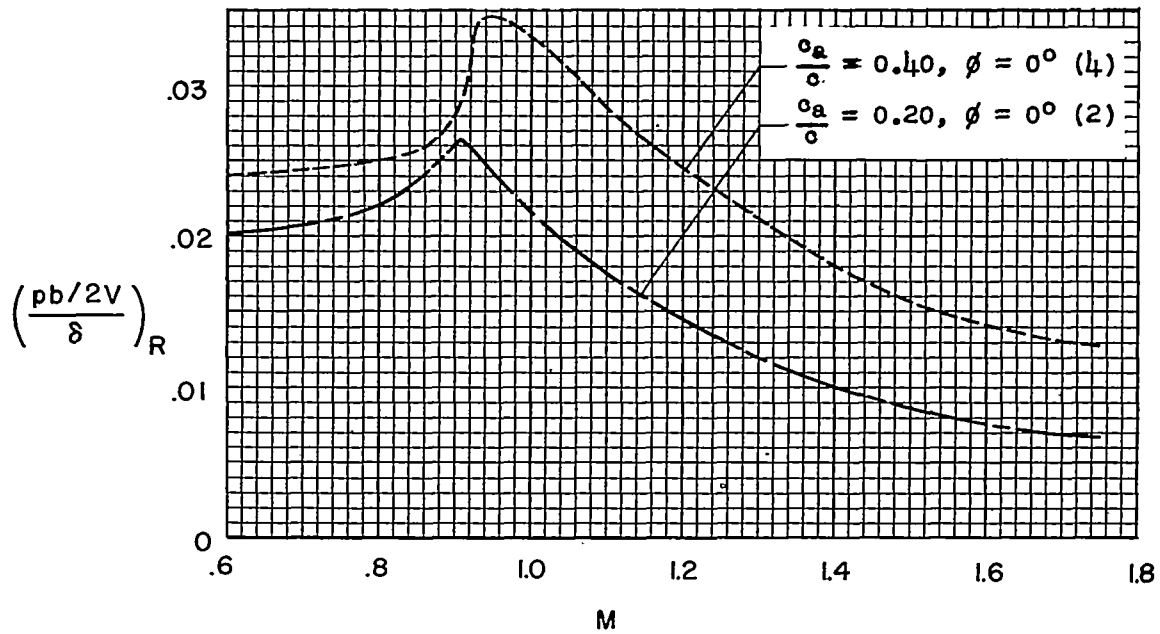
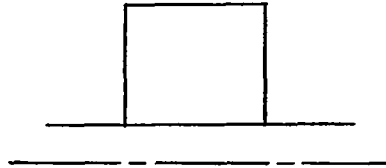
Figure 9.- Continued.



(f) $\Lambda = 45^\circ$; $A = 4.0$; $\lambda = 0.60$; NACA 65A006 airfoil sections; outboard one-quarter-span aileron.

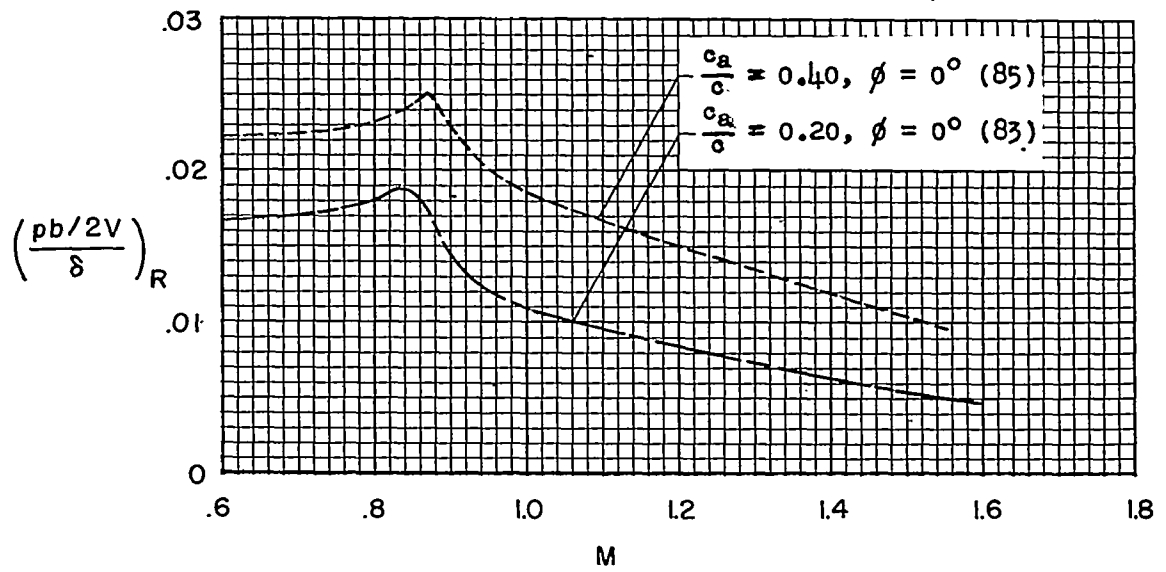
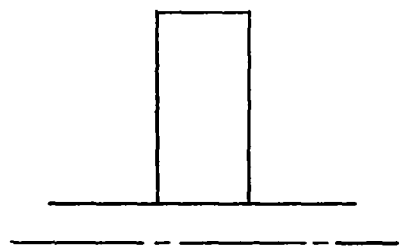
Figure 9.- Continued.





(g) $\Lambda = 0^\circ$; $A = 2.3$; $\lambda = 1.0$; flat-plate airfoil sections ($t/c = 0.054$).

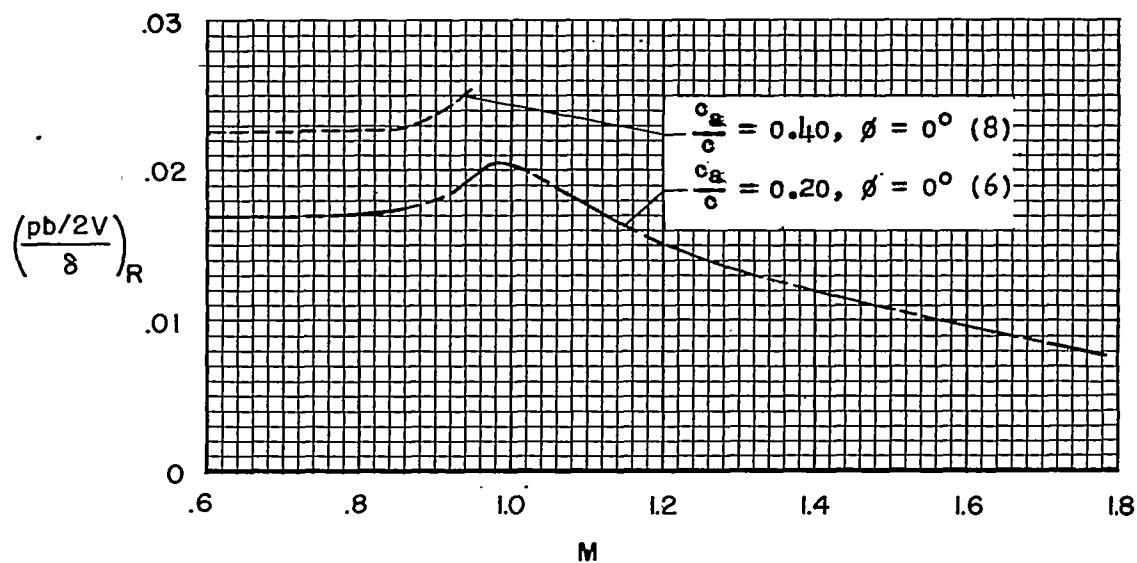
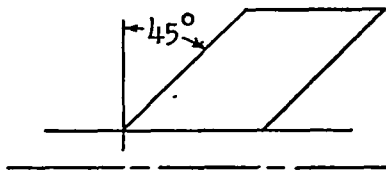
Figure 9.- Continued.



(h) $\Lambda = 0^\circ$; $A = 5.0$; $\lambda = 1.0$; flat-plate airfoil sections ($t/c = 0.083$).

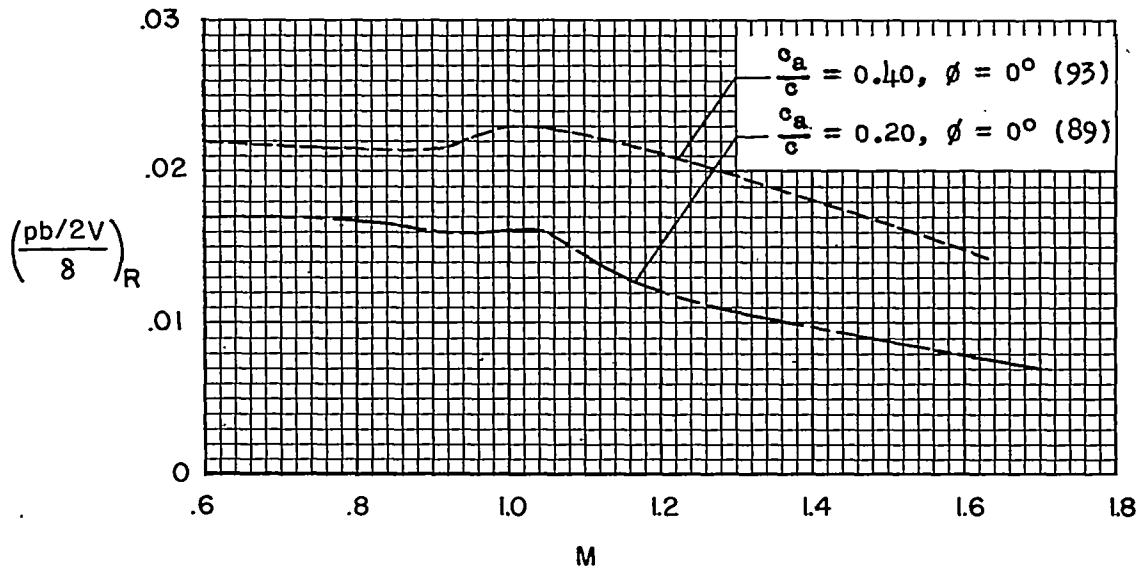
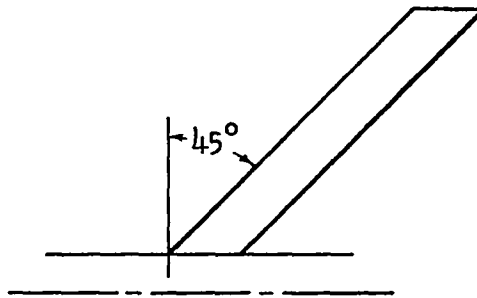
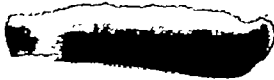
Figure 9.- Continued.





(i) $\Lambda = 45^\circ; A = 2.3; \lambda = 1.0$; flat-plate airfoil sections ($t/c = 0.054$).

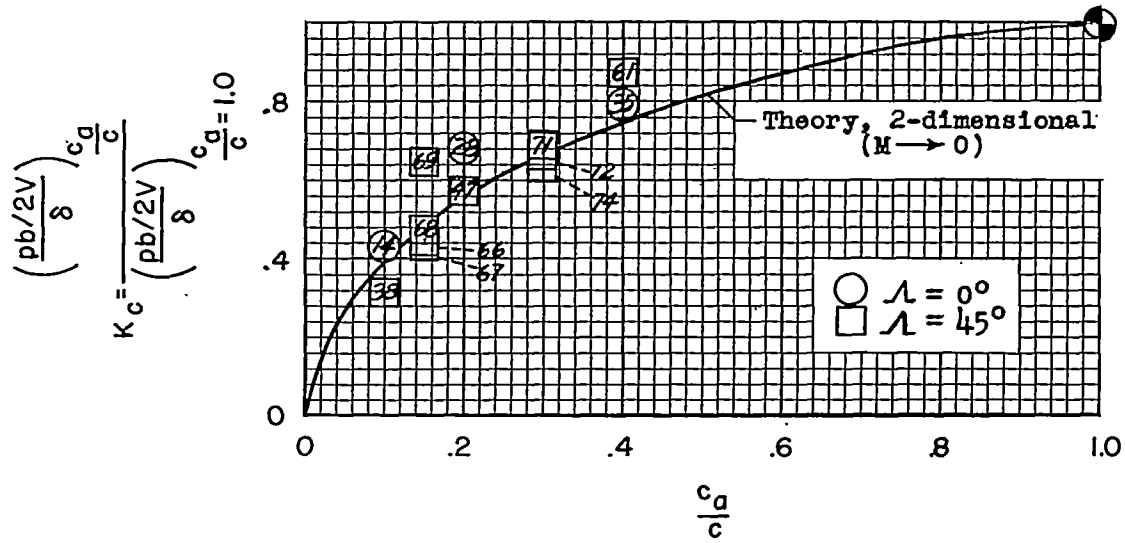
Figure 9.- Continued.



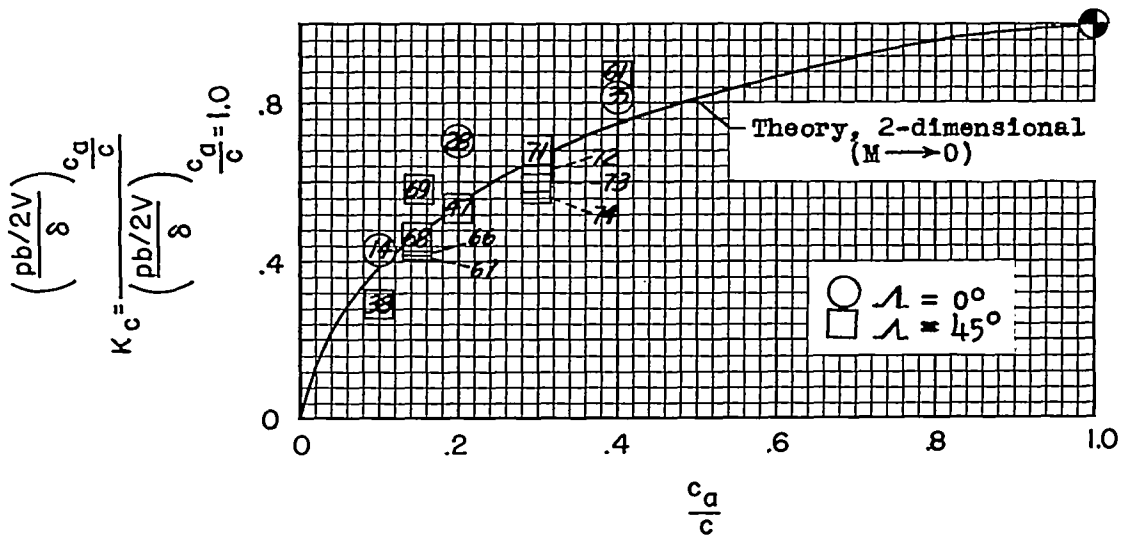
(j) $\Lambda = 45^\circ$; $A = 8.0$; $\lambda = 1.0$; flat-plate airfoil sections ($t/c = 0.108$).

Figure 9.- Concluded.



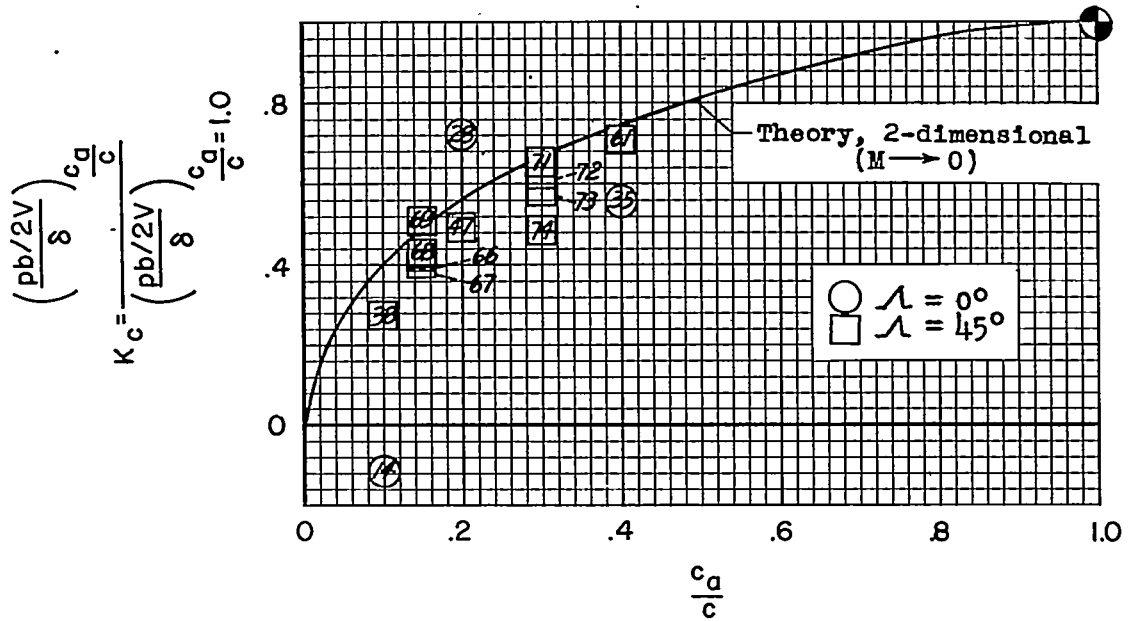


(a) M = 0.70.

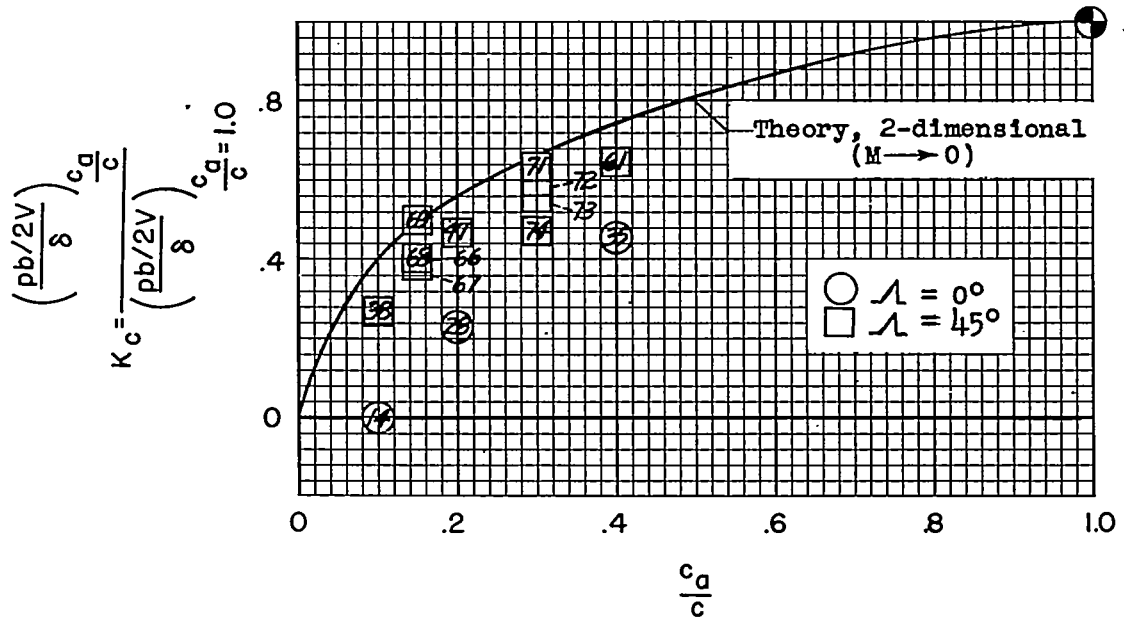


(b) M = 0.80.

Figure 10.- Variation of the effectiveness factor K_c with aileron chord ratio. $\delta \approx 3^\circ$ to 7° except for $c_a/c = 1.0$. Numbers in symbols denote model numbers.

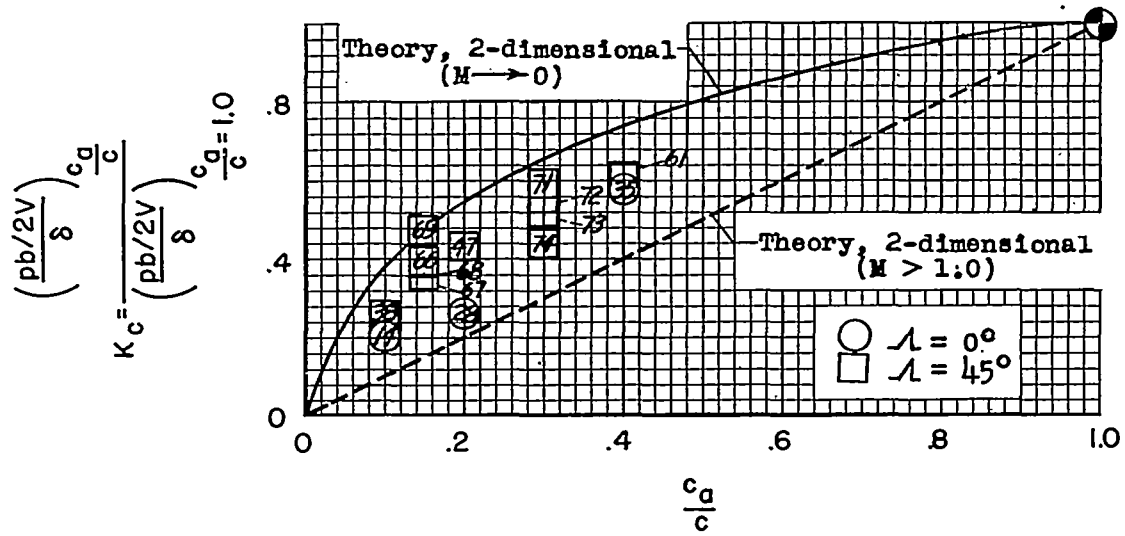


(c) $M = 0.90$.

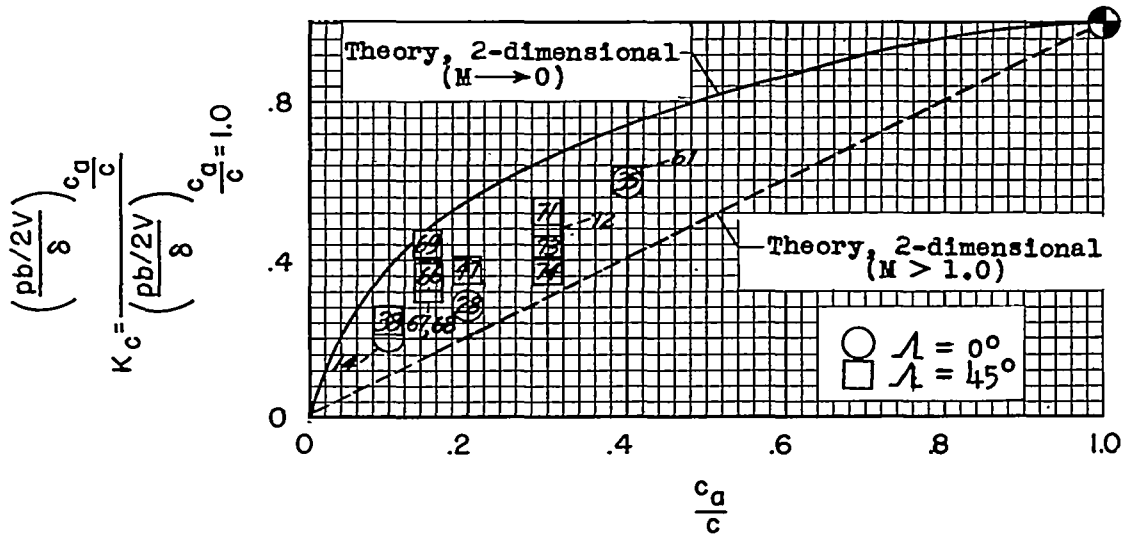


(d) $M = 0.93$.

Figure 10.- Continued.



(e) M = 0.96.



(f) M = 1.00.

Figure 10.- Continued.

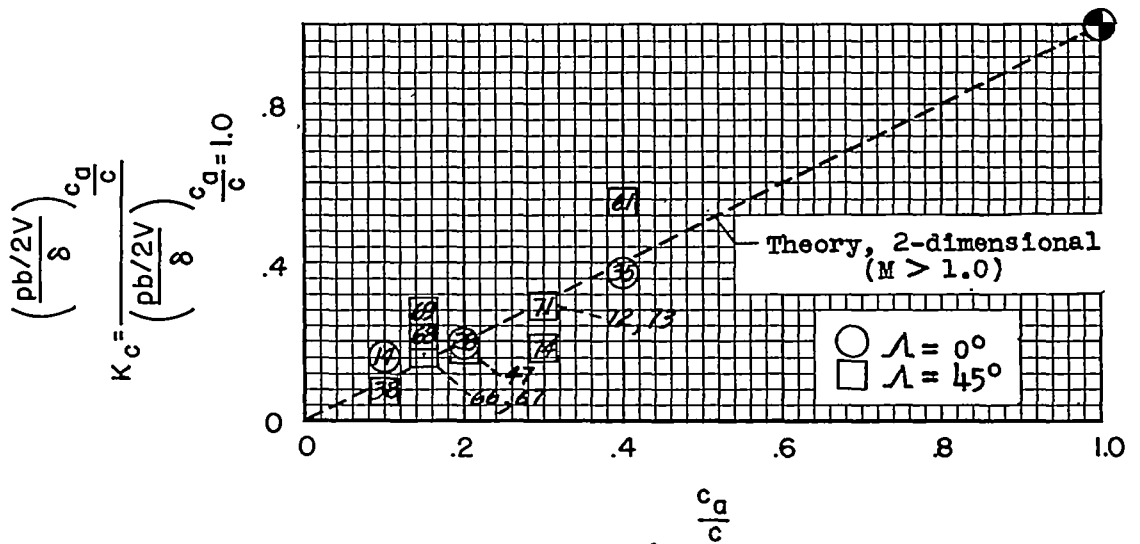
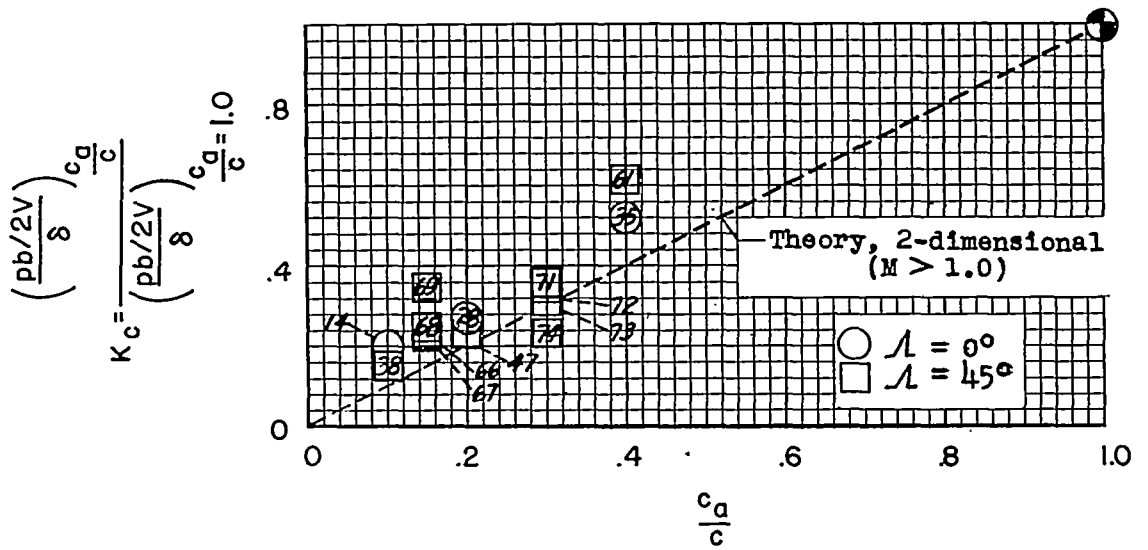
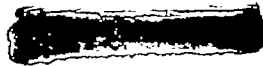
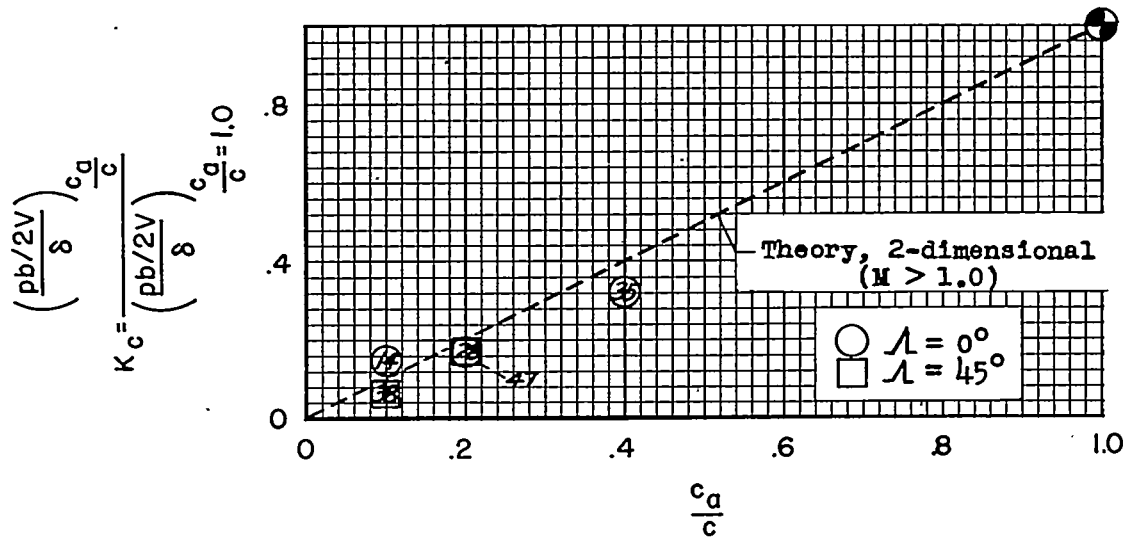


Figure 10.- Continued.



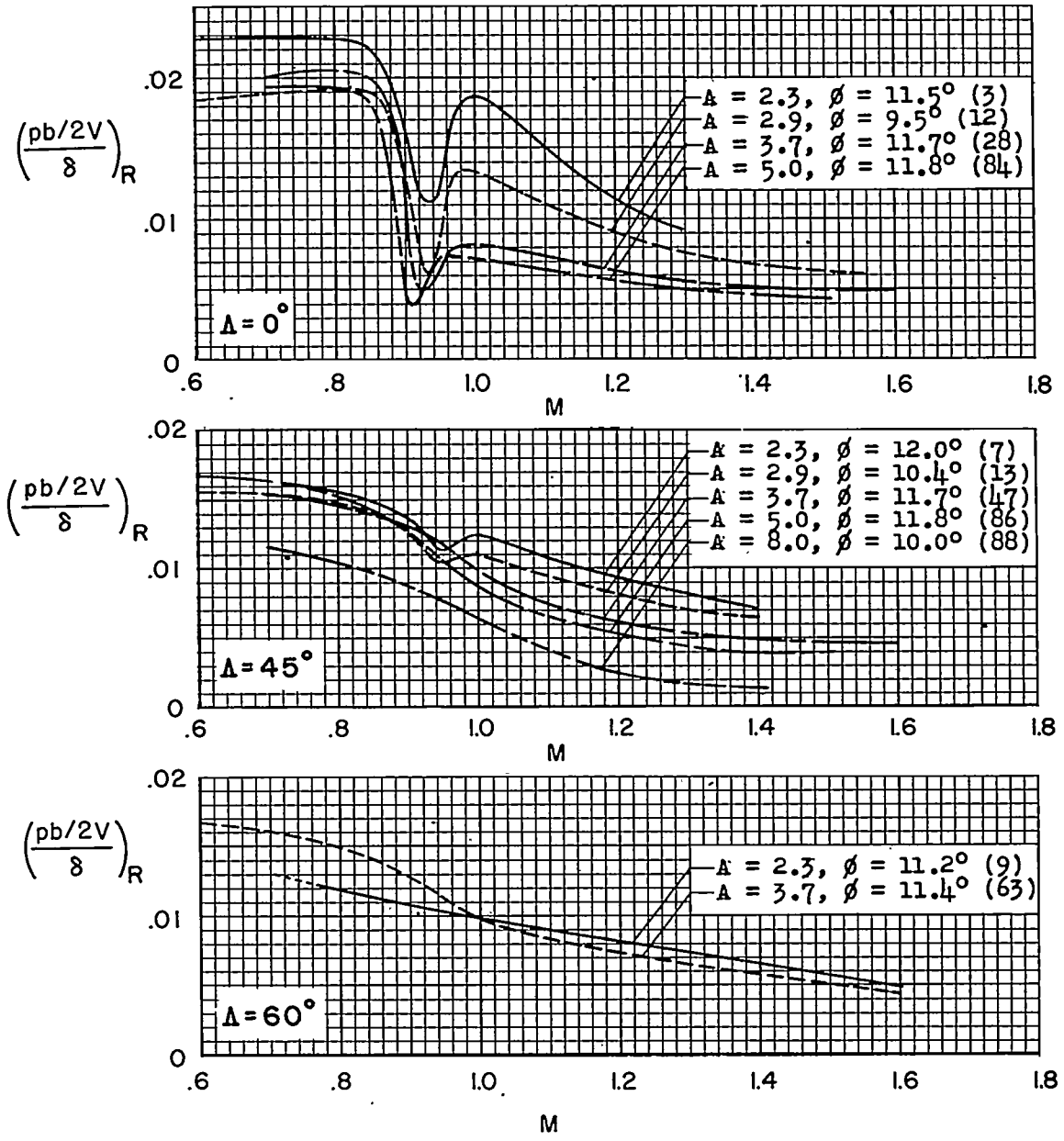
CONFIDENTIAL



(1) $M = 1.60$.

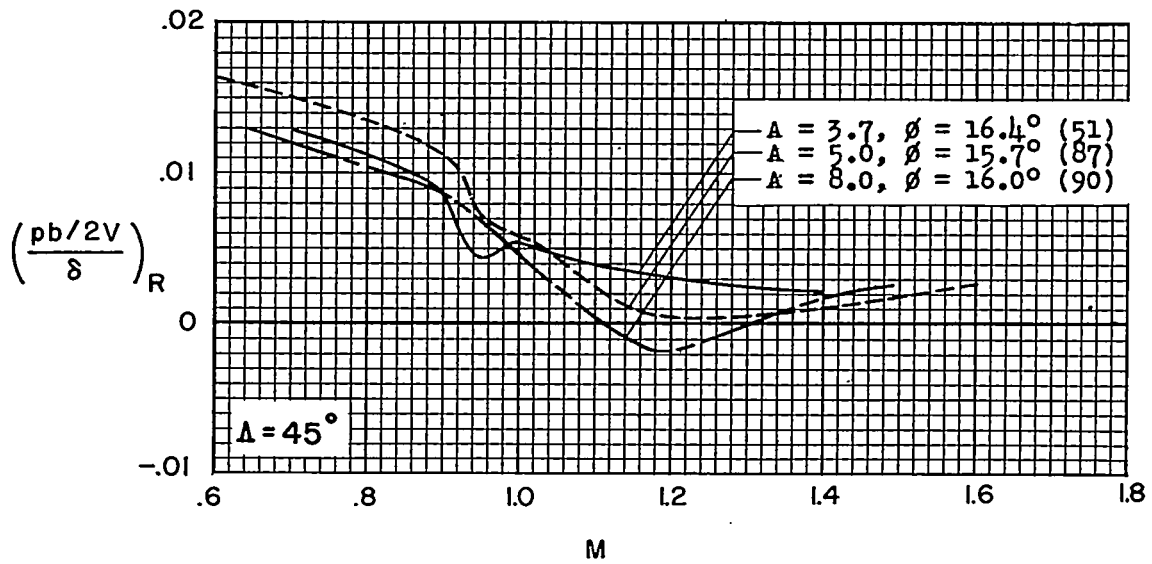
Figure 10.- Concluded.

CONFIDENTIAL



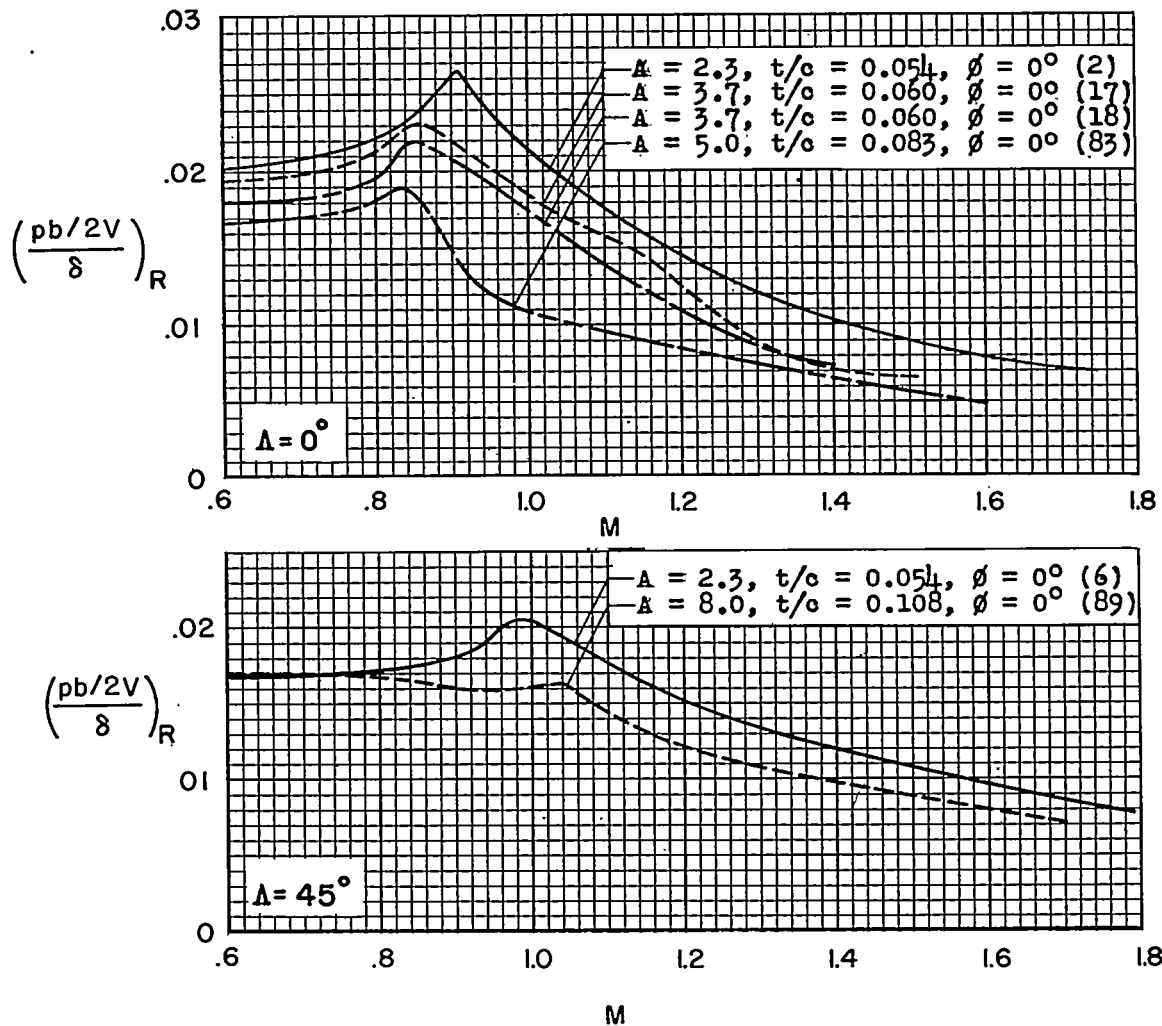
(a) NACA 65A009 airfoil sections. $c_a/c = 0.20$.

Figure 11.- Effect of aspect ratio on rolling effectiveness for full-span ailerons on untapered wings. $\delta \approx 3^\circ$ to 7° . Numbers in parentheses denote model numbers.



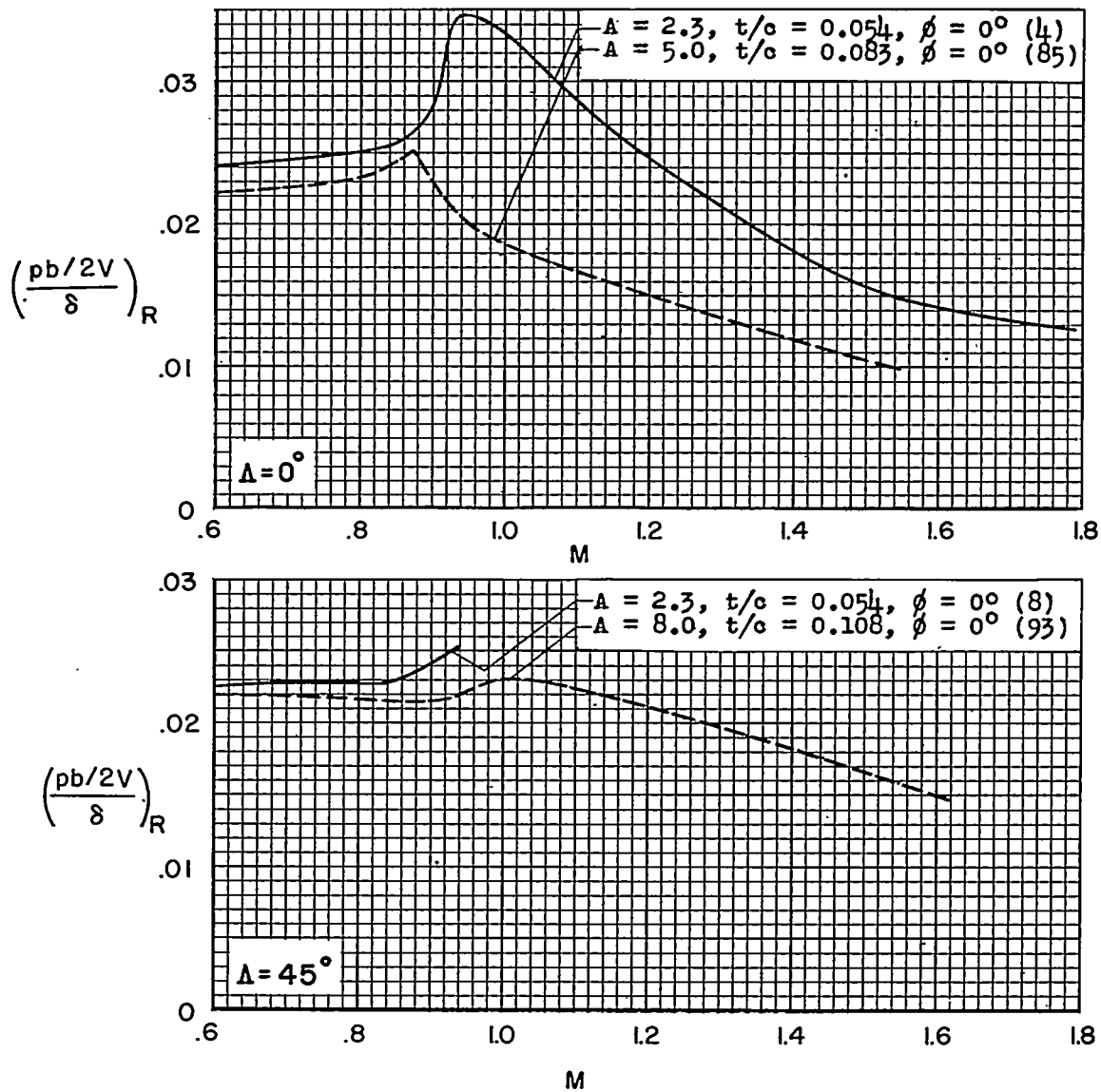
(b) NACA 65₁A012 airfoil sections. $c_a/c = 0.20$.

Figure 11.- Continued.



(c) Modified flat-plate airfoil sections. $c_a/c = 0.20$.

Figure 11.- Continued.



(d) Modified flat-plate airfoil sections. $c_a/c = 0.40$.

Figure 11.- Concluded.

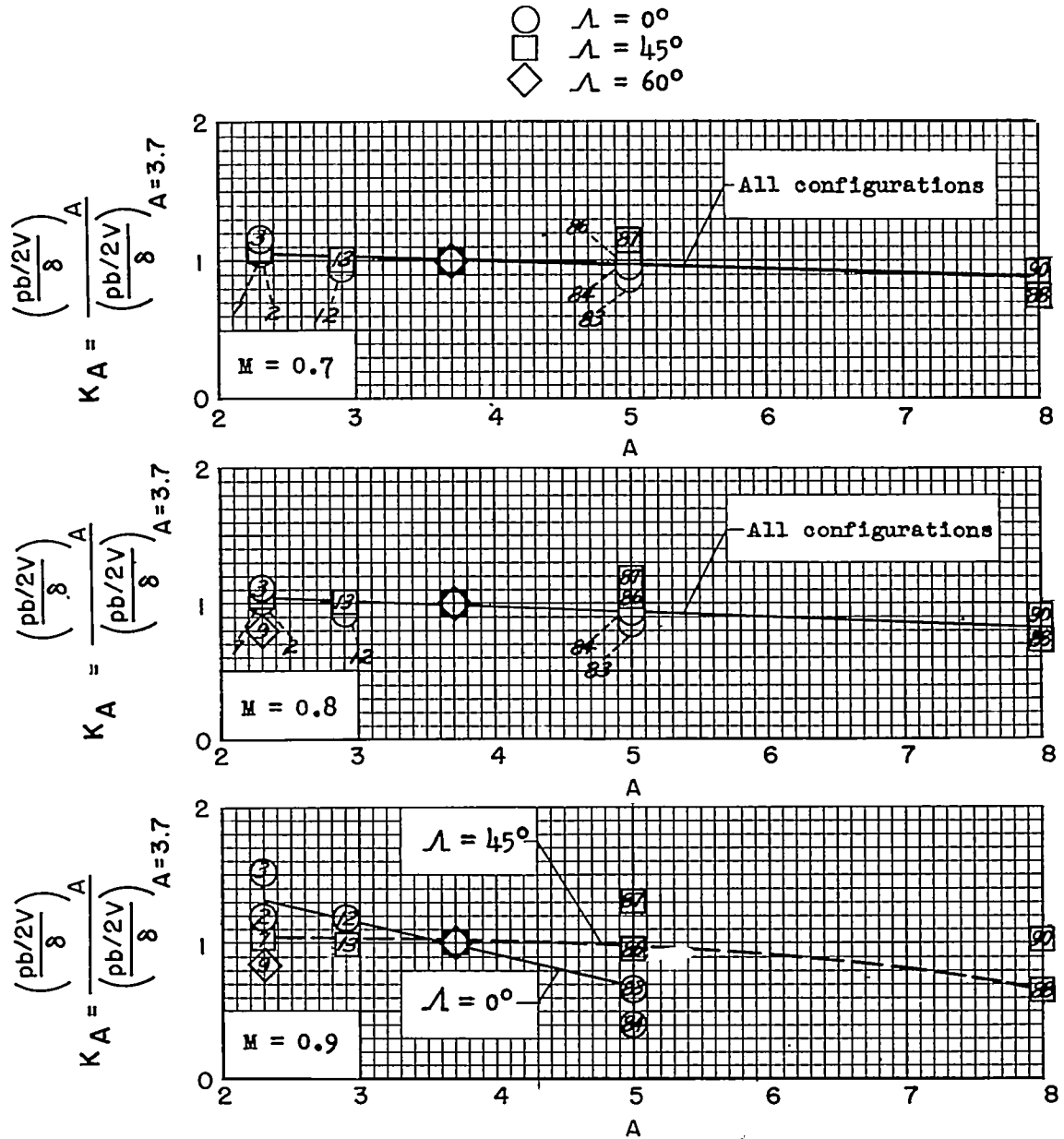


Figure 12.- Variation of the effectiveness factor K_A with aspect ratio. $\delta \approx 3^\circ$ to 7° . Numbers in symbols denote model numbers.

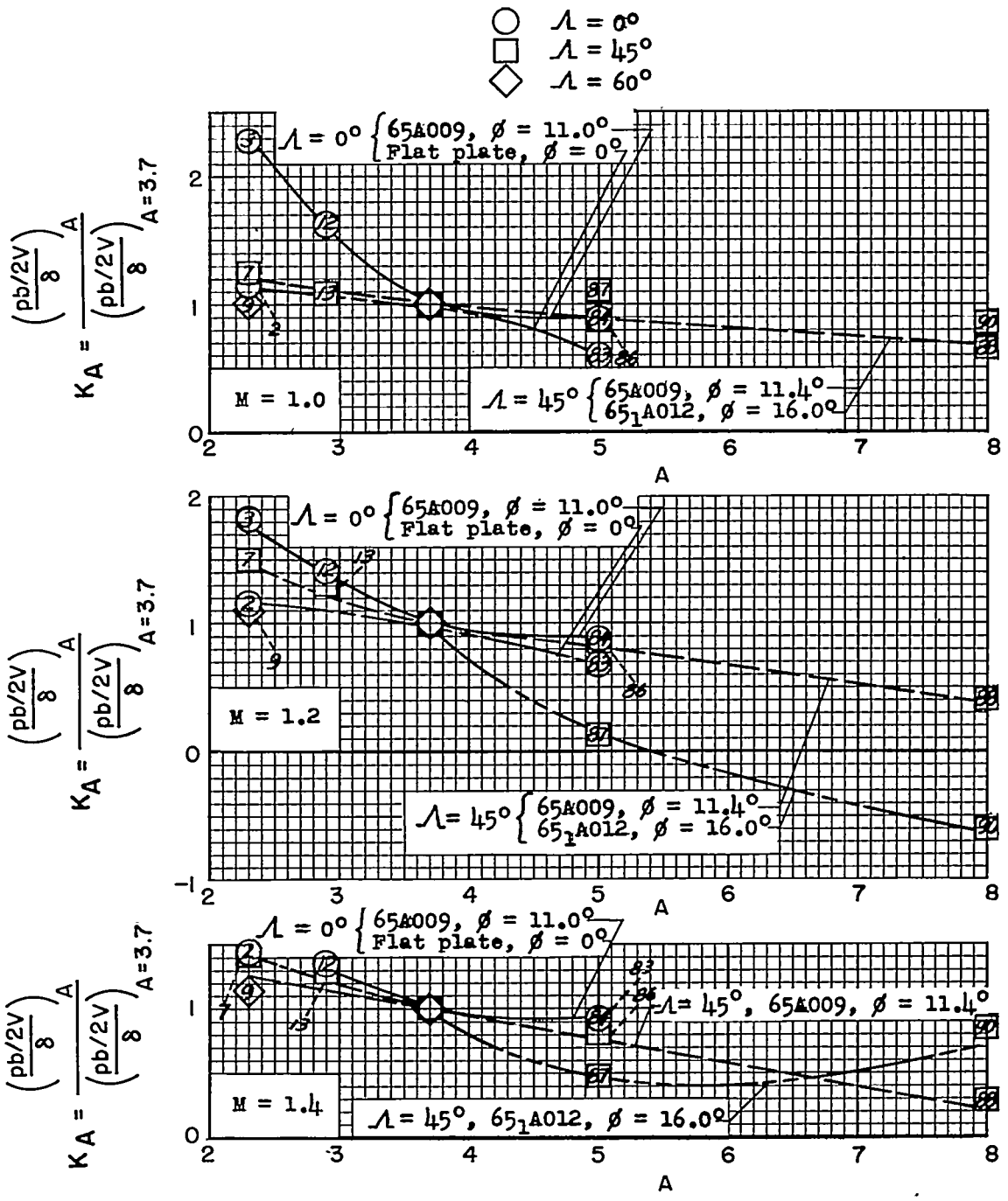
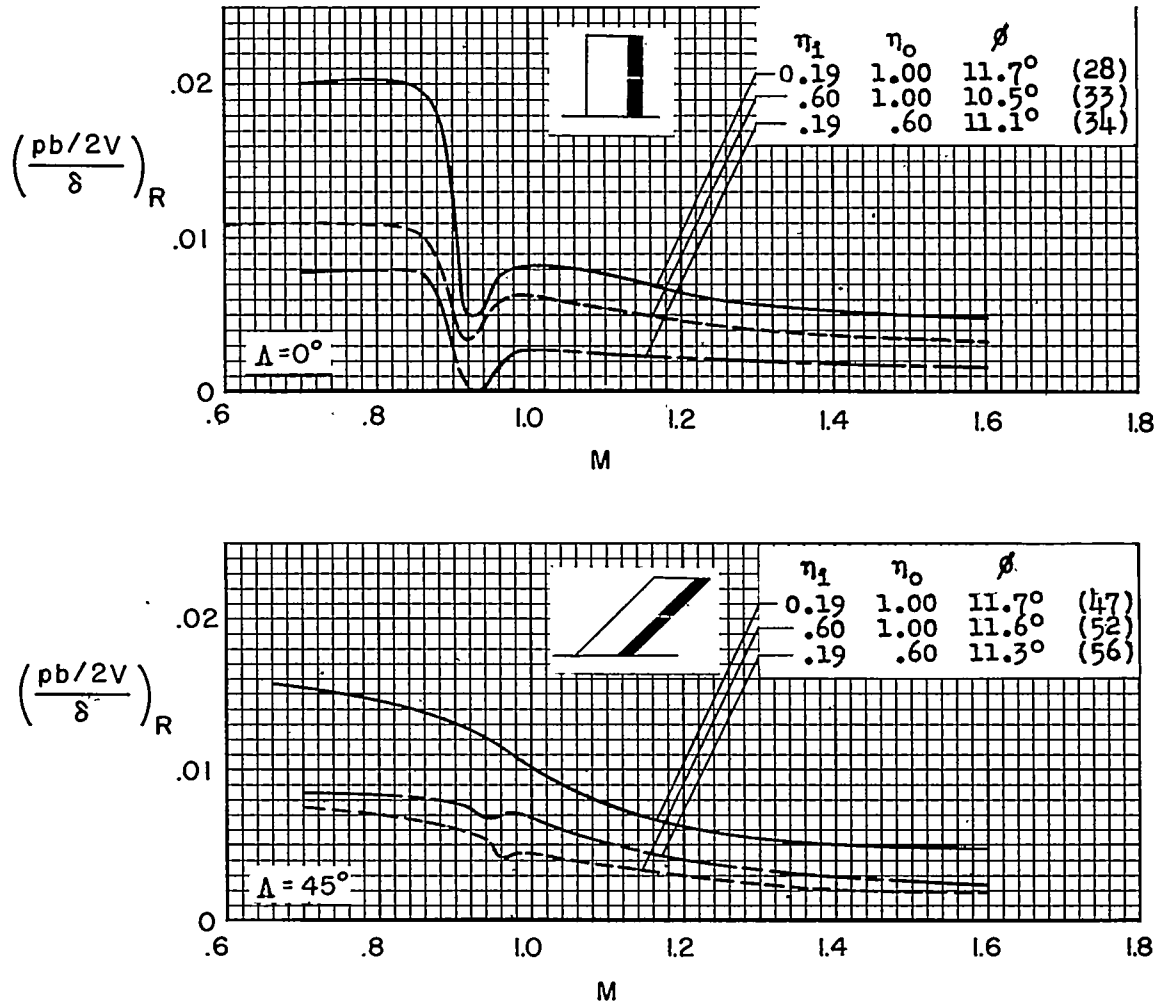
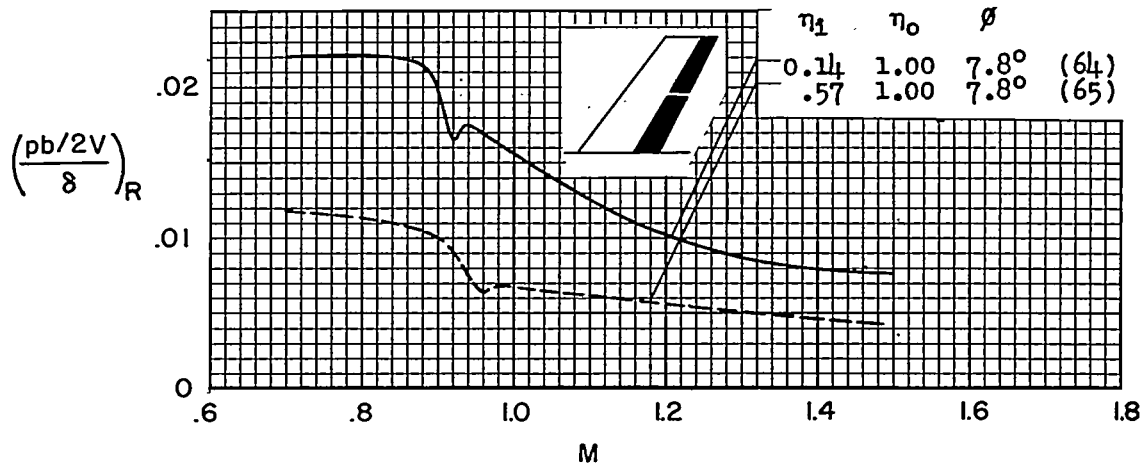


Figure 12.- Concluded.

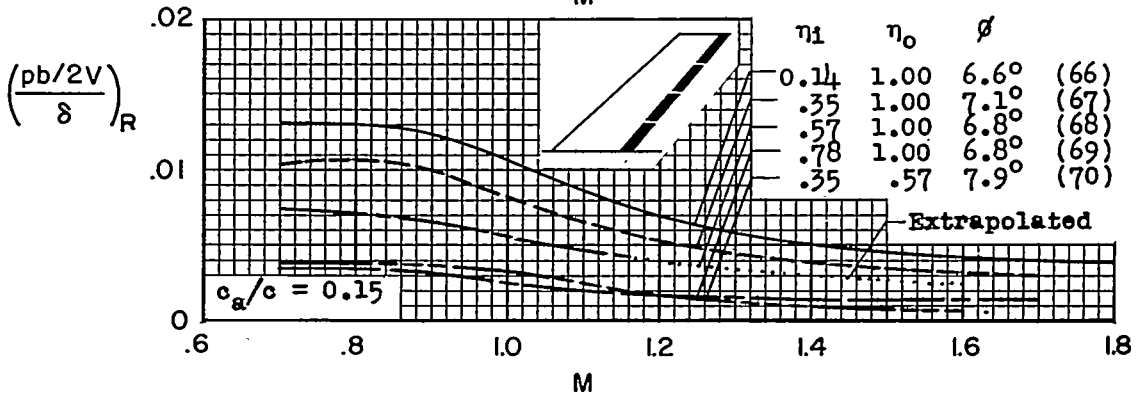
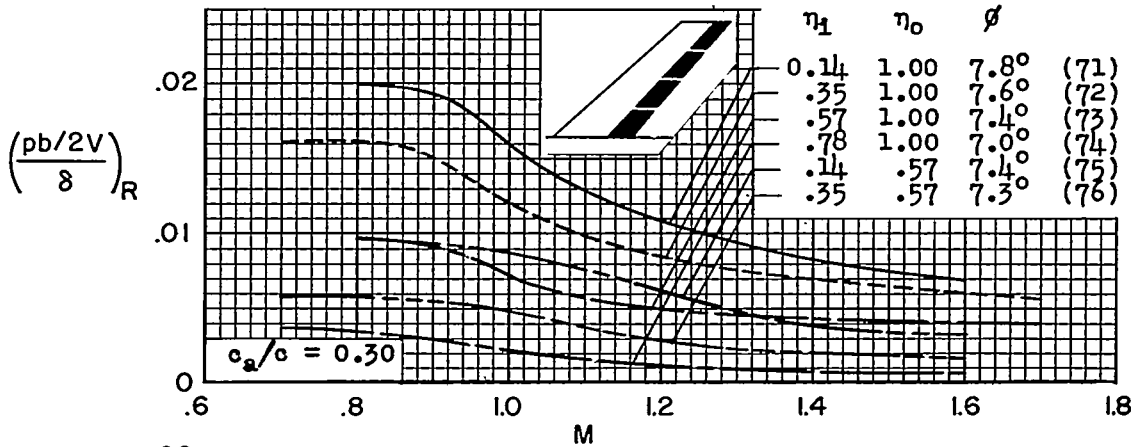


(a) NACA 65A009 airfoil sections. $A = 3.7$; $\lambda = 1.0$; $c_a/c = 0.20$.

Figure 13.- Variation of rolling effectiveness with Mach number for constant percent-chord ailerons located at various spanwise positions. $\delta \approx 3^\circ$ to 7° except for $c_a/c = 1.0$. Numbers in parentheses denote model numbers.

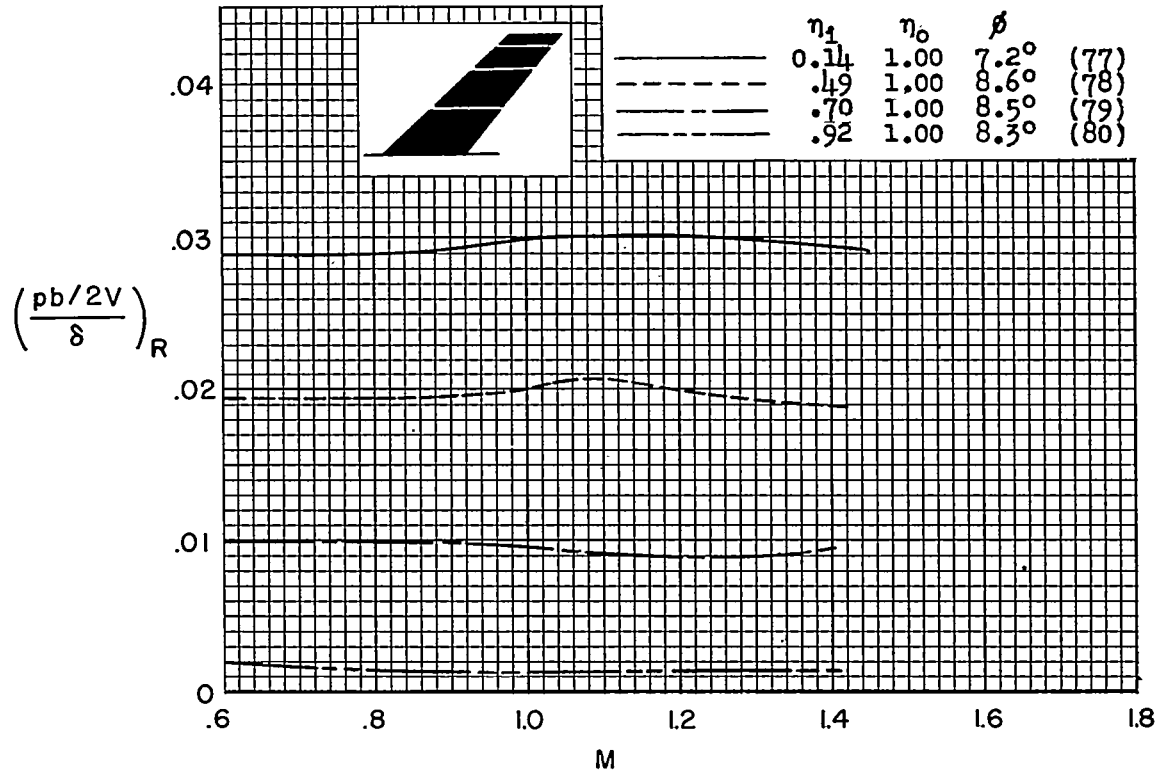


(b) NACA 65A006 airfoil sections. $A = 4.0$; $\lambda = 0.60$; $\Lambda = 35^\circ$; $c_a/c = 0.30$.



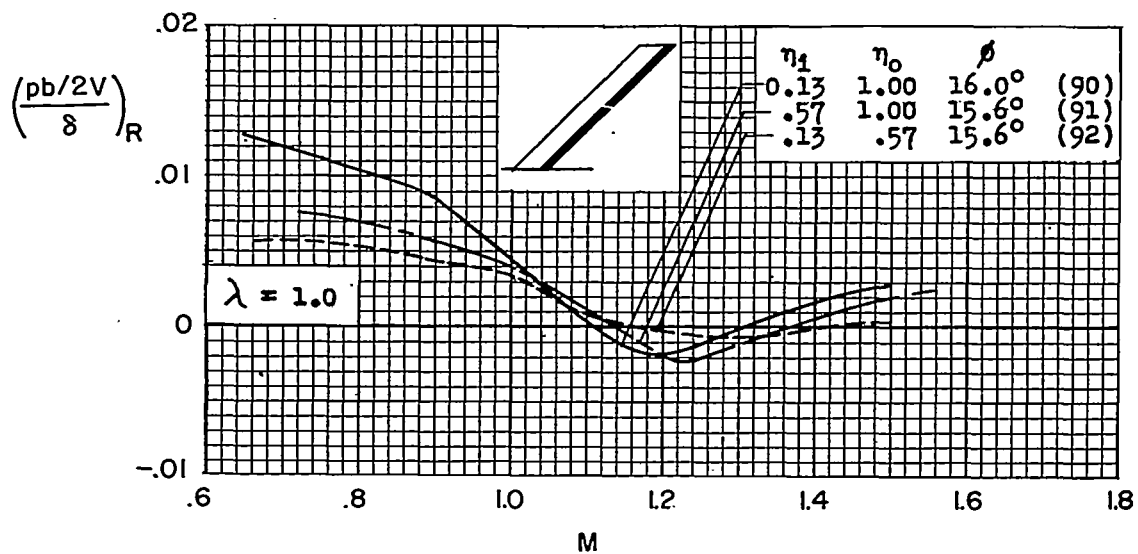
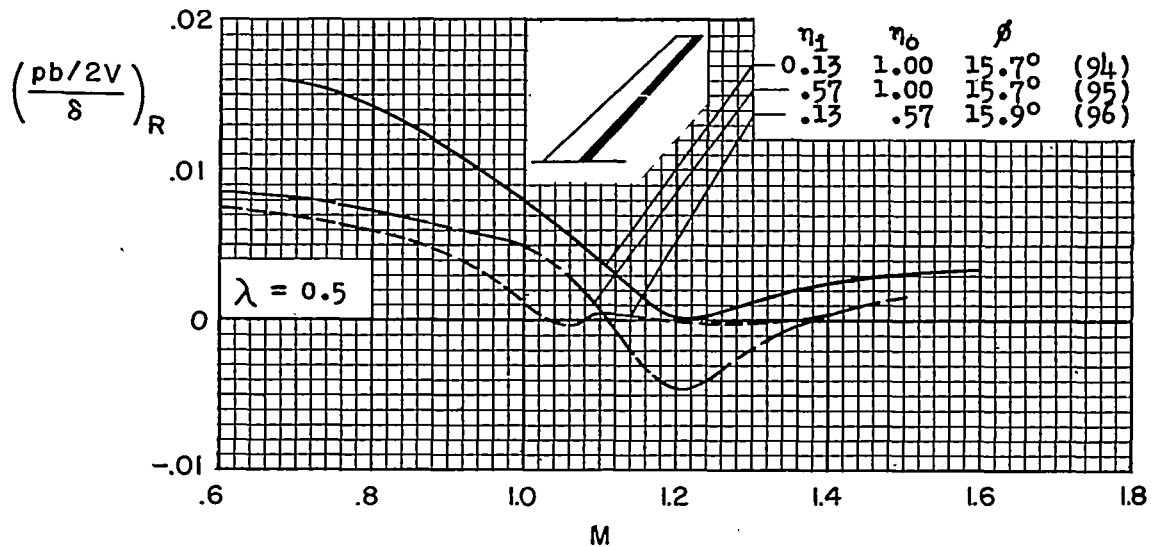
(c) NACA 65A006 airfoil sections. $A = 4.0$; $\lambda = 0.60$; $\Lambda = 45^\circ$.

Figure 13.- Continued.



(d) NACA 65A006 airfoil sections. $A = 4.0$; $\lambda = 0.60$; $\Lambda = 45^\circ$; $c_a/c = 1.0$.

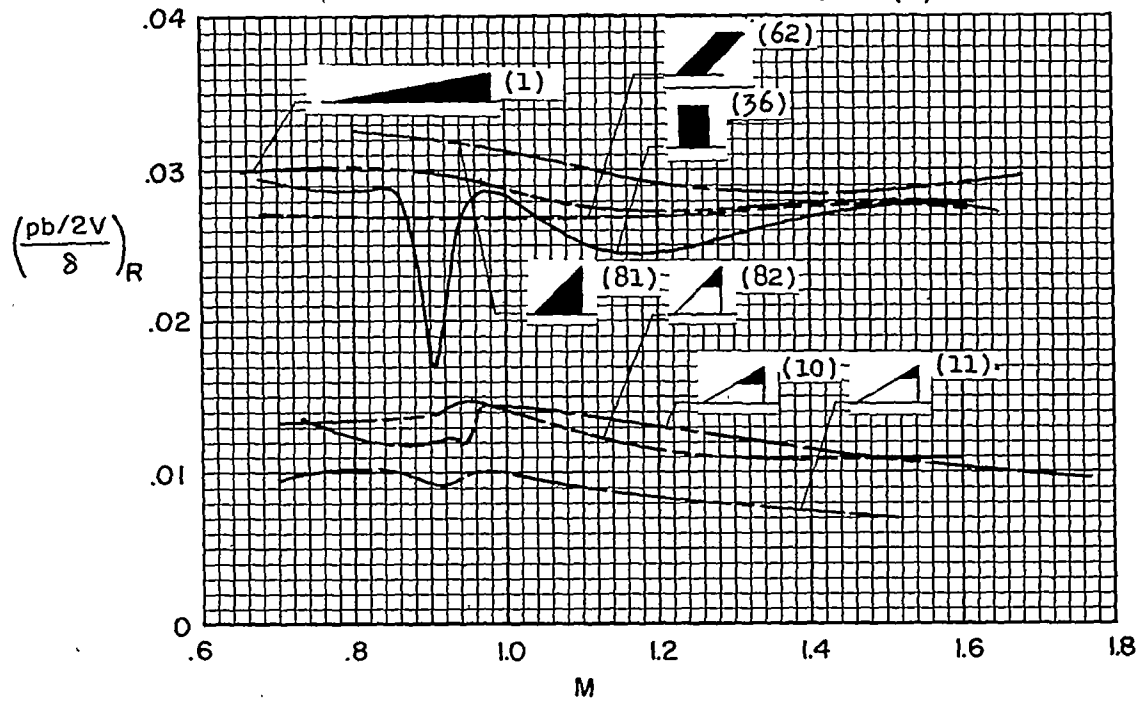
Figure 13.- Continued.



(e) NACA 65₁A012 airfoil sections. $A = 8.0$; $\Lambda = 45^\circ$; $c_a/c = 0.20$.

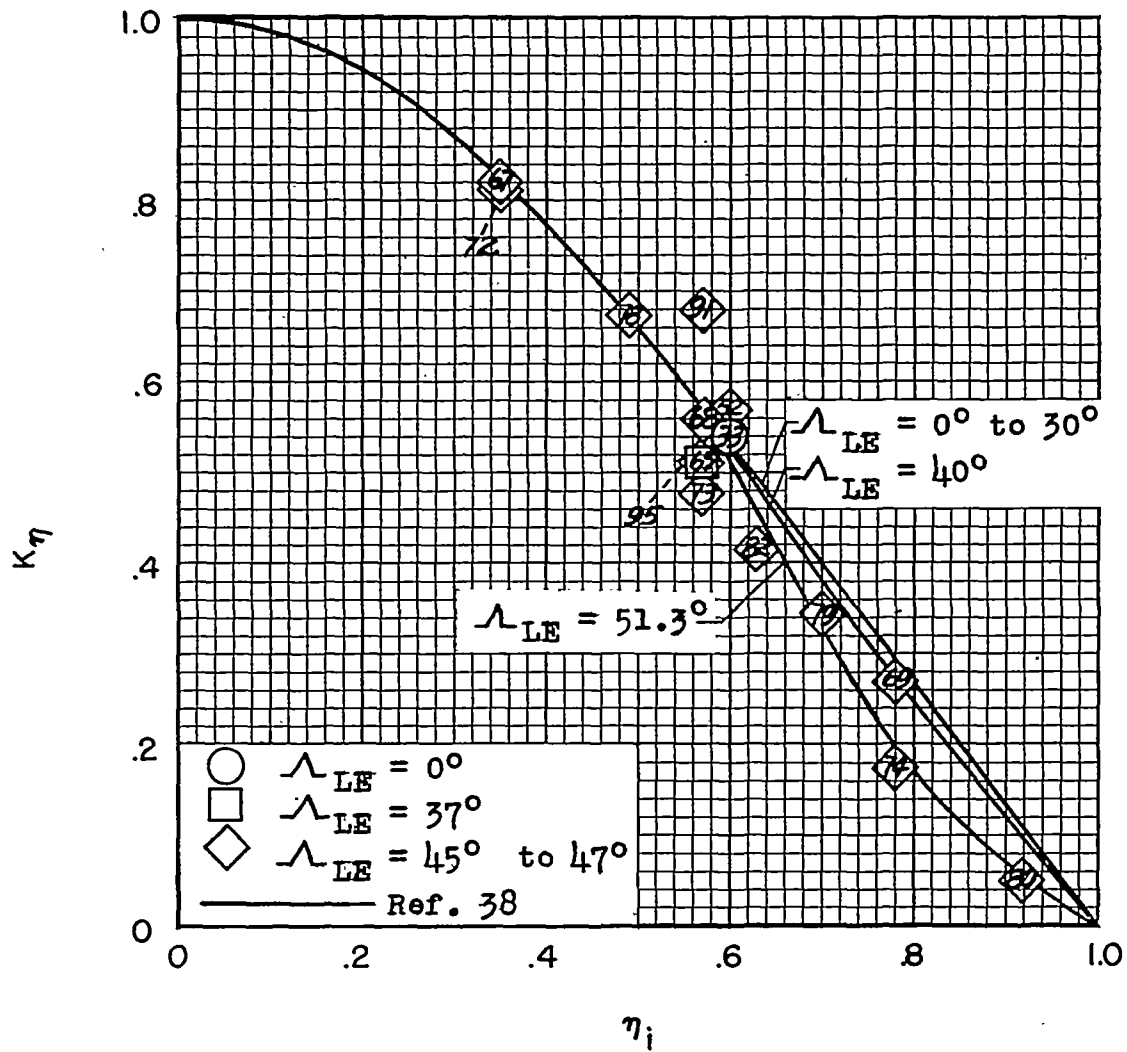
Figure 13.- Continued.

	η_1	η_0	θ	
—————	0.19	1.00	12.3°	(36)
-----	.19	1.00	11.3°	(62)
—————	.17	1.00	9.0°	(81)
-----	.63	1.00	8.6°	(82)
—————	.65	1.00	7.8°	(10)
-----	.74	1.00	4.8°	(11)
—————	.26	1.00	2.0°	(1)



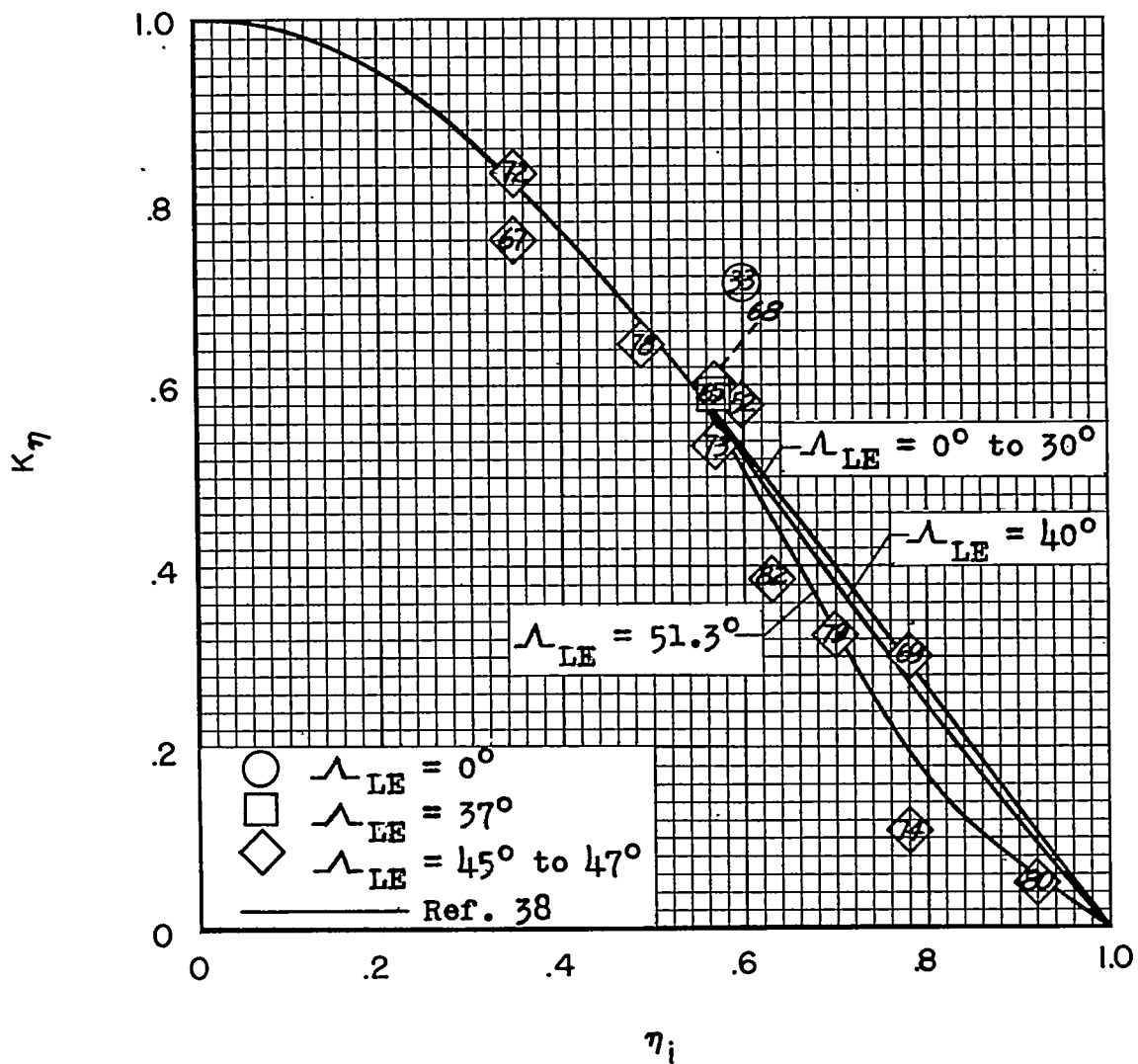
(f) Miscellaneous configurations. $c_a/c = 1.0$.

Figure 13.- Concluded.



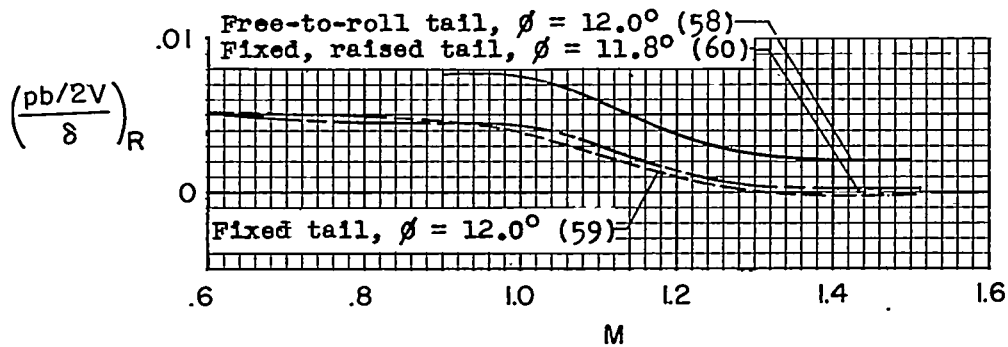
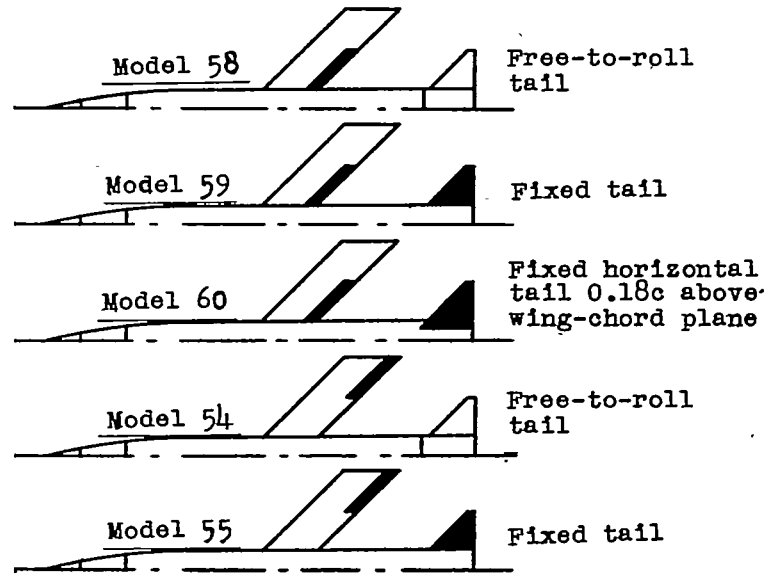
(a) $M = 0.80$.

Figure 14.- Variation of the effectiveness factor K_η with aileron span. Numbers in symbols denote model numbers.

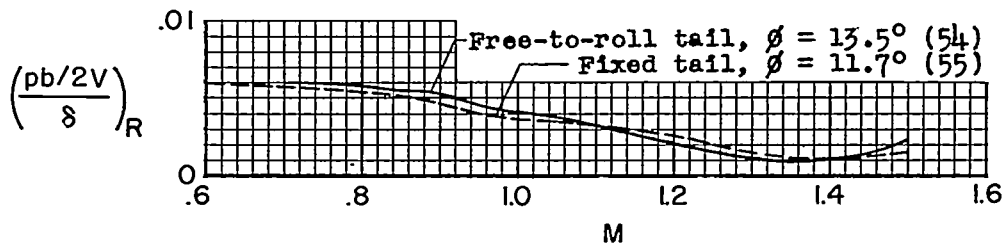


(b) $M = 1.4$.

Figure 14.- Concluded.



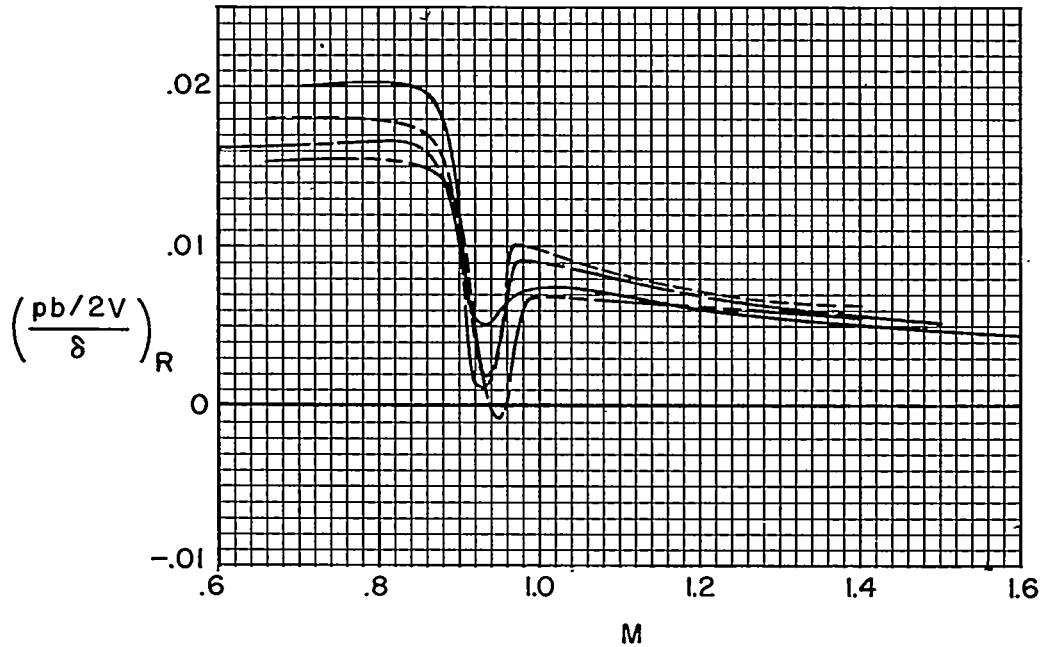
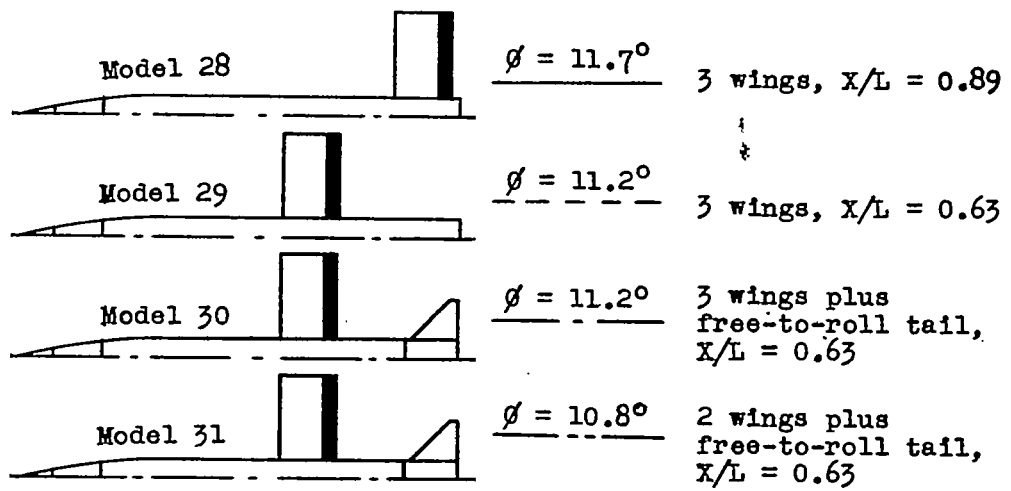
(a) Inboard ailerons.



(b) Outboard ailerons.

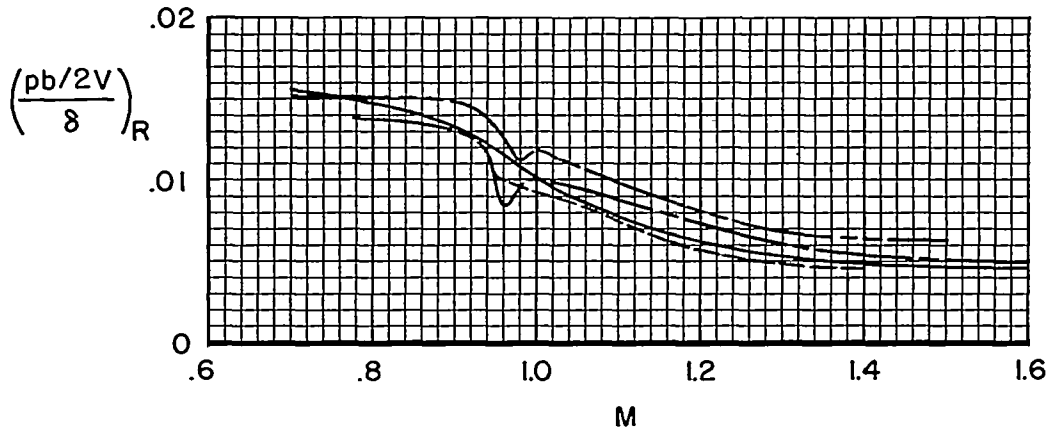
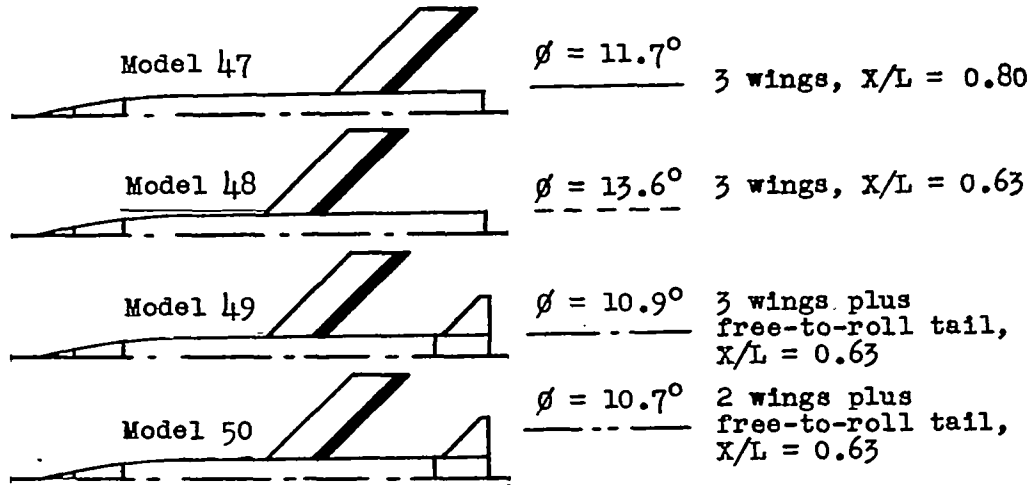
Figure 15.- Some effects of wing-tail interference on rolling effectiveness for inboard and outboard ailerons. $A = 3.7$; $\lambda = 1.0$; $\Lambda = 45^\circ$; NACA 65A009 airfoil sections; $c_a/c = 0.20$; $\delta \approx 3^\circ$ to 7° . Numbers in parentheses denote model numbers.





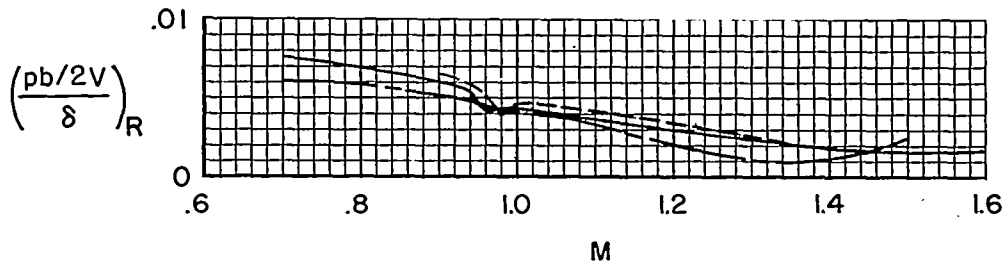
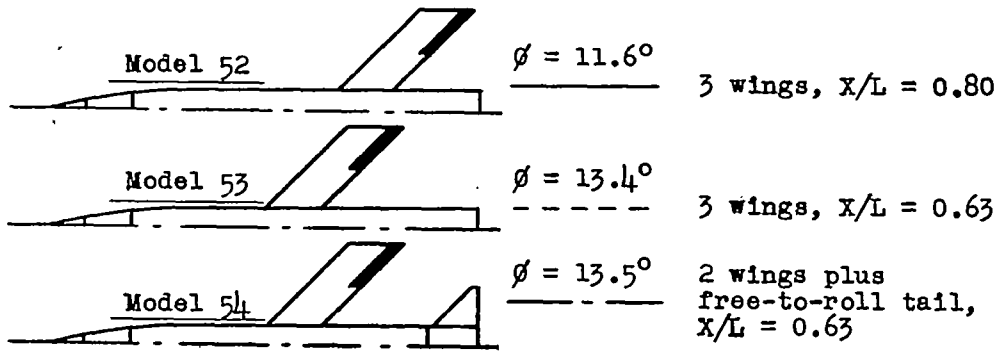
(a) Full-exposed-span aileron. $\Lambda = 0^\circ$.

Figure 16.- Some effects of wing location and number of wings. $A = 3.7$; $\lambda = 1.0$; $c_a/c = 0.20$; $\delta \approx 3^\circ$ to 7° ; NACA 65A009 airfoil sections.

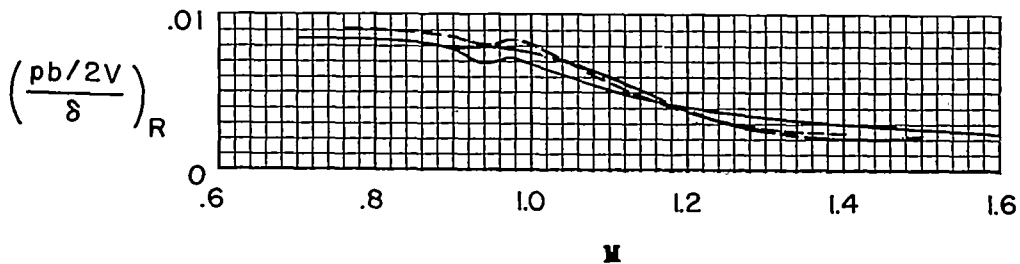
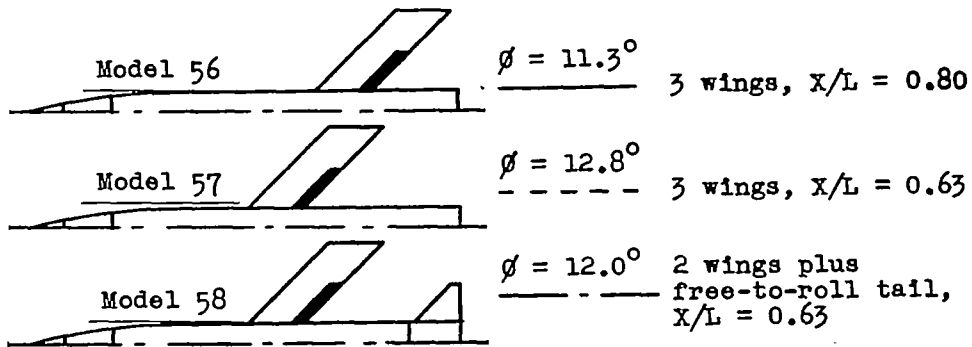


(b) Full-exposed-span ailerons. $\Lambda = 45^\circ$.

Figure 16.- Continued.



(c) Outboard half-exposed-span ailerons. $\Lambda = 45^\circ$.



(d) Inboard half-exposed-span ailerons. $\Lambda = 45^\circ$.

Figure 16.- Concluded.

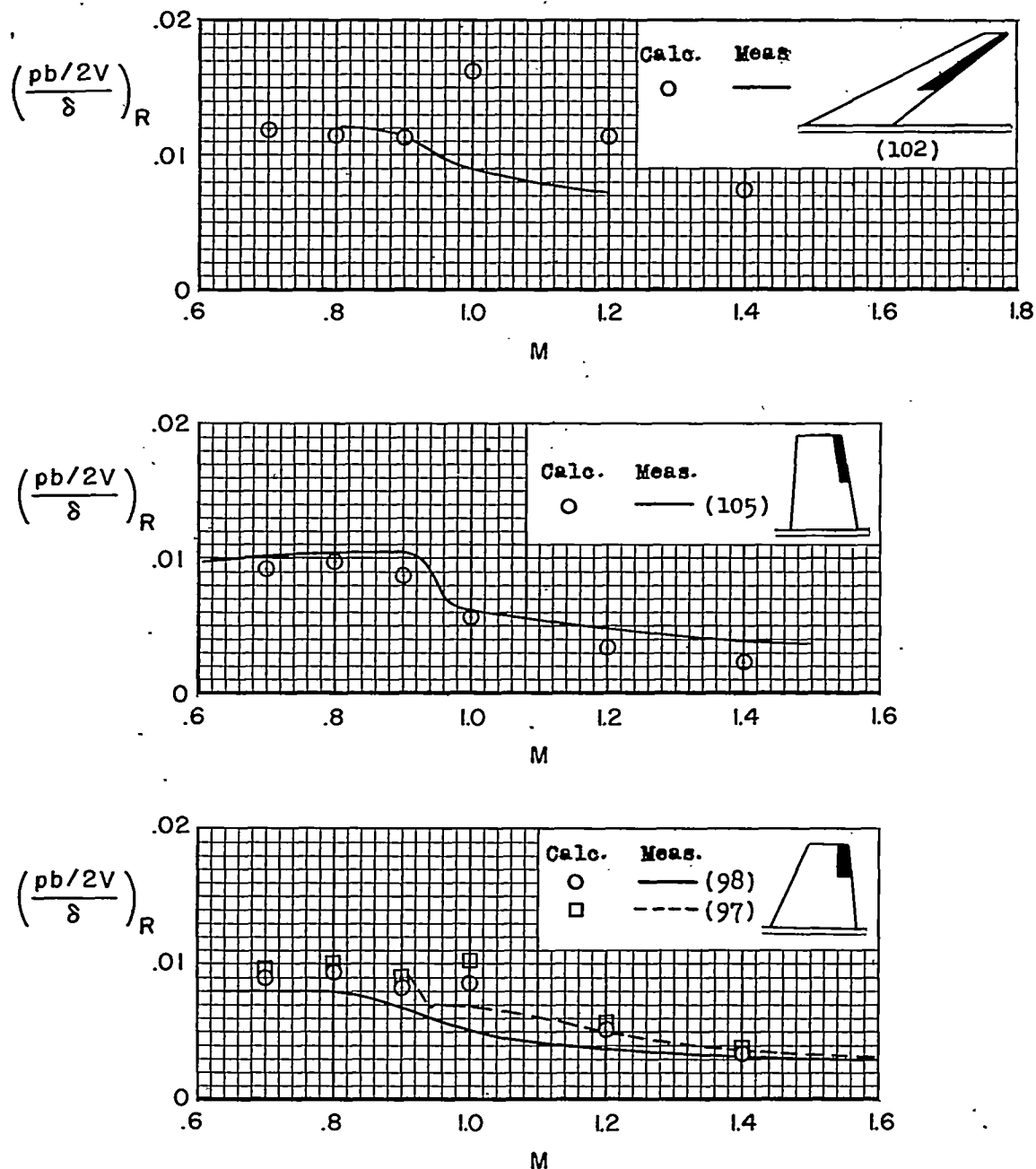


Figure 17.- Measured and estimated rolling effectiveness for several models simulating existing or proposed airplane wing-aileron configurations (without fixed tails). Estimated values were obtained from figures 6, 10, 12, and 14. Numbers in parentheses denote model numbers. $\delta \approx 3^\circ$ to 7° except for models 99, 107, and 108.

~~CONFIDENTIAL~~

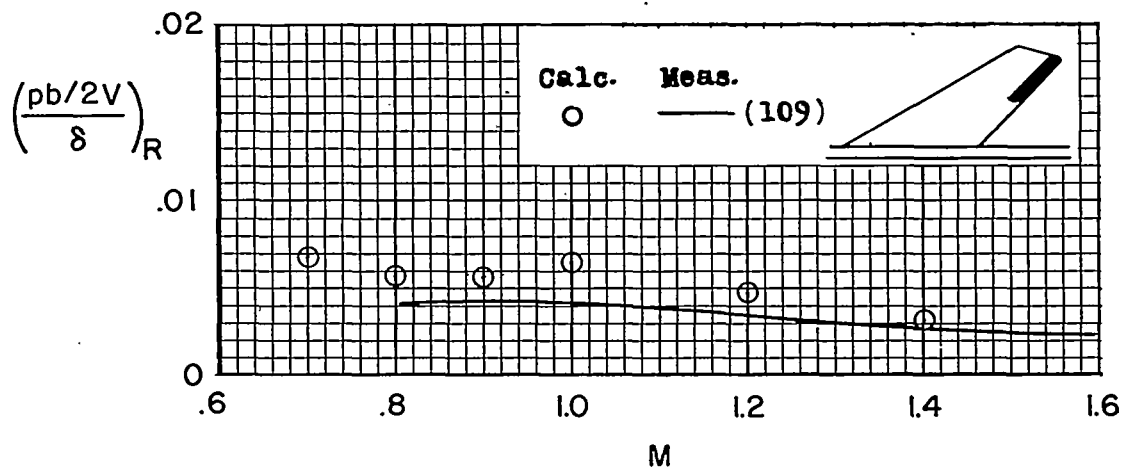
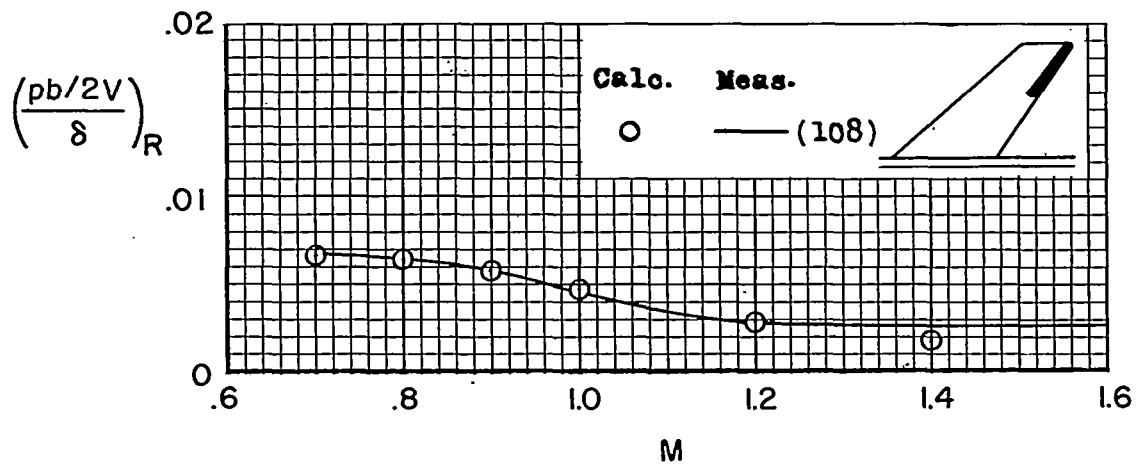
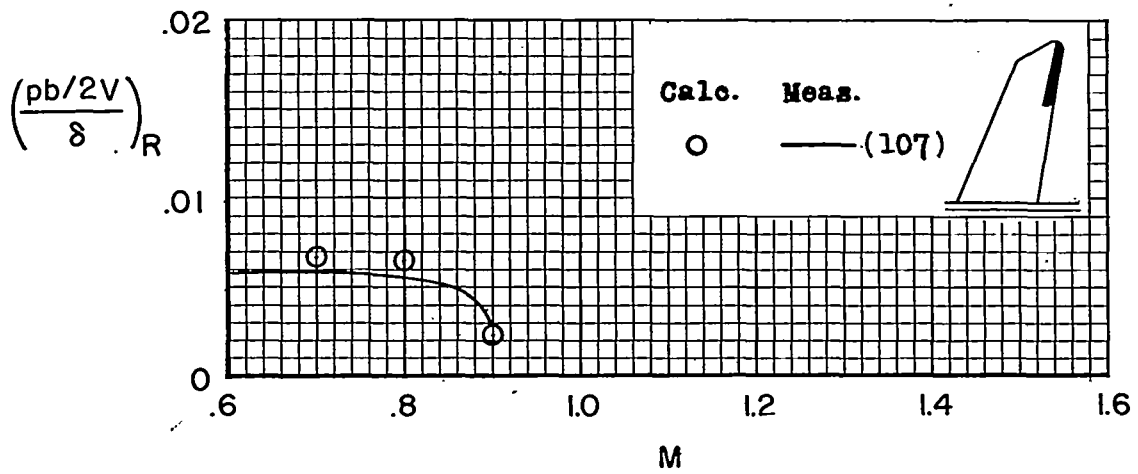


Figure 17.- Continued.

~~CONFIDENTIAL~~

~~CONFIDENTIAL~~

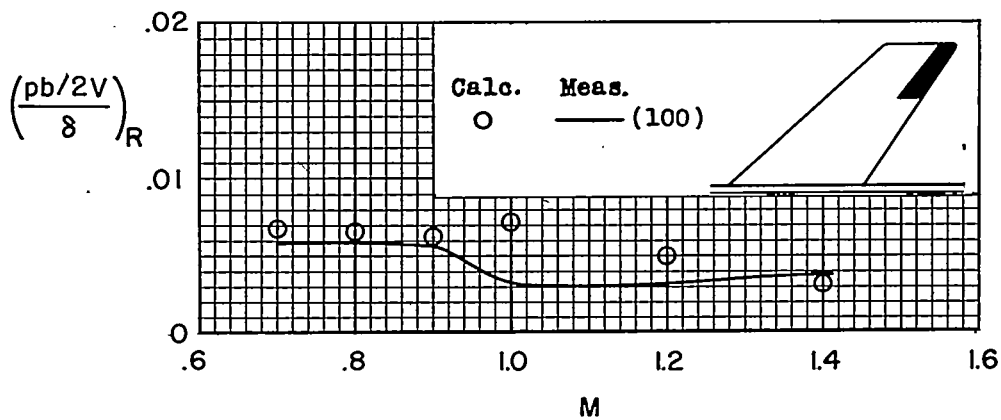
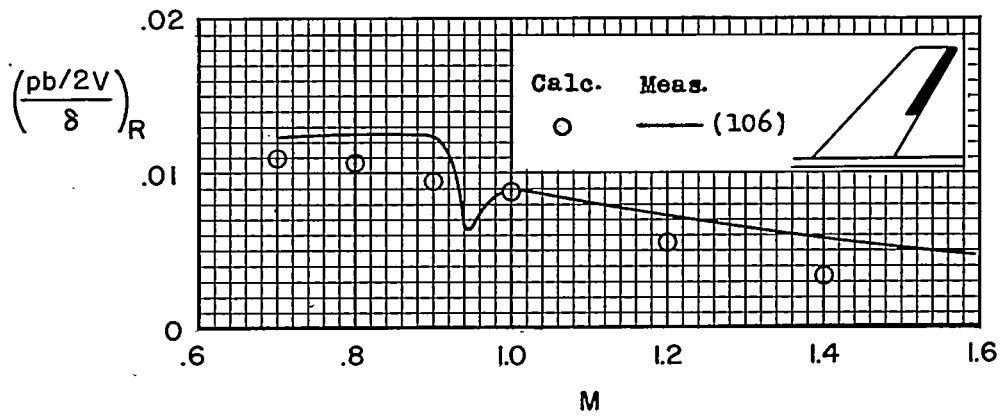
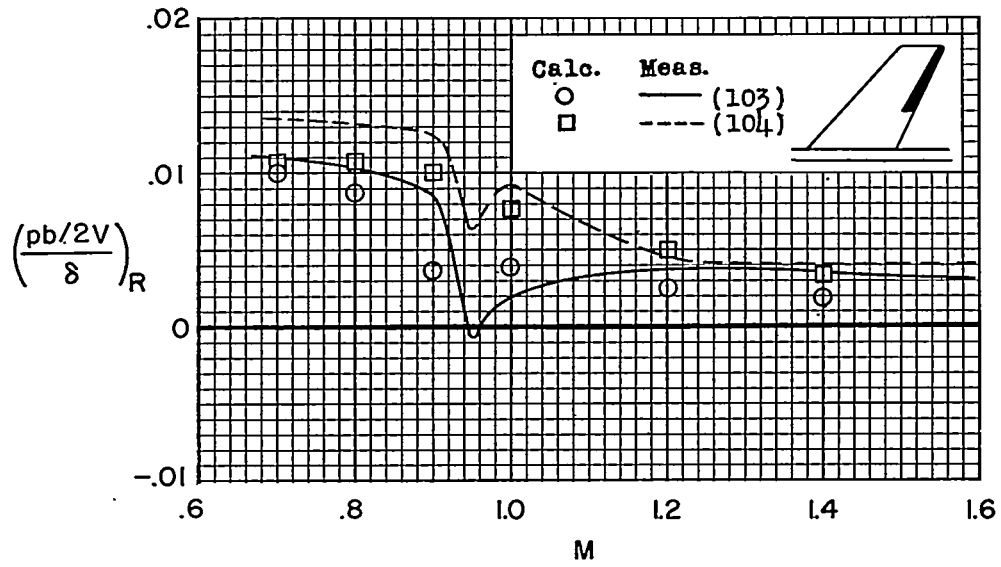


Figure 17.- Continued.

~~CONFIDENTIAL~~

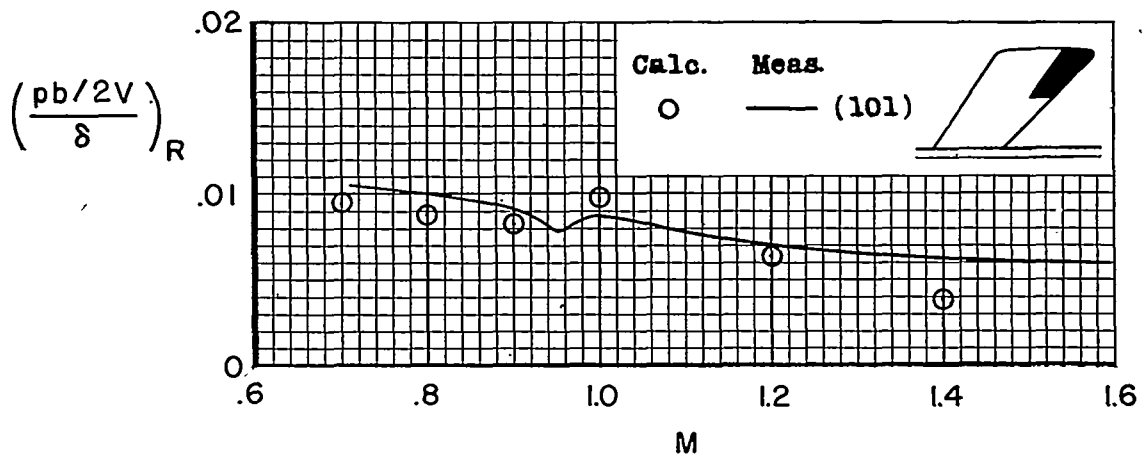
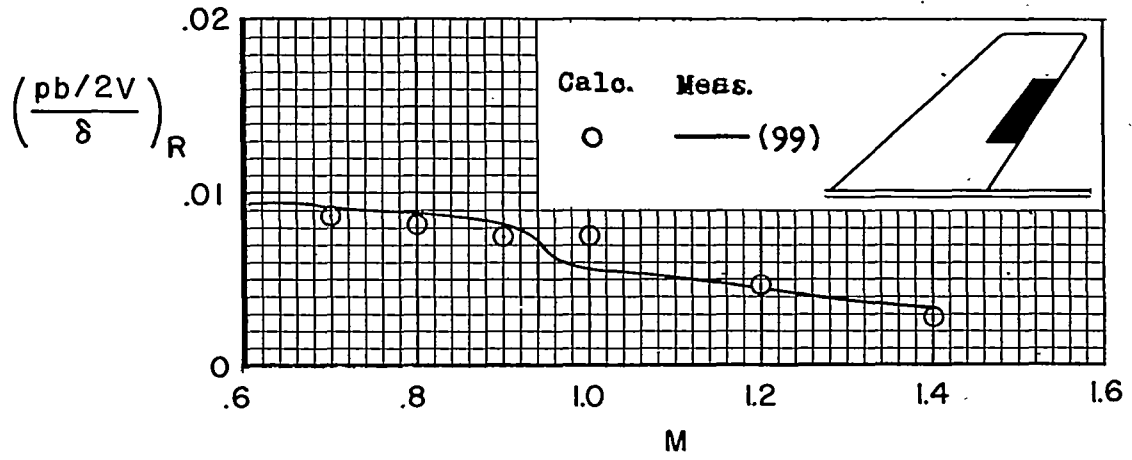


Figure 17.- Concluded.